NASA TECHNICAL NOTE

NASA TN D-4719

NASA TN D-4719

C.1

SUPERSONIC AERODYNAMICS OF LARGE-ANGLE CONES

by James F. Campbell and Dorothy T. Howell

Langley Research Center
Langley Station, Hampton, Va.

NATIONAL AERONAUTICS AND SPACE ADMINISTRATION • WASHINGTON, D. C. • AUGUST 1968

SUPERSONIC AERODYNAMICS OF LARGE-ANGLE CONES

By James F. Campbell and Dorothy T. Howell

Langley Research Center
Langley Station, Hampton, Va.

NATIONAL AERONAUTICS AND SPACE ADMINISTRATION

For sale by the Clearinghouse for Federal Scientific and Technical Information
Springfield, Virginia 22151 – CFSTI price $3.00

SUPERSONIC AERODYNAMICS OF LARGE-ANGLE CONES

By James F. Campbell and Dorothy T. Howell
Langley Research Center

SUMMARY

An investigation has been made to determine the supersonic aerodynamics of a series of conical bodies with semiapex angles from 40° to 90° (disk). The tests were performed at Mach numbers from 2.30 to 4.63, at angles of attack from -4° to 24°, and at a Reynolds number based on model (base) diameter of 0.8×10^6. These data were compared with those predicted by exact cone theory, modified Newtonian theory, and an integral relations method.

Results of this study indicated that all the configurations are statically stable with the center of gravity located at the model base. As the cone semiapex angle is increased, axial force increases, the rate of increase being largest between the 40° and 50° cone configurations. Experimental values of axial force at an angle of attack of 0° are adequately predicted for all cone semiapex angles by utilizing a combination of exact theory and an integral relations method. As the cone semiapex angle is increased, normal force decreases, normal force being zero for the flat disk. Shock standoff distance varies almost linearly with cone semiapex angle and the inverse of Mach number squared; these trends are adequately predicted by an integral relations method.

INTRODUCTION

Use of an aeroshell device during unmanned atmospheric entry has been proposed to protect the payload from the severe loading and heating environments and to provide sufficient aerodynamic braking. One of the shapes considered as an aeroshell candidate is the large-angle cone. This type of body provides a combination of the necessary high-drag characteristics with some degree of volume capacity. Several investigations (refs. 1 to 3) have been made to determine the aerodynamics of cones with semiapex angles up to (and including) 60°. To make the conical aeroshell optimum for a particular mission profile, however, it is necessary to determine the aerodynamics of cones with semiapex angles up to 90°.

Accordingly, an investigation has been conducted on a series of cone bodies with semiapex angles from 40° to 90° (disk) and the results of these tests are reported herein. For comparative purposes, results of tests on a 50° cone (from ref. 1) are included.

Static force and moment measurements and schlieren photographs were obtained at Mach numbers from 2.30 to 4.63, at angles of attack from -4° to 24°, and at a Reynolds number based on model (base) diameter of 0.8×10^6.

SYMBOLS

The results of the force tests are presented in coefficient form for both the body and stability axis systems. The pitching-moment reference center is located at the model base on the geometric center line of the cone as shown in figure 1.

C_A axial-force coefficient, $\frac{\text{Axial force}}{qS}$

C_D drag coefficient, $\frac{\text{Drag force}}{qS}$

C_L lift coefficient, $\frac{\text{Lift force}}{qS}$

C_{L_α} slope of lift-force curve with angle of attack, $\frac{\partial C_L}{\partial \alpha}$, per degree

C_m pitching-moment coefficient, $\frac{\text{Pitching moment}}{qSD}$

C_{m_α} slope of pitching-moment curve with angle of attack, $\frac{\partial C_m}{\partial \alpha}$, per degree

C_N normal-force coefficient, $\frac{\text{Normal force}}{qS}$

C_{N_α} slope of normal-force curve with angle of attack, $\frac{\partial C_N}{\partial \alpha}$, per degree

$C_{p,b}$ base pressure coefficient, $\frac{p_b - p}{q}$

$C_{p,max}$ stagnation pressure coefficient behind normal shock

D base diameter of model

l sting length, measured from base of model to sting flare

M free-stream Mach number

p free-stream static pressure

p_b static pressure at model base

p_l local static pressure

$p_{t,2}$ free-stream pitot pressure

q free-stream dynamic pressure

r radial coordinate

r_b base radius of model

S base area of model

s surface length

x axial coordinate

α angle of attack, degrees

δ standoff distance of detached shock wave, measured along geometric center line from cone apex

θ_c cone semiapex angle, degrees

θ_c^* cone semiapex angle which corresponds to sonic flow conditions on cone surface, degrees

Subscripts:

0 conditions at zero angle of attack

1 body

2 shock

APPARATUS AND TESTS

Models

Dimensional drawings of the models are shown in figure 1. The models consist of right-circular cones with semiapex angles of 40^o, 60^o, 70^o, 80^o, and 90^o (disk); they were

constructed of polished aluminum and had pointed noses and flat bases. Diameter for all the models was 4.80 inches (12.19 cm). The 40° cone model was provided with an insert which could be removed to effect an indented-base configuration. Details of the 50° cone model are found in reference 1. Two lengths of model sting supports (see fig. 2) were provided to aid in investigating sting-length effects on base pressure; the ratios of sting length to model base diameter were 2.0 and 4.0.

Tunnel

Data were obtained on the models mounted in the high Mach number test section of the Langley Unitary Plan wind tunnel, which is a variable pressure continuous-flow facility. The test section is 4.0 feet (1.22 meters) square and approximately 7.0 feet (2.13 meters) long. The nozzle leading to the test section is of the asymmetric sliding-block type which permits a continuous variation in Mach number from 2.3 to 4.7.

Test Conditions and Measurements

The models were tested at Mach numbers from 2.30 to 4.63 through an angle-of-attack range from about -4° to 24° at zero sideslip. The Reynolds number based on model (base) diameter was 0.8×10^6; the corresponding test conditions at the respective test Mach numbers are summarized in the following table:

Mach number	Total pressure		Dynamic pressure		Stagnation temperature	
	lb/ft^2	N/m^2	lb/ft^2	N/m^2	^oF	^oK
2.30	1532	73.352×10^3	453	21.690×10^3	150	338.7
2.96	2169	103.852	384	18.386	150	338.7
3.95	3863	184.960	298	14.268	175	352.6
4.63	5275	252.567	232	11.108	175	352.6

Stagnation dewpoint was maintained below -30° F (239° K) to avoid significant condensation effects in the test section. Aerodynamic forces and moments were measured by means of an electrical strain-gage balance housed partially in the models. The aft end of the balance which extended behind the base of the models was enclosed in a sleeve so that it was protected from any flow gradients. For the largest angle cones (θ_c = 70°, 80°, and 90°), which had little or no model volume in which to attach the balance, a permanent extension was affixed to the model base; this extension served as the attachment point and protective sleeve for the balance. (See fig. 1.) It is believed that this extension had no significant effect on the data presented in this paper.

Chamber and base pressures were measured on all the cone configurations, the base pressure orifice being located at a point 1.20 in. (3.05 cm) above the model center line

in the plane of symmetry. Because of the similarity exhibited between the chamber and base pressures on all the cone configurations, the base pressures measured on the 40° cone are presented along with the chamber pressures obtained on all the cones. The axial-force measurements presented in this paper, however, are gross values and were not corrected for base pressure. Angles of attack have been corrected for both tunnel-flow angularity and deflection of the balance and sting due to aerodynamic loads. Boundary layer trips were not affixed to the models.

RESULTS AND DISCUSSION

Aerodynamic Characteristics

Experimental.- The basic aerodynamic characteristics in pitch for the test models are presented in figures 3 to 6; the modified Newtonian theory shown for comparison is discussed in a subsequent section. These data indicate that all the configurations are statically stable $\left(-C_{m_{\alpha}}\right)$, the pitching moment being nearly linear through the angle-of-attack range. This stability is illustrated in the summary plots of figures 7 and 8 where pitching-moment slope at zero angle of attack is shown as a function of semiapex angle and Mach number, respectively. The stability of the 50° cone is highly dependent on Mach number, a decrease in stability occurring with increase in Mach number for Mach numbers less than that for shock attachment (about 3.2), and an increase in stability occurring with increase in Mach number for Mach numbers greater than that for shock attachment. This trend of stability with Mach number applies to the other cone configurations, where for the 40° cone the shock is attached in the test Mach number range and the stability increases with Mach number increase. Cones with semiapex angles equal to or greater than 60° have detached shocks regardless of Mach number so that their stability decreases with Mach number increase. It is interesting to note that the pitching moment of the flat disk $\left(\theta_c = 90^{\circ}\right)$ is due solely to axial force, since normal force for this configuration is equal to zero.

The variation of normal force with angle of attack for the cone configurations (figs. 3 to 6) is seen to be essentially linear. As cone angle is increased, there is a corresponding decrease in normal force so that for the flat disk, normal force goes to zero. Similar trends of normal-force slope at zero angle of attack $\left(C_{N_{\alpha,0}}\right)$ with cone semiapex angle are seen in figure 9. An increase in Mach number results in a corresponding increase in $C_{N_{\alpha,0}}$ for the 50° cone (fig. 10); cones with semiapex angles equal to or greater than 60° are virtually insensitive to Mach number.

The basic aerodynamic data of figures 3 to 6 indicate that maximum axial force (and drag) occurs at angles of attack near zero for the cone bodies. Increasing the cone semiapex angle results in increases in axial force throughout the angle-of-attack range,

a maximum being approached for the flat-disk configuration. Of the cones tested, the largest rate of increase in axial force with increase in cone semiapex angle occurs between the 40° and 50° cones. (See summary plot of fig. 11.) Increasing semiapex angle from $\theta_c = 50^{\circ}$ leads to a nearly linear increase in axial force, although at a rate not as great as that between $\theta_c = 40^{\circ}$ and 50°. The effect of Mach number on axial force for the family of cones is shown in figure 12. The 40° cone shows a significant reduction in $C_{A,0}$ with Mach number increase and the 50° cone decreases slightly, whereas axial force for the other cone semiapex angles is essentially constant in the test Mach number range. Experimental frontal surface pressure distributions on a 60° semiapex angle cone are shown in figure 13.

As seen in the basic data of figures 3 to 6, the lift-curve slope is negative for cones with semiapex angles equal to or greater than 50°. This effect, of course, is due to a larger contribution of axial force than of normal force in generating lift force. (See expression below.) An increase in cone semiapex angle results in a decrease in lift-curve slope, a maximum negative value being obtained for the flat disk. The magnitude of the lift-curve slope at zero angle of attack (see fig. 14) is obtained from the expression $C_{L_{\alpha,0}} = C_{N_{\alpha,0}} - C_{A,0}$ and is equal to the axial force (in radians) in the case of the flat disk where $C_{N_{\alpha,0}} = 0$.

Theoretical.- The basic aerodynamic characteristics in pitch predicted by the modified Newtonian theory (using $C_{p,max}$) are shown in figures 3 to 6 superimposed on the experimental data. This theory predicts the trends in aerodynamic characteristics resulting from changes in cone semiapex angle and/or angle of attack, but generally does not accurately predict absolute magnitudes.

The agreement between experimental pitching moment and that predicted by modified Newtonian theory is seen in figures 3 to 6 to be dependent on cone semiapex angle; this dependence is best illustrated by the pitching-moment slope data of figure 7. Pitching-moment slopes predicted by modified Newtonian theory and by exact theory (ref. 4) are little different in the range of cone semiapex angles where both theories are applicable. Modified Newtonian theory is seen to predict a maximum stability level for a particular cone semiapex angle; this semiapex angle is calculated in the appendix to be 58.8°. Another interesting point concerning the modified Newtonian theory is that it predicts pitching-moment slope to be zero for the flat disk. Comparison of experiment and theory indicates that the pitching-moment slope for the 40° cone is adequately predicted by theory throughout the Mach number range, and that the value of $C_{m_{\alpha,0}}$ for the 50° cone approaches theory at the highest test Mach numbers. Because of inherent assumptions in modified Newtonian theory, the value of $C_{m_{\alpha,0}}$ predicted by this theory is not susceptible to shock-detachment conditions, in contrast to the 50° cone experimental data discussed previously.

Modified Newtonian theory predicts a lower normal-force slope than does exact cone theory (ref. 5) as shown in figure 9. A continual decrease in $C_{N_{\alpha,0}}$ occurs with increases in cone semiapex angle for each test Mach number, $C_{N_{\alpha,0}}$ predicted by modified Newtonian theory approaching zero as θ_c approaches 90^o. This trend agrees with that established by the experimental data. Modified Newtonian theory generally underpredicts normal-force slope for cones with attached shocks and overpredicts normal-force slope for cones with detached shocks. Normal-force slope for the 40^o cone is generally predicted by exact theory throughout the test Mach number range, whereas the value of $C_{N_{\alpha,0}}$ for the 50^o cone is predicted by exact theory at the highest test Mach number. Use of the coefficient of 2.0 instead of $C_{p,max}$ in the Newtonian theory would provide better agreement between theory and experiment for cones with attached shocks and greater disagreement for cones with detached shocks.

Theoretical methods available for predicting axial force of conical bodies at zero angle of attack represent only the pressure drag due to the frontal surface of the cone. To compare these theories with the axial-force data presented in figures 3 to 6, it is necessary to adjust these theories to account for base drag. Accordingly, the theoretical methods shown in the summary plots of figures 11 and 12 were adjusted by the values of base drag measured during the tests with the exception of the 40^o and 50^o cones whose base pressures were influenced by sting effects (see subsequent discussion); the theoretical methods for these cone configurations (and those with smaller semiapex angles) were adjusted by base pressures measured on the 60^o cone. It will be shown in a subsequent discussion that these measured values are closely approximated by the empirical expression, $C_{p,b} = -\frac{1}{M^2}$.

Modified Newtonian theory predicts lower values of axial force than does exact theory (ref. 6) in the range of cone semiapex angles where both theories are applicable (fig. 11). The experimental data show that modified Newtonian theory predicts the trends of $C_{A,0}$ with cone semiapex angle, but is inherently poor in estimating absolute magnitudes. A combination of exact cone theory with an integral relations method (ref. 7) adequately predicts the magnitudes of axial force for all cone semiapex angles. The exact cone theory is utilized when supersonic flow conditions exist on the cone surface, and the integral relations method when mixed flow conditions exist. The point where the integral relations method fairs into exact theory at $M = 2.30$ is seen to be at that cone semiapex angle which supports sonic flow on its surface, θ_c^*; this condition is not true at the higher test Mach numbers. A detailed discussion of these characteristics of the integral relations method can be found in reference 7.

The trends of axial force with Mach number discussed previously are seen in figure 12 to be generally predicted by the combination of exact theory and the integral relations method. Modified Newtonian theory is not presented in this figure because of poor agreement.

The experimental data presented in figure 13 were obtained in the Langley Unitary Plan wind tunnel by Robert L. Stallings, Jr., of the Langley Research Center and are compared with the pressure distributions predicted by the integral relations and modified Newtonian theories. These data demonstrate the excellent agreement between the integral relations method and experiment at the three test Mach numbers; as expected, the modified Newtonian theory is limited in its agreement.

Variation of the lift-curve slope with cone semiapex angle predicted by the modified Newtonian and exact theories is shown in figure 14. Small differences are seen between the two theories in the range of cone semiapex angles where both theories are applicable. Comparison with experimental data shows that the modified Newtonian theory predicts the trends of $C_{L_{\alpha,0}}$ with θ_c. It should be noted that zero lift-curve slope is predicted by modified Newtonian theory for a cone with a semiapex angle somewhat less than 45^o. This condition results from inclusion of base drag in the theory. If base drag was not considered, a value of $C_{L_{\alpha,0}} = 0$ would be predicted for $\theta_c = 45^o$.

Base Drag

The magnitudes of the base pressure coefficients for the various test configurations are presented in figure 15. Also included in this figure are the effects of indenting the base of the 40^o cone and the effects of various radial positions for the base pressure $\left(\frac{r}{r_b} = 0 \text{ corresponds to the model chamber}\right)$. Indenting the base region of the 40^o cone is seen to have little or no effect on base pressure throughout the angle-of-attack range. Comparison of the base pressures at the two radial locations for $\theta_c = 40^o$ indicates only a slight radial gradient of base pressure in the test angle-of-attack range. This result is similar to the results obtained on a 60^o cone. In light of these results, it appears that chamber pressures are representative of the pressures existing over the base region.

It is seen that base pressure remains essentially constant throughout the angle-of-attack range at each test Mach number for cones with semiapex angles equal to or greater than 60^o. The 40^o and 50^o cones produce some variation of base pressure with angle of attack at $M = 2.30$, but little or no variation at $M = 4.63$. It should be pointed out, however, that the 40^o and 50^o cones were tested by using a sting length of 2.0 times the cone base diameter, whereas the other cone models were tested by using a ratio of sting length to model base diameter of 4.0. To determine the significance of this difference in sting length, the 70^o and 80^o cone configurations were tested with a shortened sting (see fig. 2)

having a ratio of sting length to model base diameter of 2.0. The effect of sting length on the longitudinal aerodynamic characteristics of these two cone models is shown in figures 16 and 17 for Mach numbers of 2.30 and 2.96. The data indicate that the shorter sting ($l/D = 2.0$) causes a reduction in total axial force near zero angle of attack at $M = 2.30$; at $M = 2.96$ there is little difference in axial force due to the different sting lengths. Visual evidence of the effect of sting length can be seen in the schlieren photographs of figure 18, where the presence of the sting support in the vicinity of the wake recompression shock results in an altered wake structure at $M = 2.30$.

The effects of sting length on the base pressure coefficient for the models at zero angle of attack are shown as a function of Mach number in figure 19. The data indicate little or no sting effect at Mach numbers from 2.96 to 4.63. At $M = 2.30$, the upstream communication effects caused by the shorter stings result in increases in base pressure (and thus decreases in total axial force as seen in figures 16 and 17). Shown for comparison in this figure are the values of base pressure coefficient predicted by the empirical expression, $C_{p,b} = -\frac{1}{M^2}$ (ref. 8). The data obtained by using the sting with $l/D = 4.0$ show excellent agreement with the empirical values throughout the test Mach number range.

Shock Shape and Standoff Distance

Schlieren photographs for the test models at zero angle of attack are shown in figure 20. Measurements of the detached shock waves are obtained from these photographs and are presented in figure 21 compared with the shock shapes predicted by an integral relations method (ref. 7). The predicted detached shock shape is in good agreement with experiment at all test Mach numbers for the 60° cone configuration. Increase in cone semiapex angle leads to some degradation in agreement, particularly for the flat disk $(\theta_c = 90^\circ)$. The standoff distance of the shock from the nose of the cones is shown in figure 22 as a function of cone semiapex angle. Shock standoff increases almost linearly with semiapex angle; this increase is adequately predicted by the integral relations method. Shown for comparison is an algebraic solution for shock standoff at $M = \infty$. (See ref. 9.)

The linear nature of shock standoff distance with cone semiapex angle is also reflected in figure 23 where the variation of shock standoff distance with Mach number is presented for the family of cone bodies. For all the cones shock standoff distance decreases with Mach number increase, the largest variation occurring at the lowest test Mach number. Data obtained from other studies (refs. 10 to 13) are presented and show reasonable agreement with the results of the present investigation. The integral relations method adequately predicts the trends of shock standoff distance with Mach number for all the cones. It is noted that the results of the theory developed by Serbin (ref. 13)

for the flat disk are virtually identical to the results of the integral relations method in the test Mach number range.

The uniformity of the data yields the possibility of extrapolating the results to $M = \infty$. This condition is illustrated in figure 24 where shock standoff distance is shown to vary linearly with $1/M^2$. Both experimental and theoretical data appear to lend themselves to this extrapolation, the extrapolated integral relations method showing good agreement with other theories at $M = \infty$.

CONCLUSIONS

A study has been conducted to determine the supersonic aerodynamics of a series of conical bodies with semiapex angles from 40° to 90° (disk); results of this study lead to the following conclusions:

1. All the configurations are statically stable, the center of gravity being located at the model base.

2. As the cone semiapex angle is increased, axial force increases, the rate of increase being largest between the 40° and 50° cone configurations. Experimental values of axial force at zero angle of attack are adequately predicted for all cone semiapex angles by utilizing a combination of exact theory and an integral relations method.

3. As the cone semiapex angle is increased, normal force decreases, normal force being zero for the flat disk.

4. Shock standoff distance varies almost linearly with cone semiapex angle and the inverse of Mach number squared; these trends are adequately predicted by an integral relations method.

Langley Research Center,
National Aeronautics and Space Administration,
Langley Station, Hampton, Va., May 17, 1968,
124-07-03-12-23.

APPENDIX

PITCHING-MOMENT SLOPE PREDICTED BY MODIFIED NEWTONIAN THEORY

The aerodynamic forces and moments were calculated for the conical bodies by use of a form of the Newtonian theory presented in reference 3. Multiplying the aerodynamic coefficients obtained from this reference by $\frac{C_{p,max}}{2}$ yields the modified Newtonian theory used in the present investigation. The stagnation pressure behind a normal shock $(C_{p,max})$ was evaluated by using the expression given in reference 3. Aerodynamic coefficients were calculated for angles of attack from -4° to 25° at the four test Mach numbers. These coefficients were referenced to base area and diameter to be compatible with the experimental data. To afford a more realistic comparison between modified Newtonian theory and the basic experimental data (figs. 3 to 6), the modified Newtonian axial-force results were adjusted to account for base pressure by means of base pressures measured during the tests.

By use of the base diameter as the reference length for the modified Newtonian pitching-moment coefficients (ref. 3), the pitching-moment slope at zero angle of attack can be shown to be

$$C_{m_{\alpha,0}} = \frac{1}{6}\cot\theta_c\left(1 - 2\tan^2\theta_c\right)C_{N_{\alpha,0}} \tag{1}$$

where

$$C_{N_{\alpha,0}} = C_{p,max}\cos^2\theta_c$$

The combination of trigonometric functions in this expression dictates that $C_{m_{\alpha,0}}$ will approach the following limits with θ_c:

$$C_{m_{\alpha,0}} \to +\infty \qquad (\theta_c \to 0^{\circ})$$

$$C_{m_{\alpha,0}} \to 0 \qquad (\theta_c \to 90^{\circ})$$

It is interesting to note that expression (1) has a minimum point (see fig. 7); thus Newtonian theory predicts a cone of a particular semiapex angle to have the largest stability level. This semiapex angle is calculated as follows:

APPENDIX

The pitching-moment slope at zero angle of attack predicted by modified Newtonian theory is expressed from equation (1) as

$$C_{m_{\alpha,0}} = \frac{1}{6} \cot \theta_c \left(1 - 2 \tan^2 \theta_c\right) C_{p,max} \cos^2 \theta_c$$

or

$$C_{m_{\alpha,0}} = \frac{C_{p,max}}{6} \cot \theta_c \left(\cos^2 \theta_c - 2 \sin^2 \theta_c\right)$$

where

$$\sin^2 \theta_c = 1 - \cos^2 \theta_c$$

Thus,

$$C_{m_{\alpha,0}} = \frac{C_{p,max}}{6} \cot \theta_c \left(3 \cos^2 \theta_c - 2\right) \tag{2}$$

To find the value of θ_c where $C_{m_{\alpha,0}}$ reaches a minimum, the derivative of expression (2) is taken and set equal to zero.

$$\frac{dC_{m_{\alpha,0}}}{d\theta_c} = \frac{d}{d\theta_c}\left[\frac{C_{p,max}}{6} \cot \theta_c \left(3 \cos^2 \theta_c - 2\right)\right] = 0$$

After differentiating, this equation becomes

$$\left(3 \cos^2 \theta_c - 2\right)\left(-\csc^2 \theta_c\right) + \cot \theta_c \left(-6 \cos \theta_c \sin \theta_c\right) = 0$$

Substituting for $\csc \theta_c$ and $\cot \theta_c$ in terms of $\sin \theta_c$ and $\cos \theta_c$ yields

$$-3 \cos^2 \theta_c \left(1 + 2 \sin^2 \theta_c\right) + 2 = 0$$

or, since $\sin^2 \theta_c = 1 - \cos^2 \theta_c$,

$$6 \cos^4 \theta_c - 9 \cos^2 \theta_c + 2 = 0 \tag{3}$$

Solving equation (3) yields $\cos \theta_c = \pm 1.11$ and ± 0.5185. Since it is impossible for the cosine of an angle to be greater than one, the desired solution of expression (3) is

$$\theta_c = \cos^{-1} 0.5185$$

$$\theta_c = 58.8^\circ$$

This semiapex angle is independent of Mach number.

REFERENCES

1. Campbell, James F.: Longitudinal Aerodynamic Characteristics of Several High-Drag Bodies at Mach Numbers From 1.50 to 4.63. NASA TN D-3915, 1967.

2. Nichols, James O.; and Nierengarten, Edward A.: Aerodynamic Characteristics of Blunt Bodies. Tech. Rep. No. 32-677 (Contract NAS7-100), Jet Propulsion Lab., California Inst. Technol., Nov. 19, 1964.

3. Wells, William R.; and Armstrong, William O.: Tables of Aerodynamic Coefficients Obtained From Developed Newtonian Expressions for Complete and Partial Conic and Spheric Bodies at Combined Angles of Attack and Sideslip With Some Comparisons With Hypersonic Experimental Data. NASA TR R-127, 1962.

4. Sims, Joseph L.: Tables for Supersonic Flow Around Right Circular Cones at Small Angles of Attack. NASA SP-3007, 1964.

5. Ames Research Staff: Equations, Tables, and Charts for Compressible Flow. NACA Rep. 1135, 1953. (Supersedes NACA TN 1428.)

6. Staff of Comput. Section, Center of Anal. (under dir. of Zdeněk Kopal): Tables of Supersonic Flow Around Cones. Tech. Rep. No. 1 (NOrd Contract No. 9169), Massachusetts Inst. Technol., 1947.

7. South, Jerry C., Jr.: Calculation of Axisymmetric Supersonic Flow Past Blunt Bodies With Sonic Corners, Including a Program Description and Listing. NASA TN D-4563, 1968.

8. Saltzman, Edwin J.: Base Pressure Coefficients Obtained From the X-15 Airplane for Mach Numbers Up to 6. NASA TN D-2420, 1964.

9. Aleksenko, I. I.; Barantsev, R. G.; and Panteleyeva, I. N.: The Method of Transverse Approximation in a Hypersonic Flow. FTD-TT-65-1806, U.S. Air Force, Jan. 6, 1966. (Available from DDC as AD 626968.)

10. Johnston, G. W.: An Investigation of the Flow About Cones and Wedges at and Beyond the Critical Angle. Rep. No. 24, Inst. Aerophys., Univ. of Toronto, Dec. 1952.

11. Boison, J. Christopher; and Curtiss, Howard A.: An Experimental Investigation of Blunt Body Stagnation Point Velocity Gradient. ARS J., vol. 29, no. 2, Feb. 1959, pp. 130-135.

12. Serbin, H.: Hypersonic, Non-Viscous Flow Around a Circular Disk Normal to the Stream. U.S. Air Force Project RAND Res. Memo. RM-1713, the RAND Corp., May 3, 1956.

13. Serbin, Hyman: Supersonic Flow Around Blunt Bodies. J. Aeronaut. Sci. (Readers' Forum), vol. 25, no. 1, Jan. 1958, pp. 58-59.

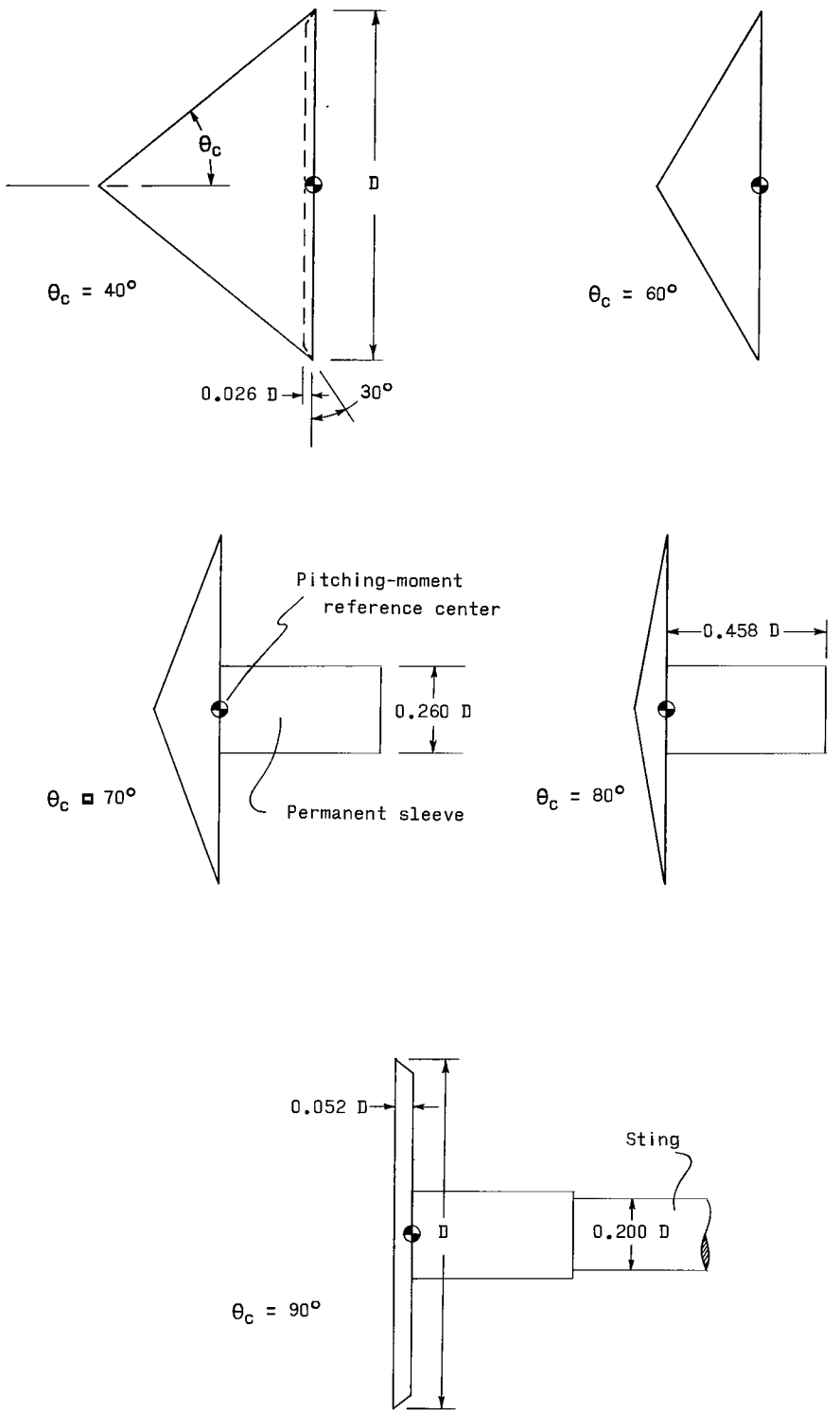

Figure 1.- Model details. Dimensions are presented as fractions of the base diameter D. All configurations have same diameter, D = 4.80 in. (12.19 cm).

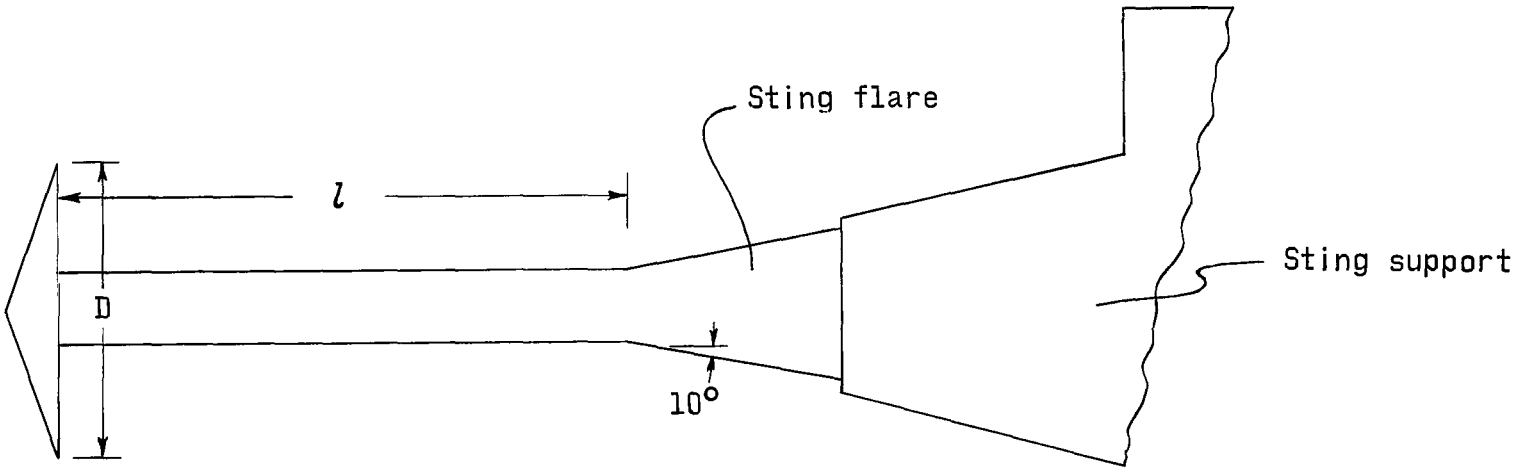

Sting length used to obtain basic data in figures 3 to 6

θ_c, deg	l/D
40	2.0
50	2.0
60	4.0
70	4.0
80	4.0
90	4.0

Figure 2.- Illustration of sting length.

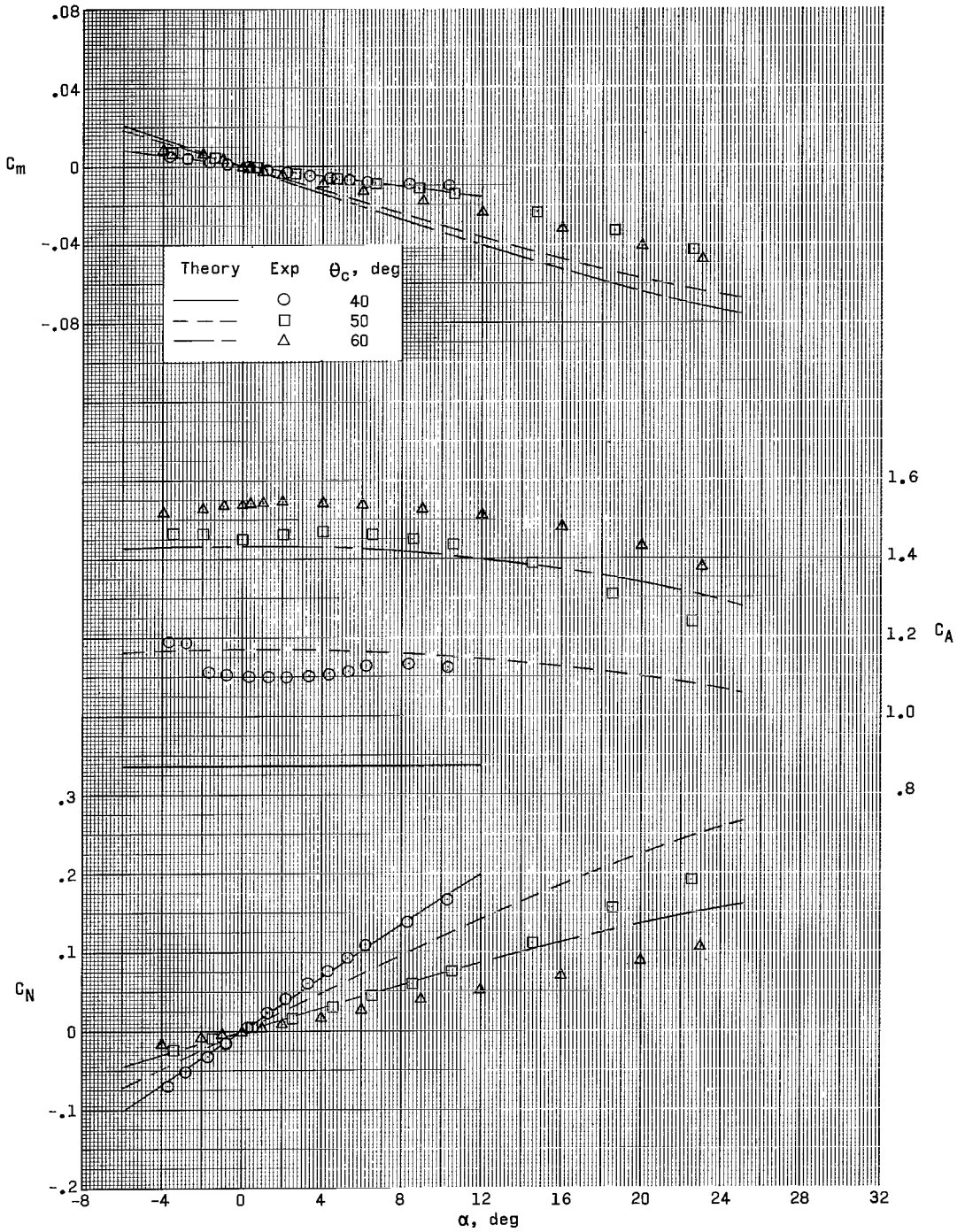

(a) Body axis.

Figure 3.- Comparison of experimental aerodynamic characteristics with those predicted by modified Newtonian theory for family of cone models. M = 2.30.

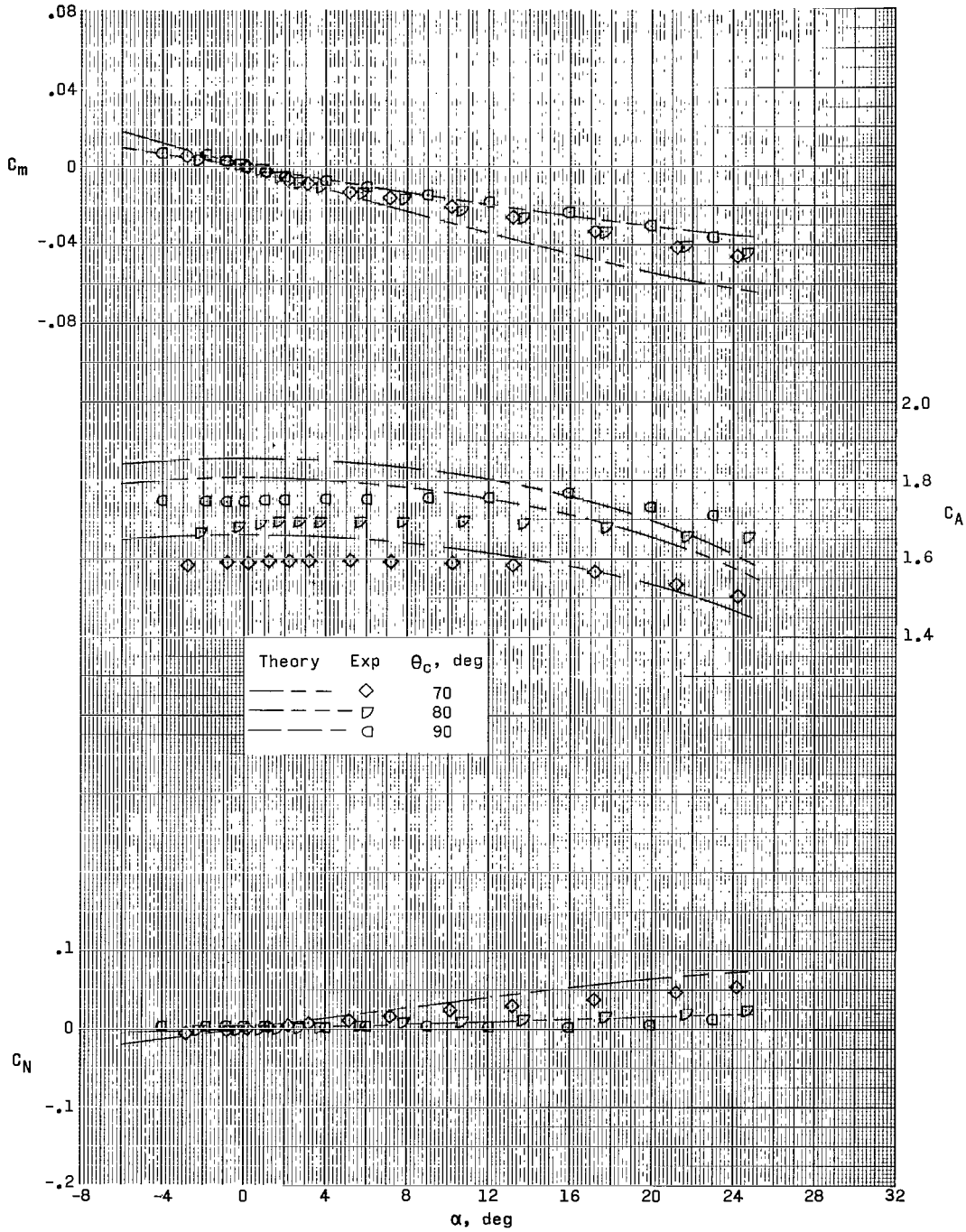

(a) Concluded.

Figure 3.- Continued.

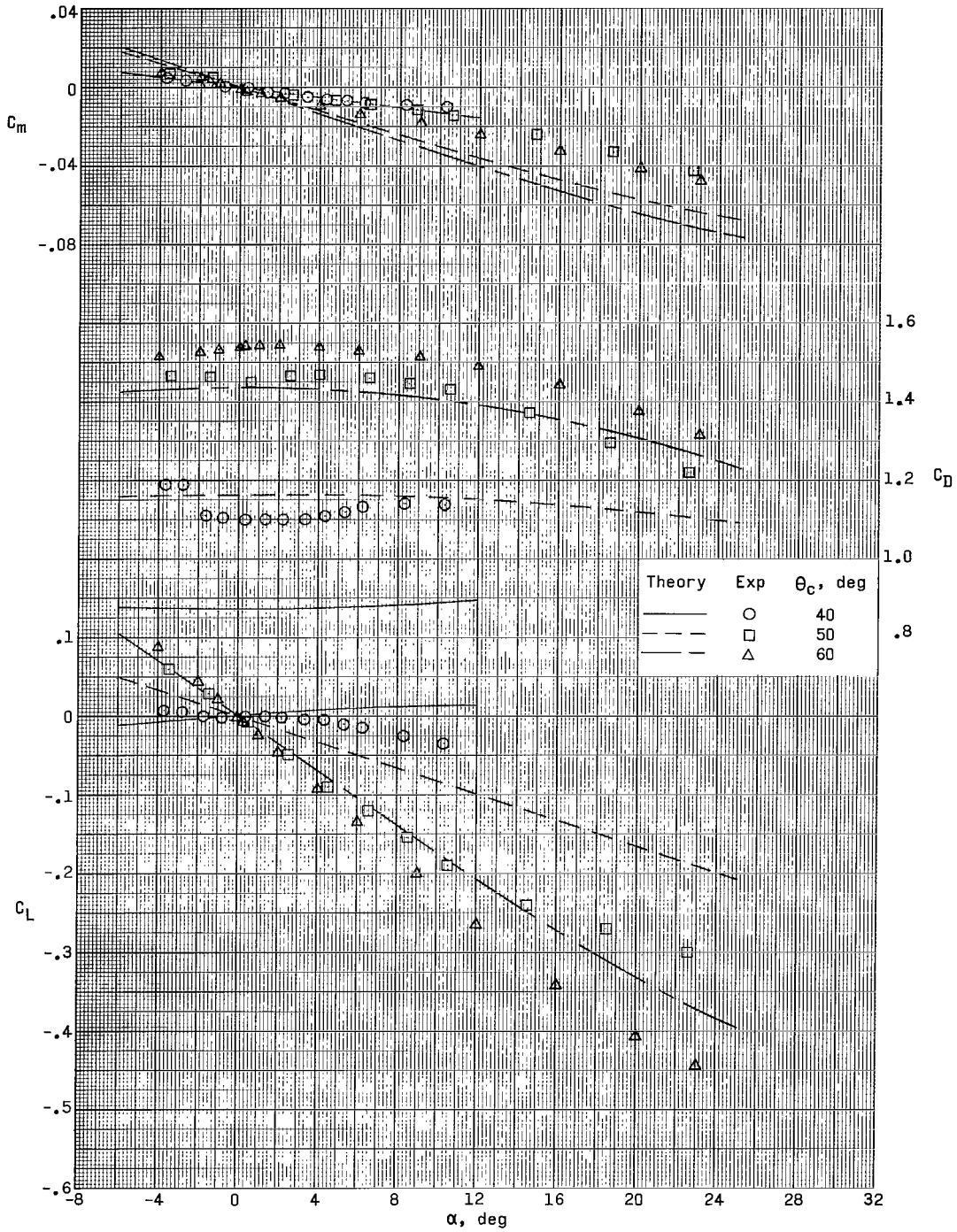

(b) Stability axis.

Figure 3.- Continued.

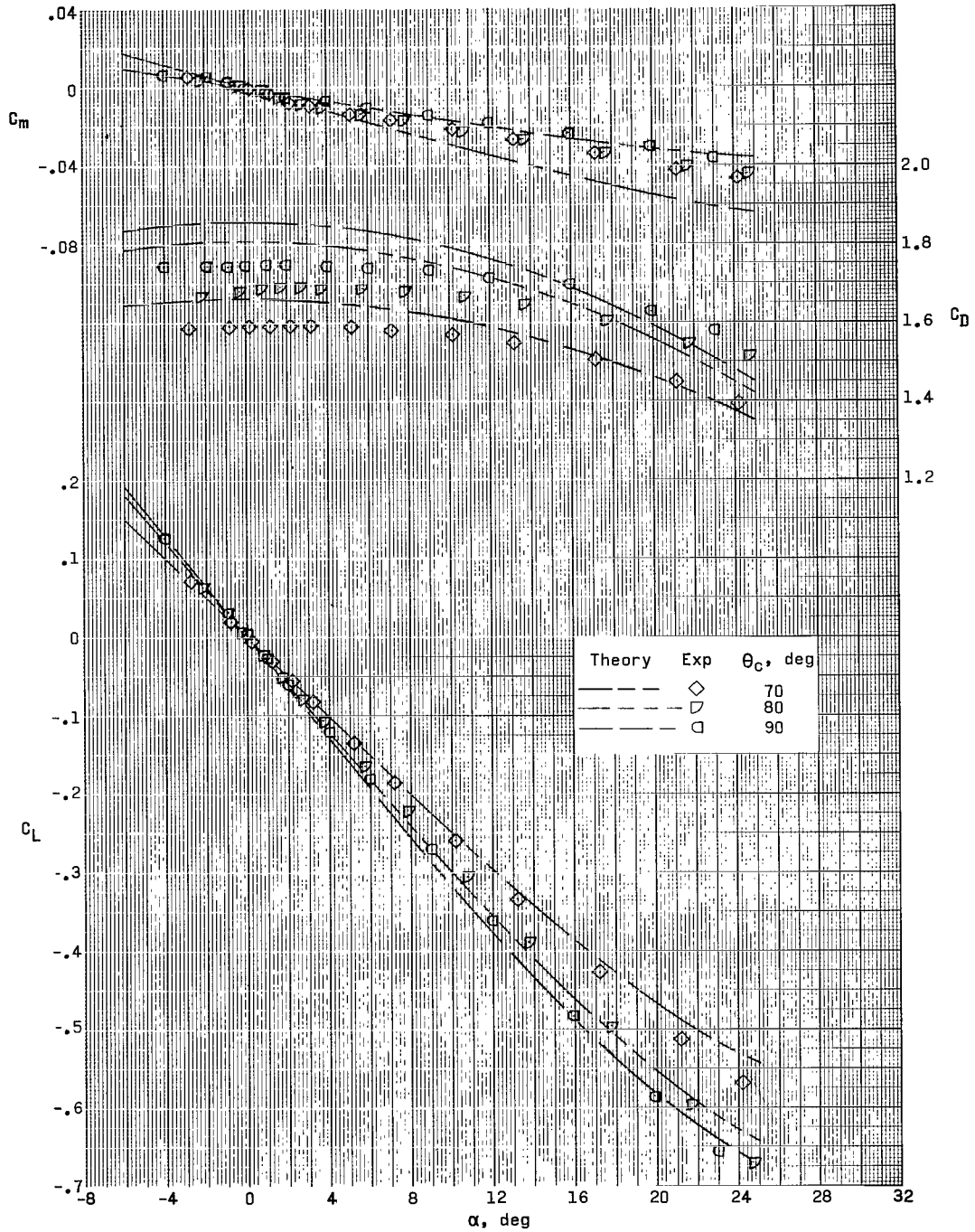

(b) Concluded.

Figure 3.- Concluded.

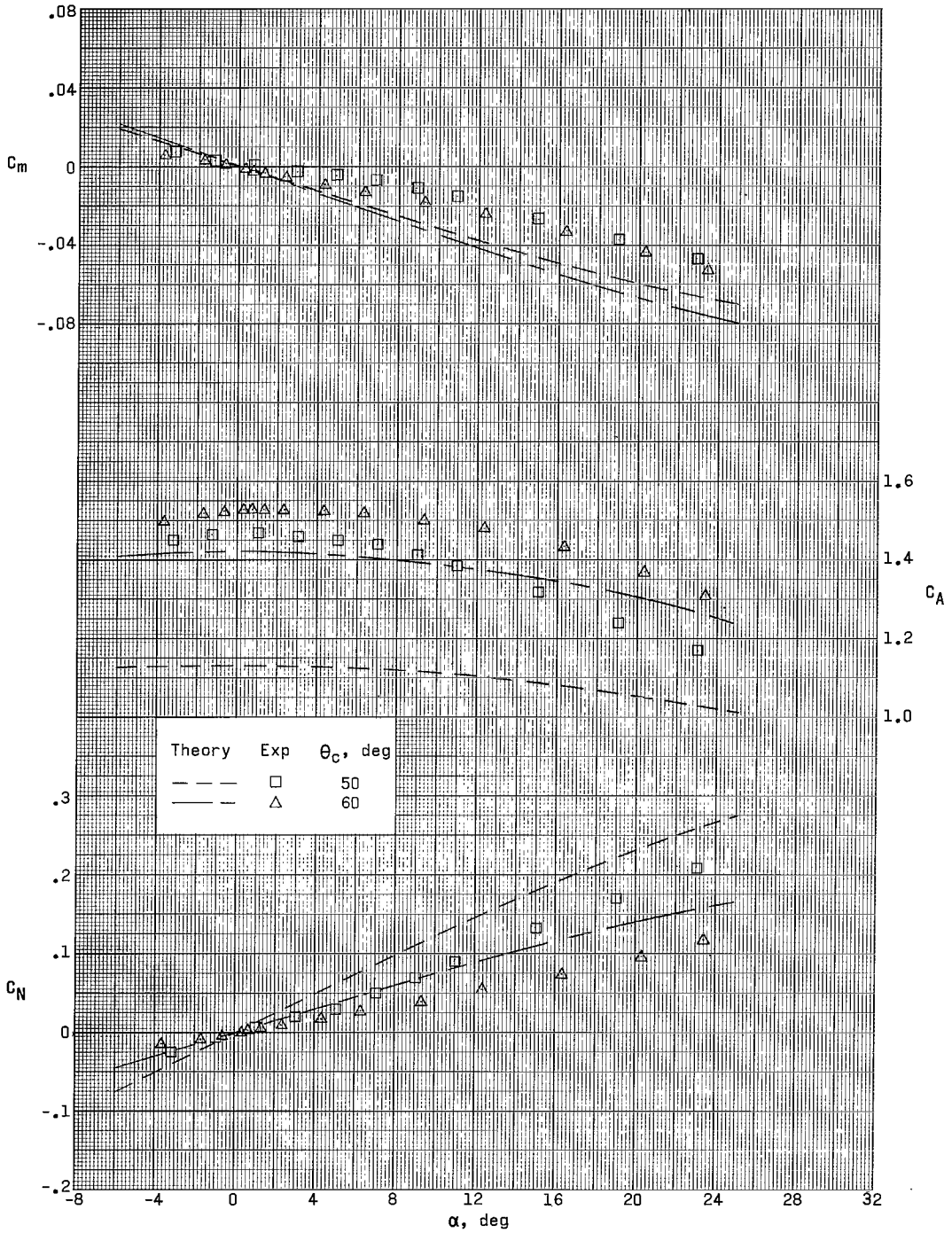

(a) Body axis.

Figure 4.- Comparison of experimental aerodynamic characteristics with those predicted by modified Newtonian theory for family of cone models. M = 2.96.

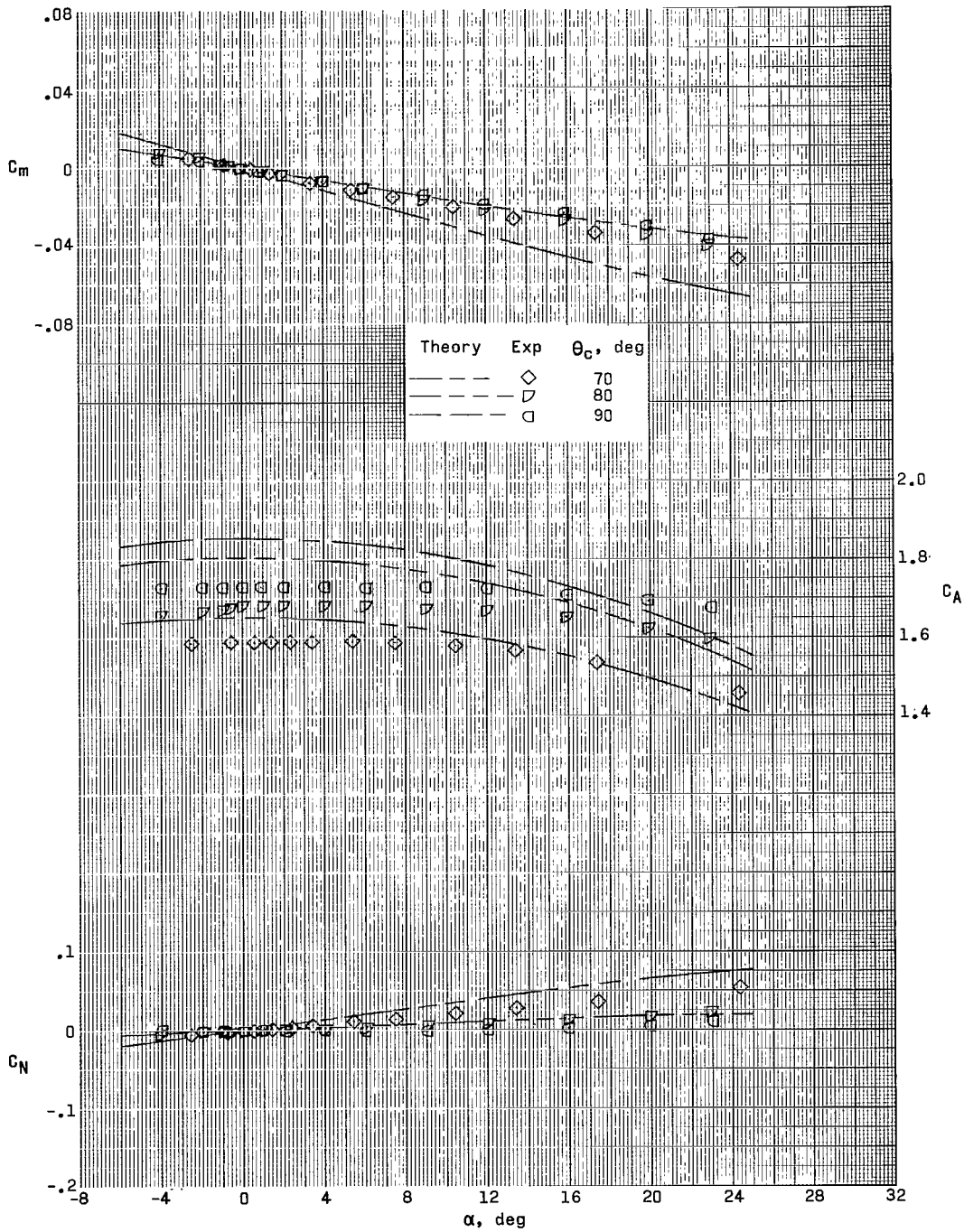

(a) Concluded.

Figure 4.- Continued.

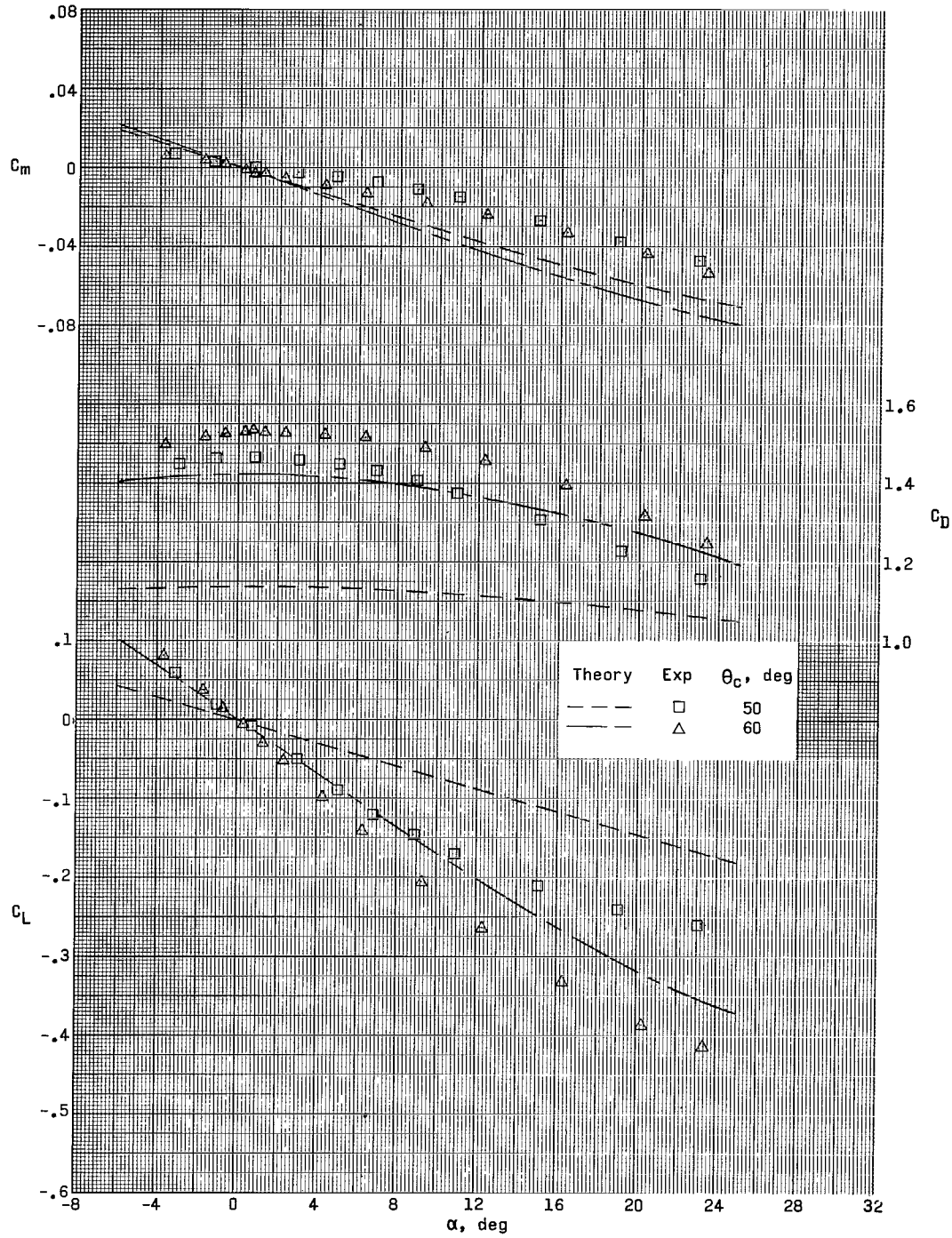

(b) Stability axis.

Figure 4.- Continued.

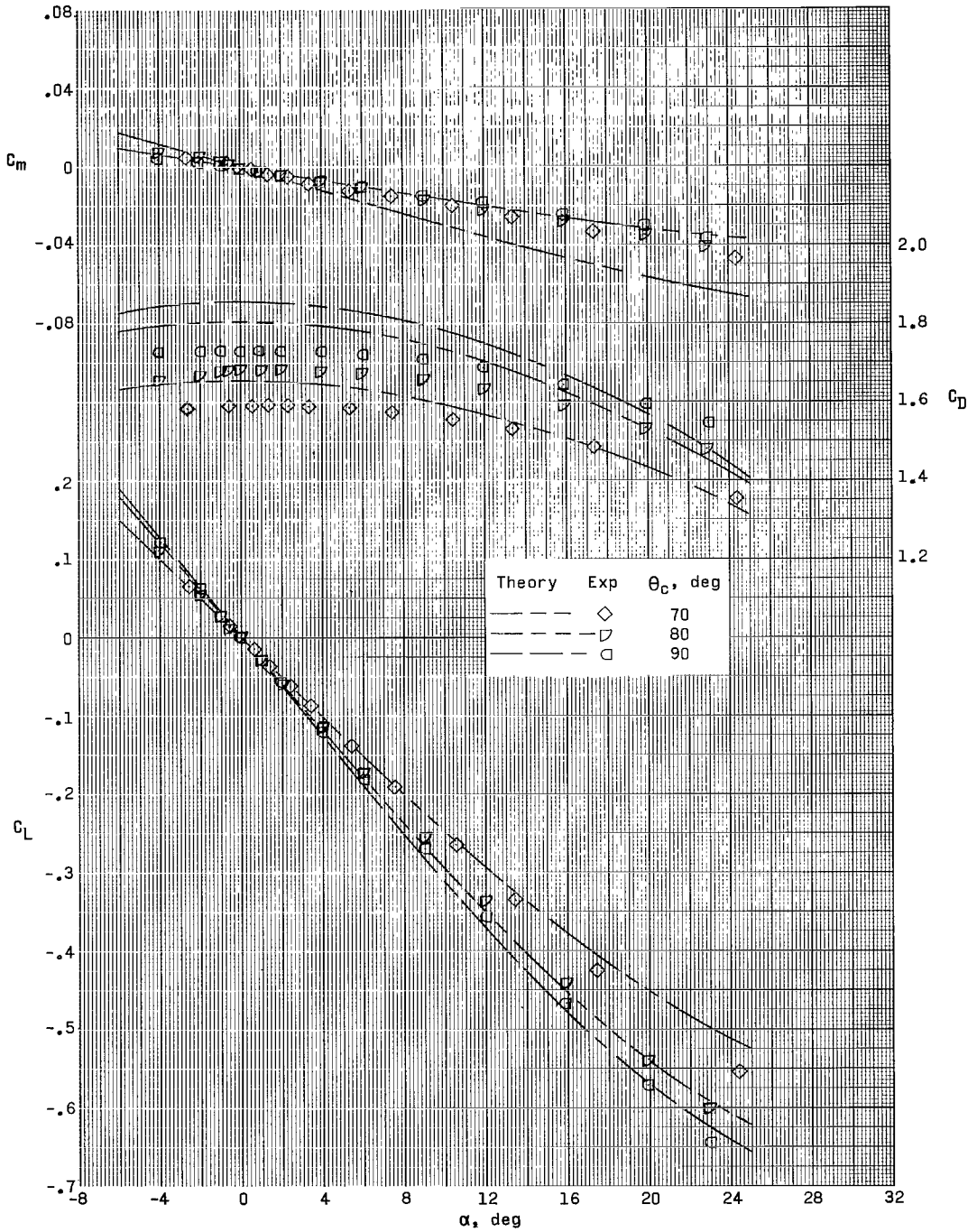

(b) Concluded.

Figure 4.- Concluded.

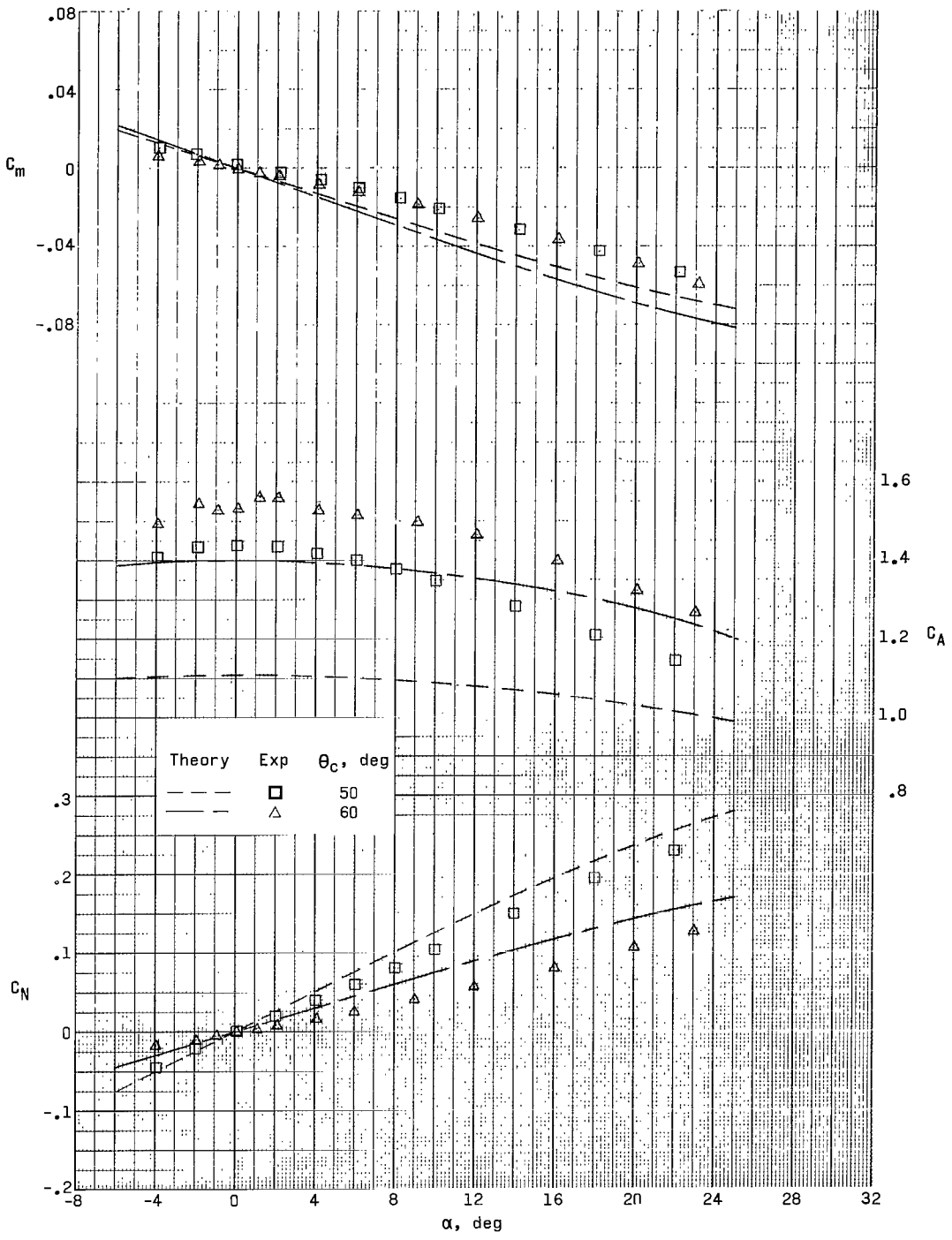

(a) Body axis.

Figure 5.- Comparison of experimental aerodynamic characteristics with those predicted by modified Newtonian theory for family of cone models. M = 3.95.

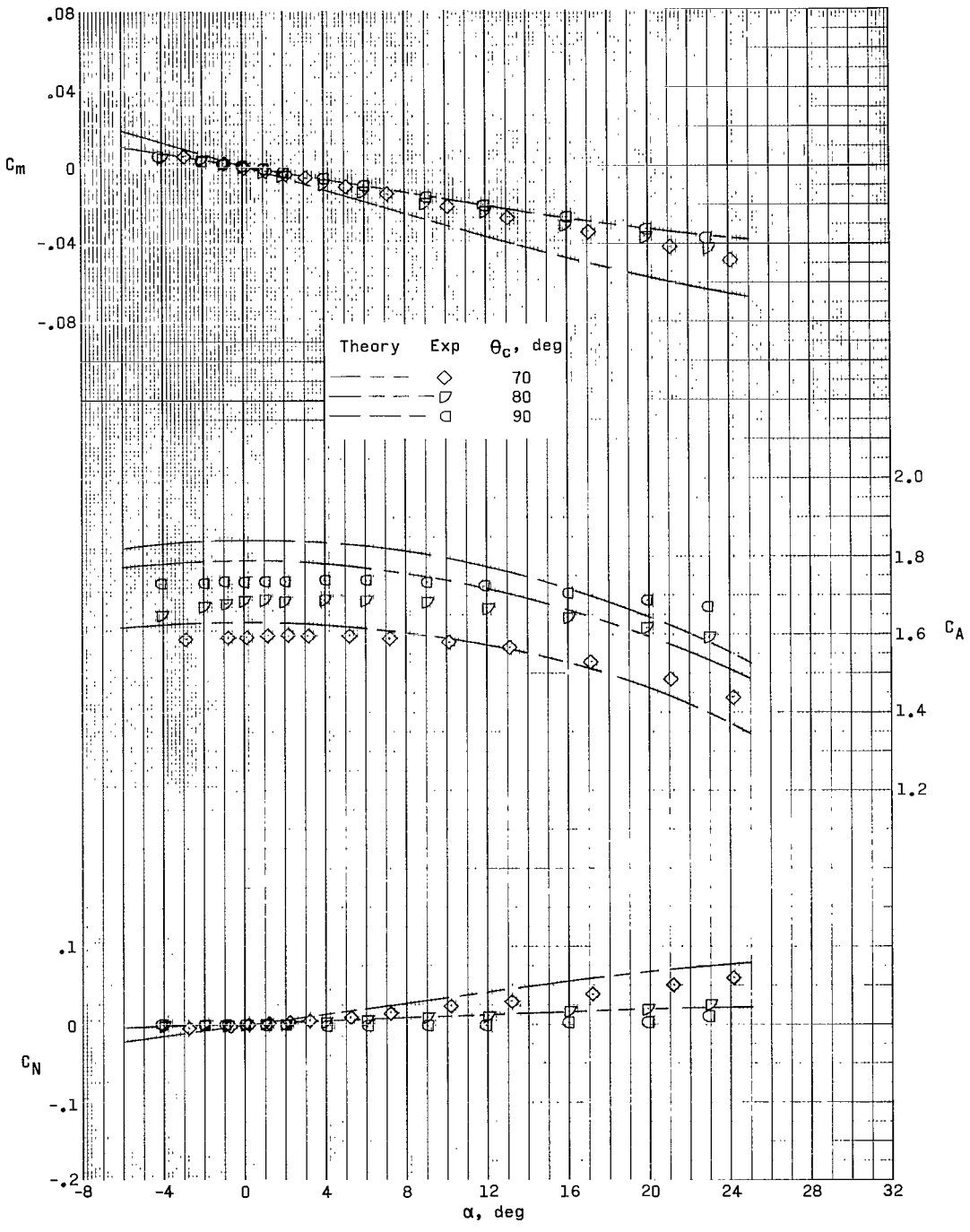

(a) Concluded.

Figure 5.- Continued.

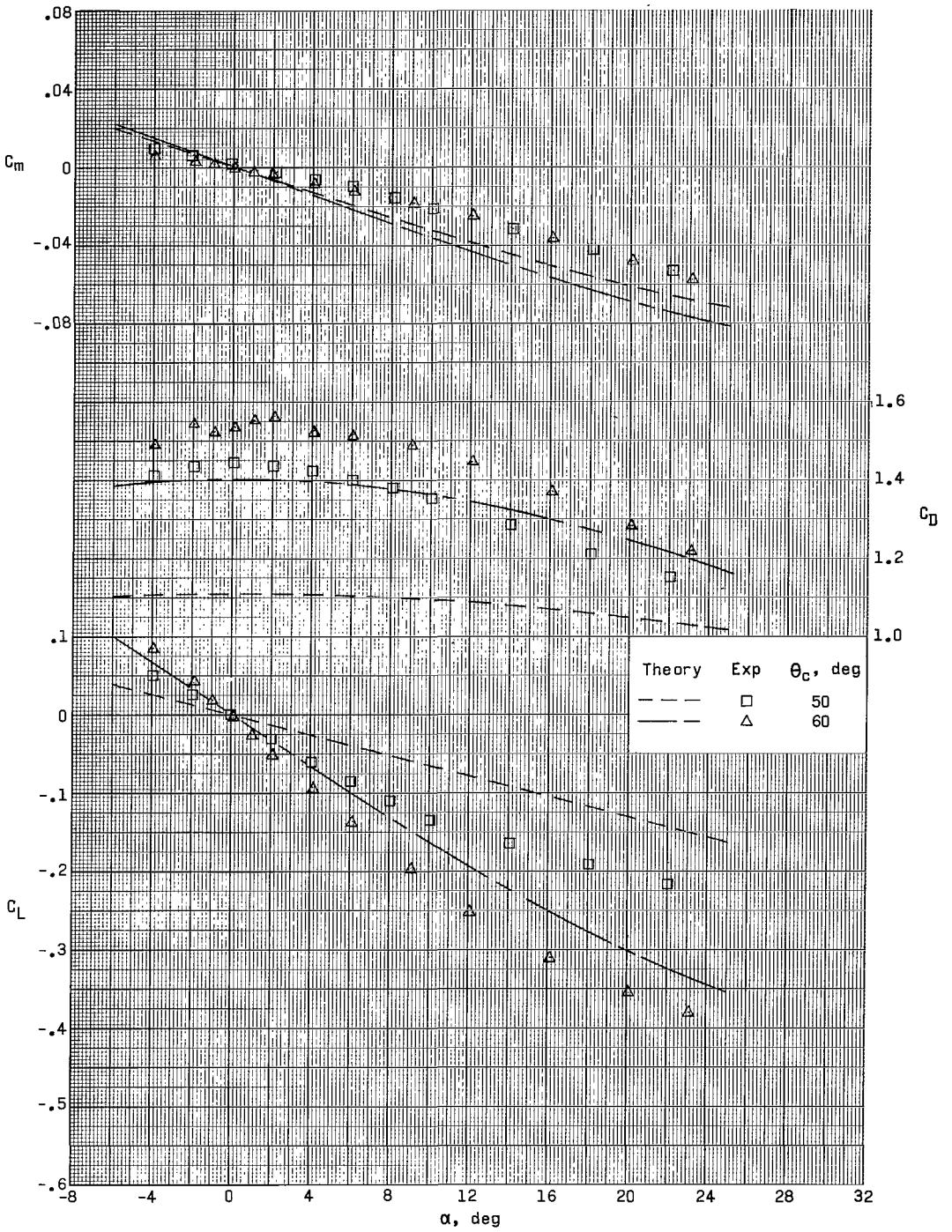

(b) Stability axis.

Figure 5.- Continued.

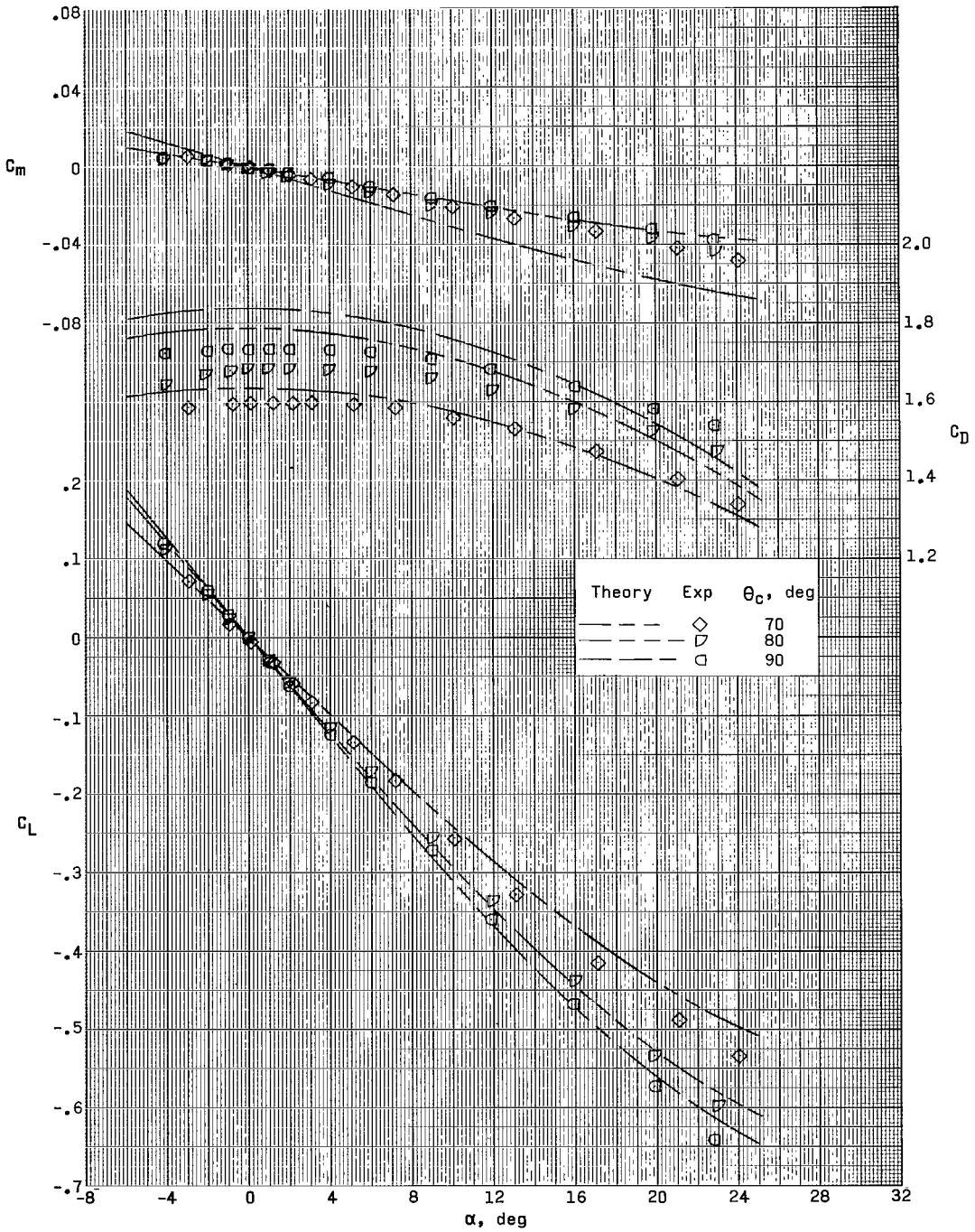

(b) Concluded.

Figure 5.- Concluded.

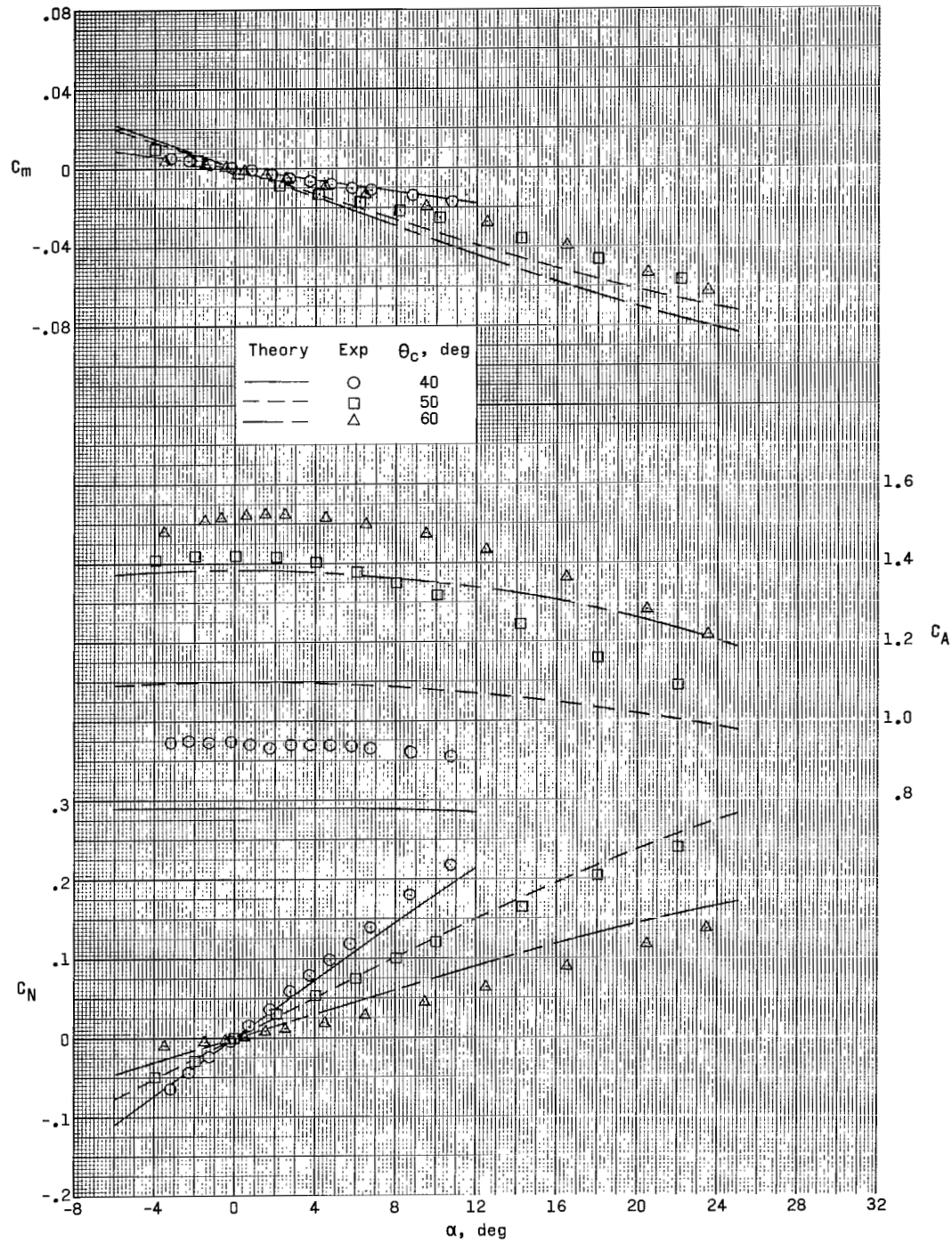

(a) Body axis.

Figure 6.- Comparison of experimental aerodynamic characteristics with those prediced by modified Newtonian theory for family of cone models. M = 4.63.

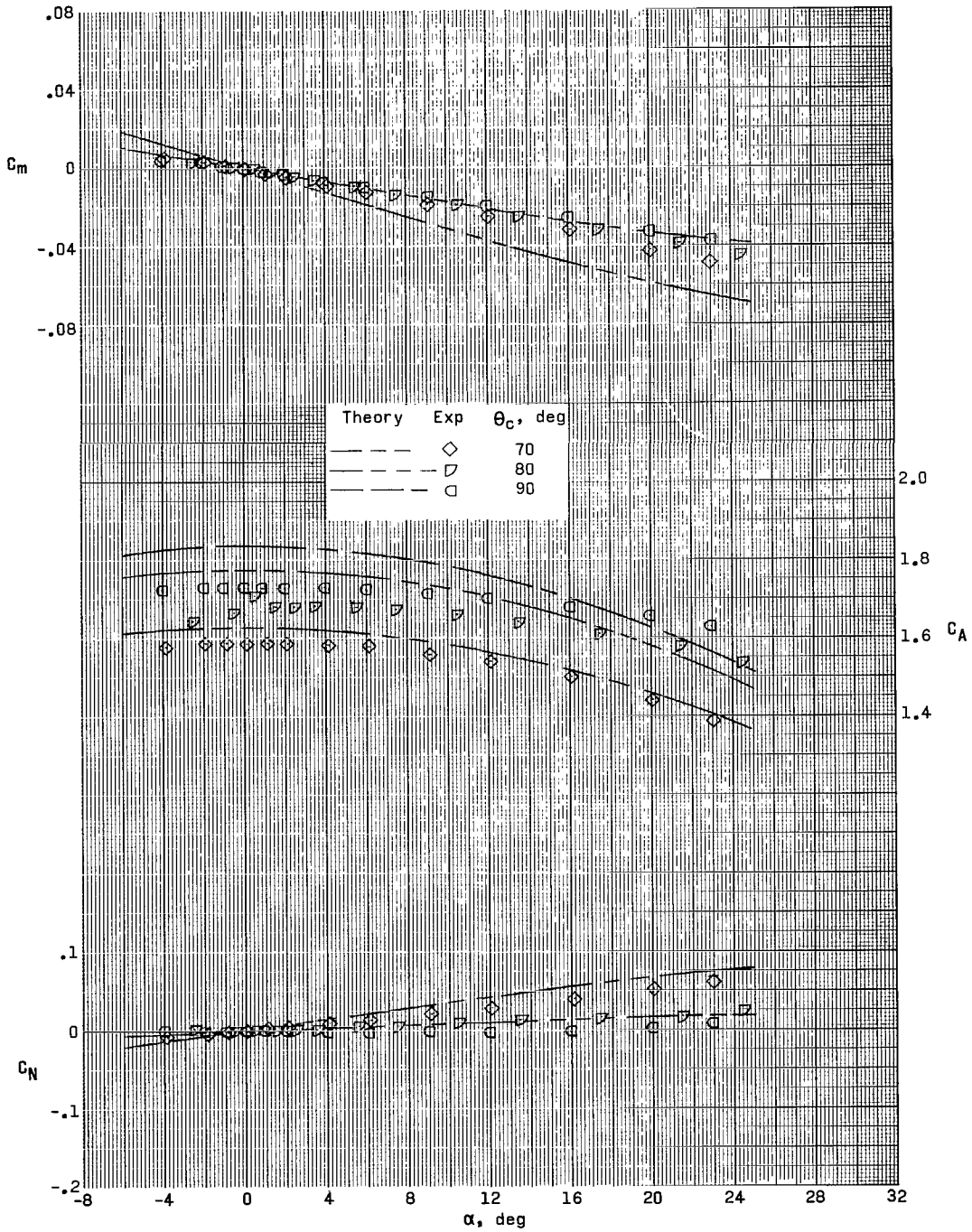

(a) Concluded.

Figure 6.- Continued.

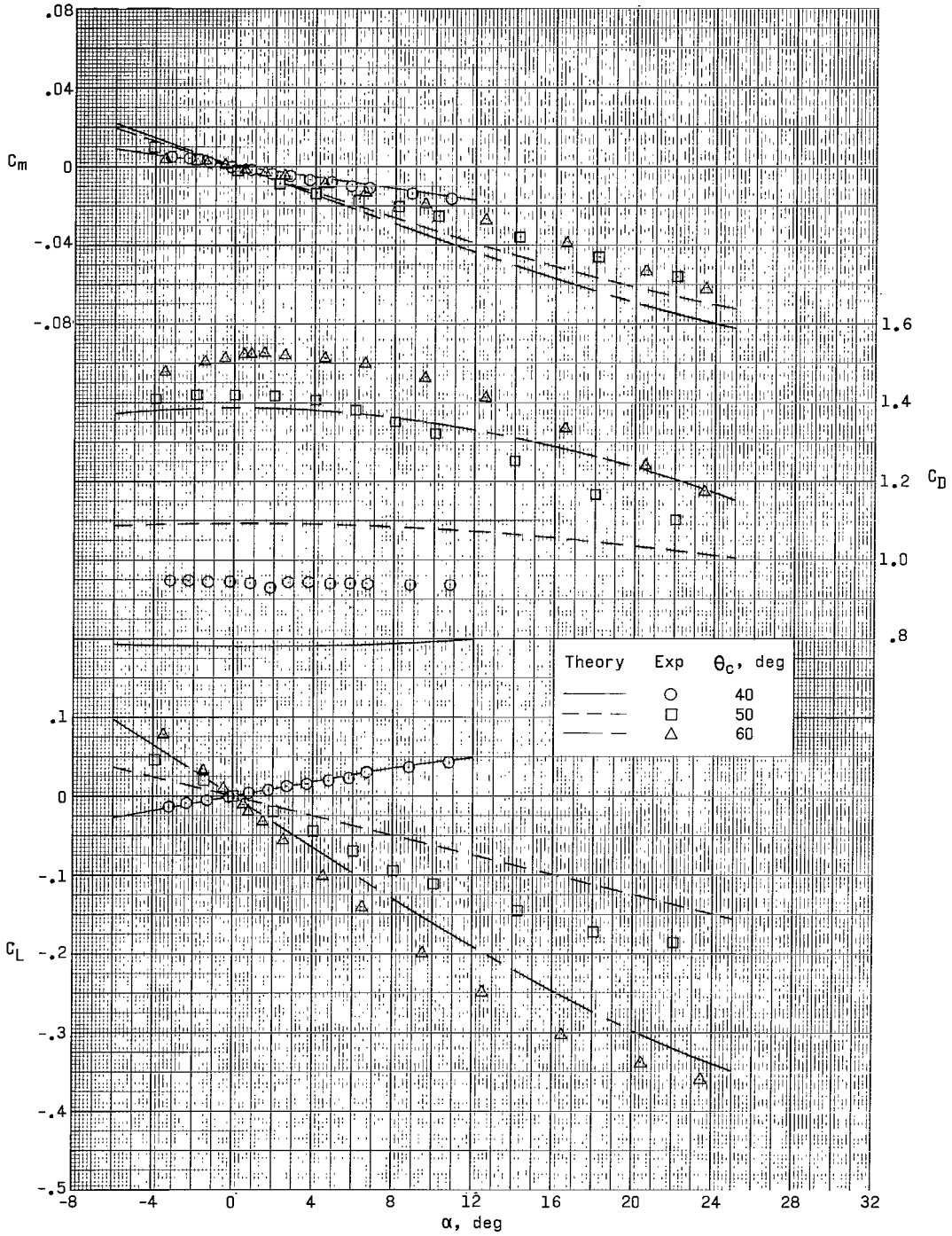

(b) Stability axis.

Figure 6.- Continued.

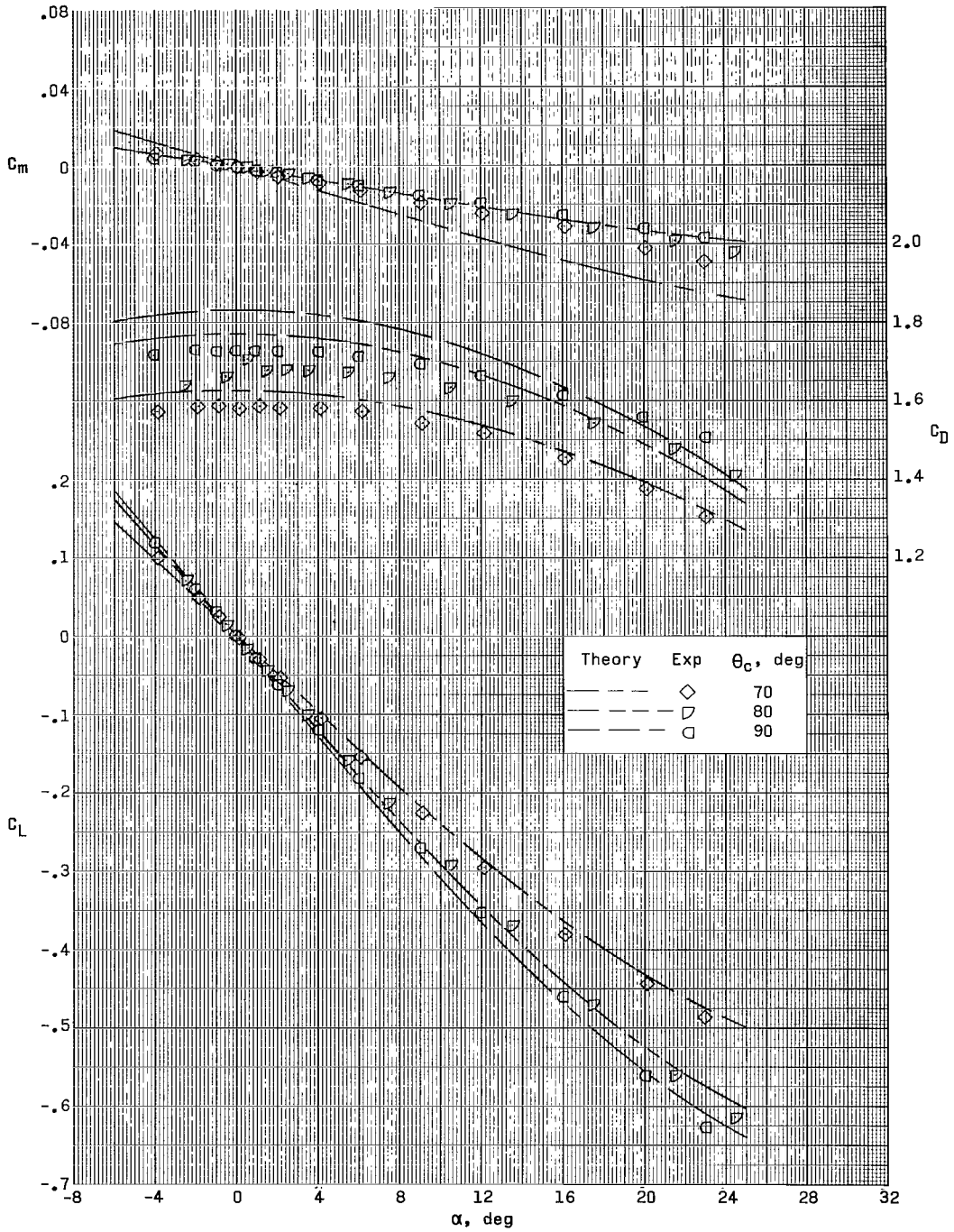

(b) Concluded.

Figure 6.- Concluded.

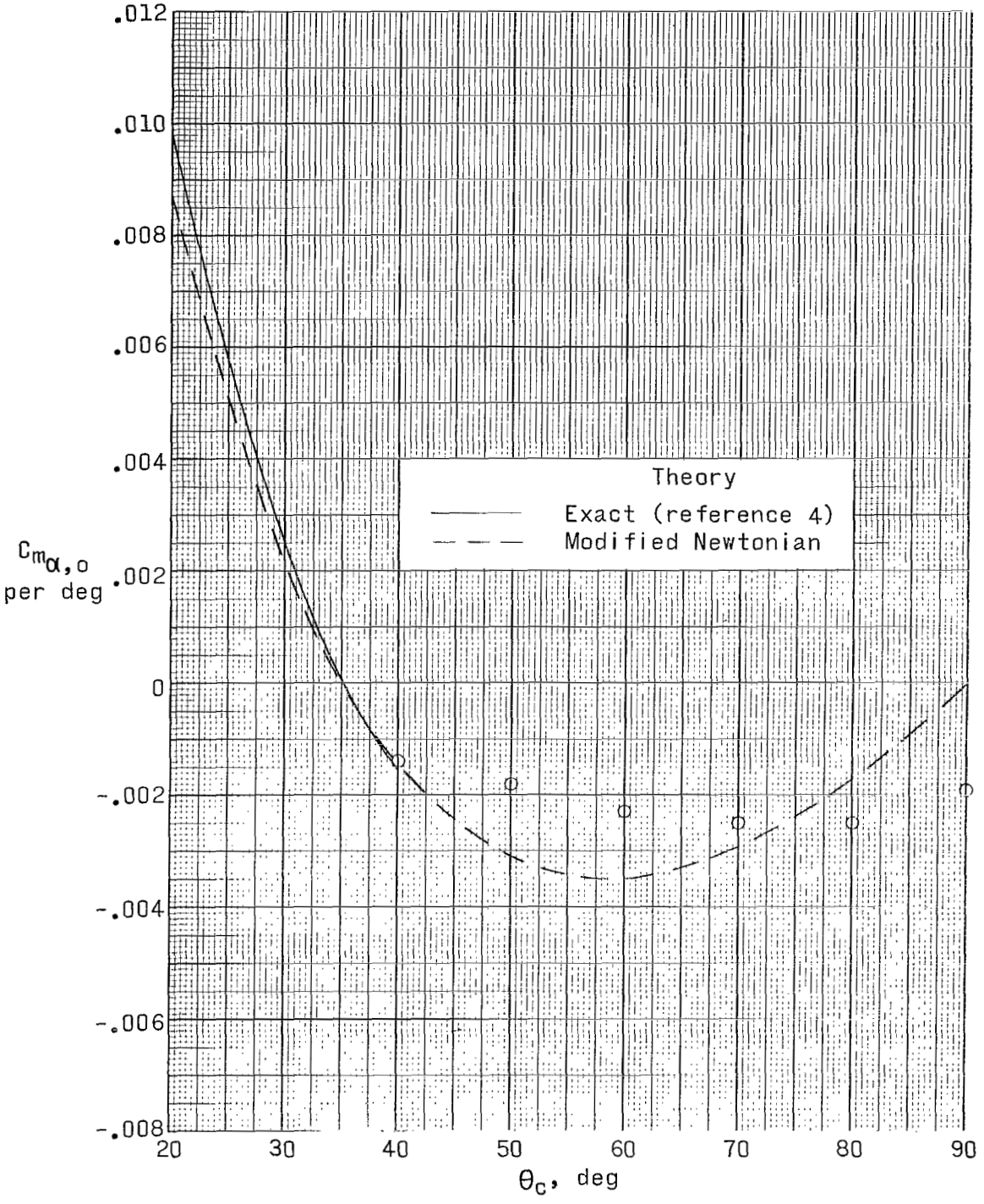

(a) M = 2.30.

Figure 7.- Variation of pitching-moment slope at zero angle of attack with cone semiapex angle.

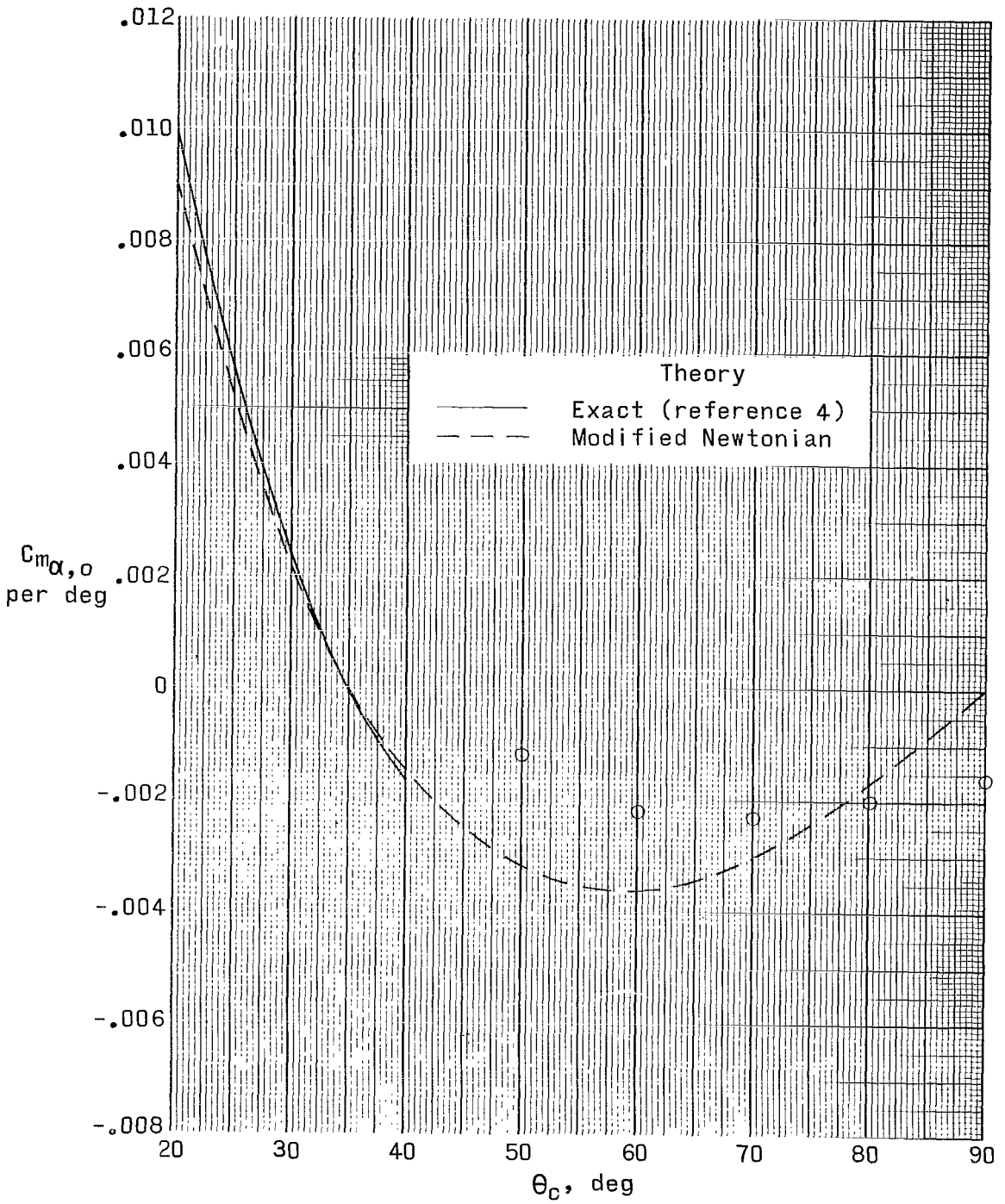

(b) $M = 2.96$.

Figure 7.- Continued.

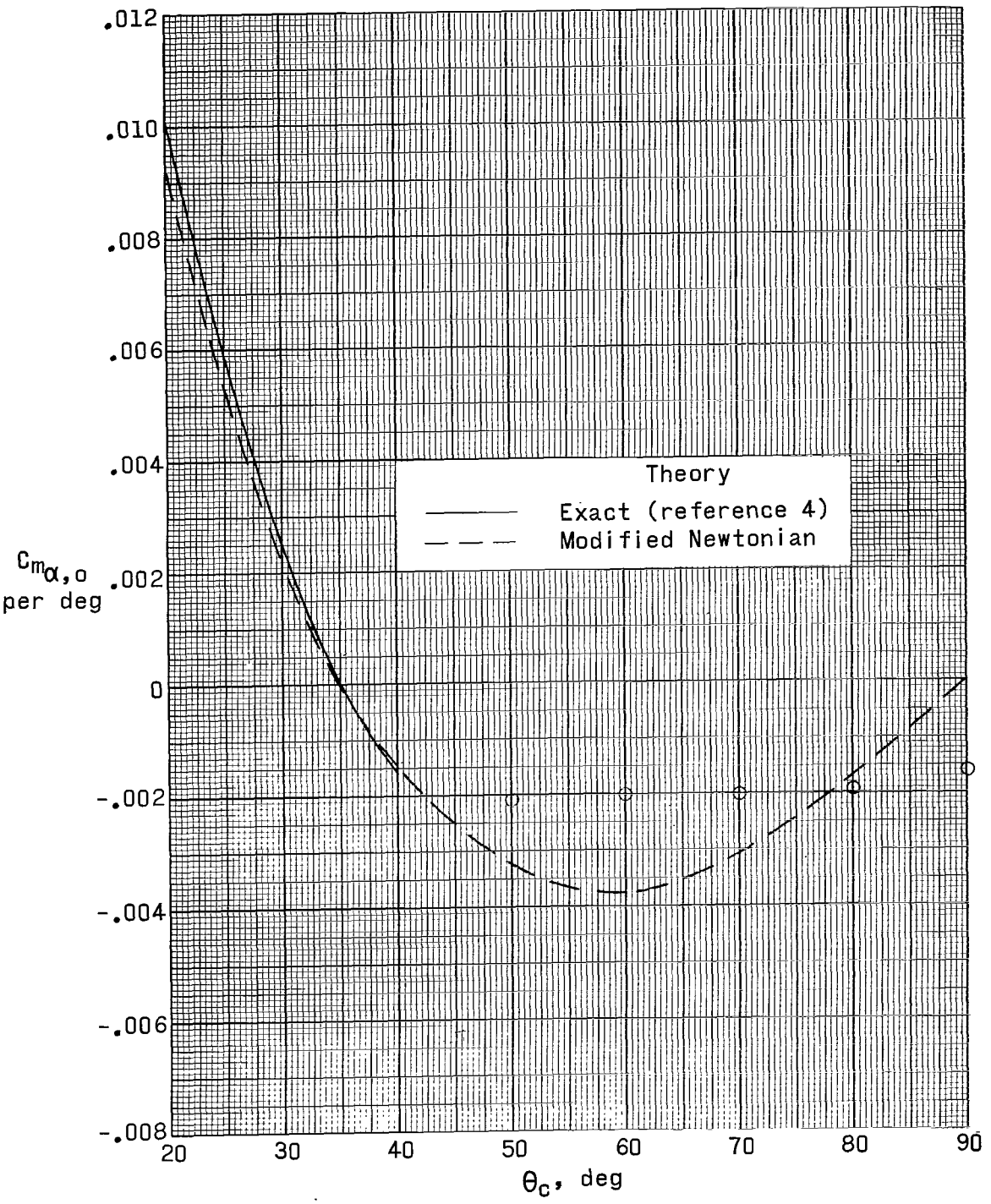

(c) M = 3.95.

Figure 7.- Continued.

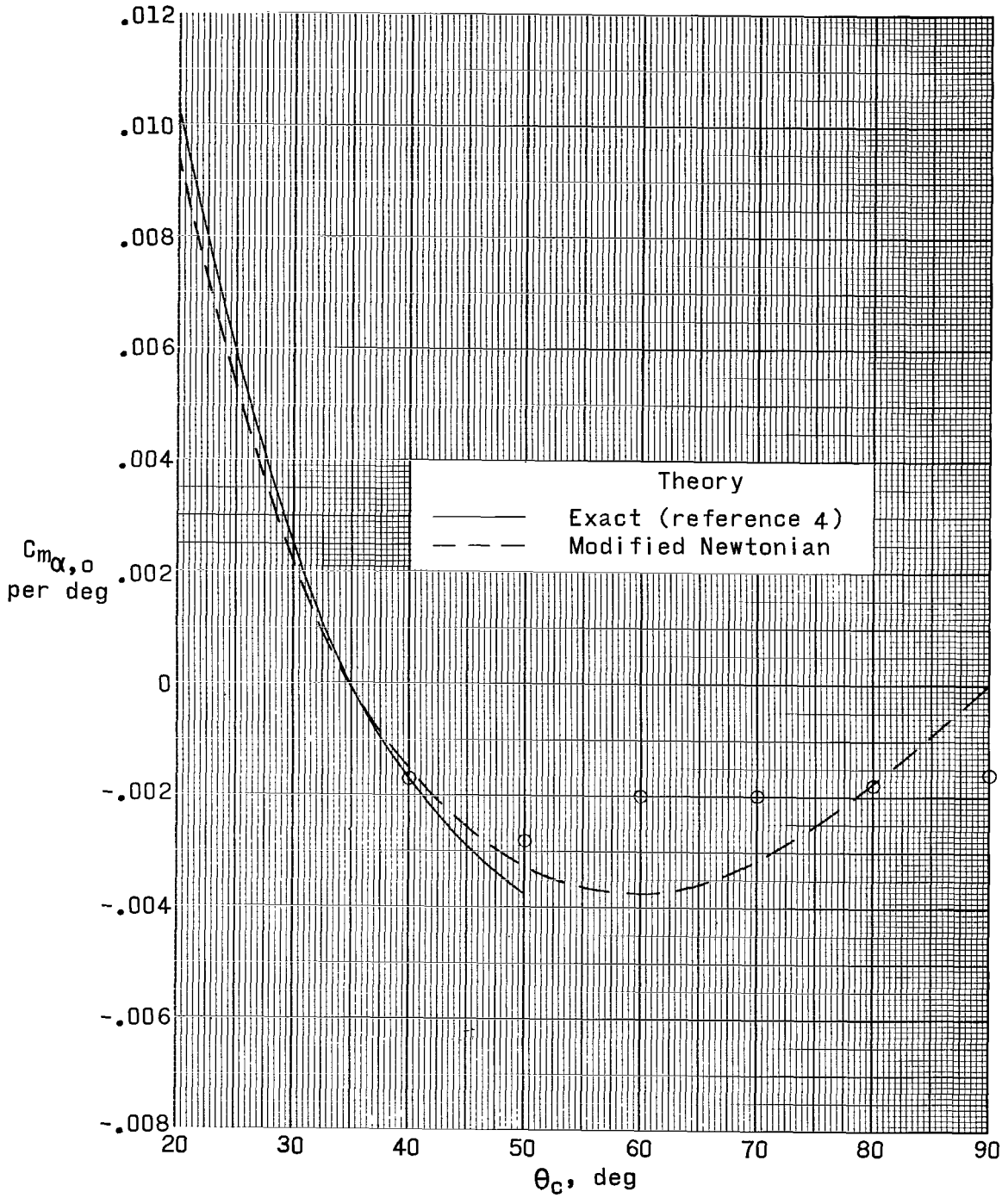

(d) M = 4.63.

Figure 7.- Concluded.

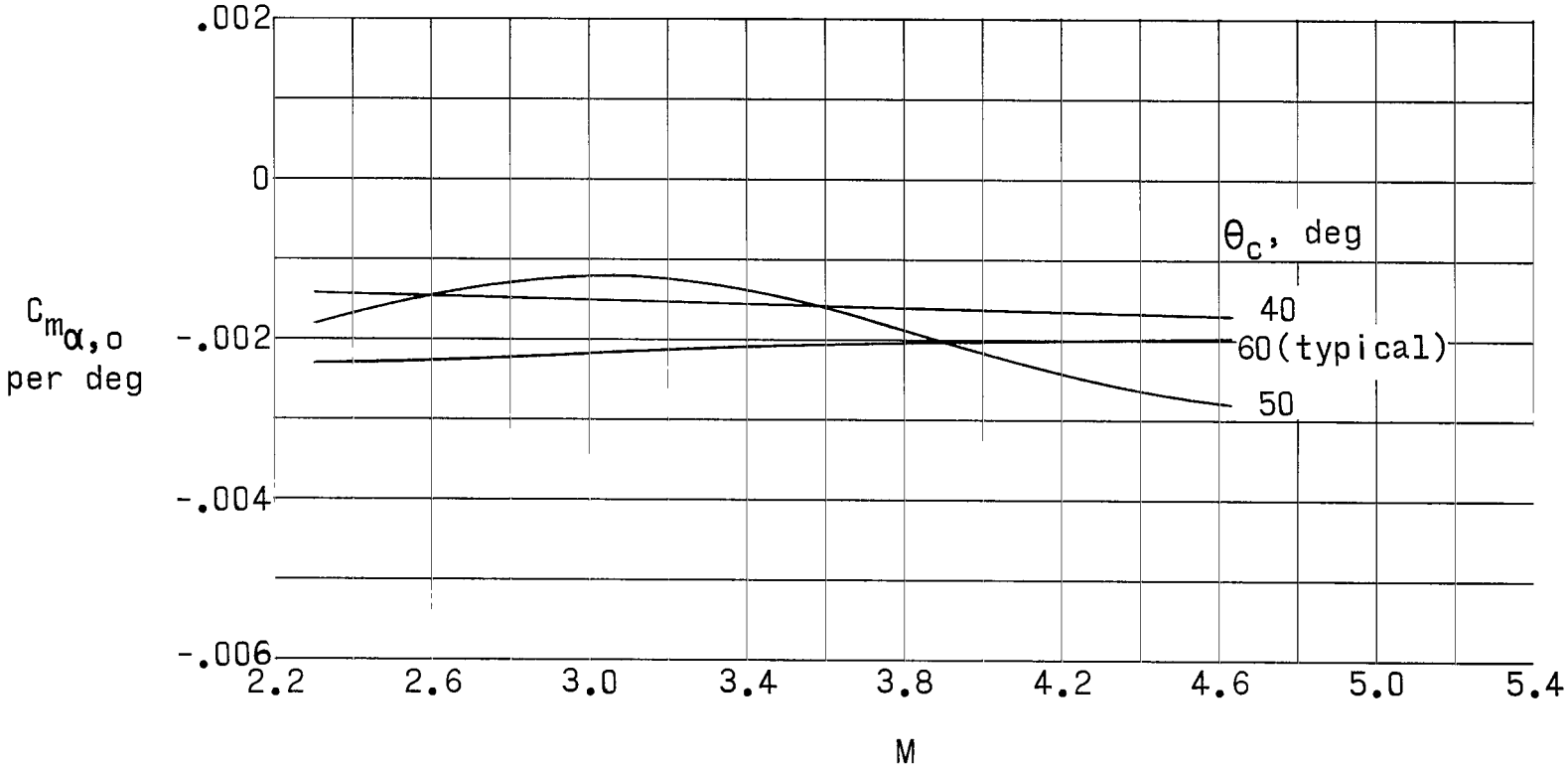

Figure 8.- Variation of pitching-moment slope at zero angle of attack with Mach number.

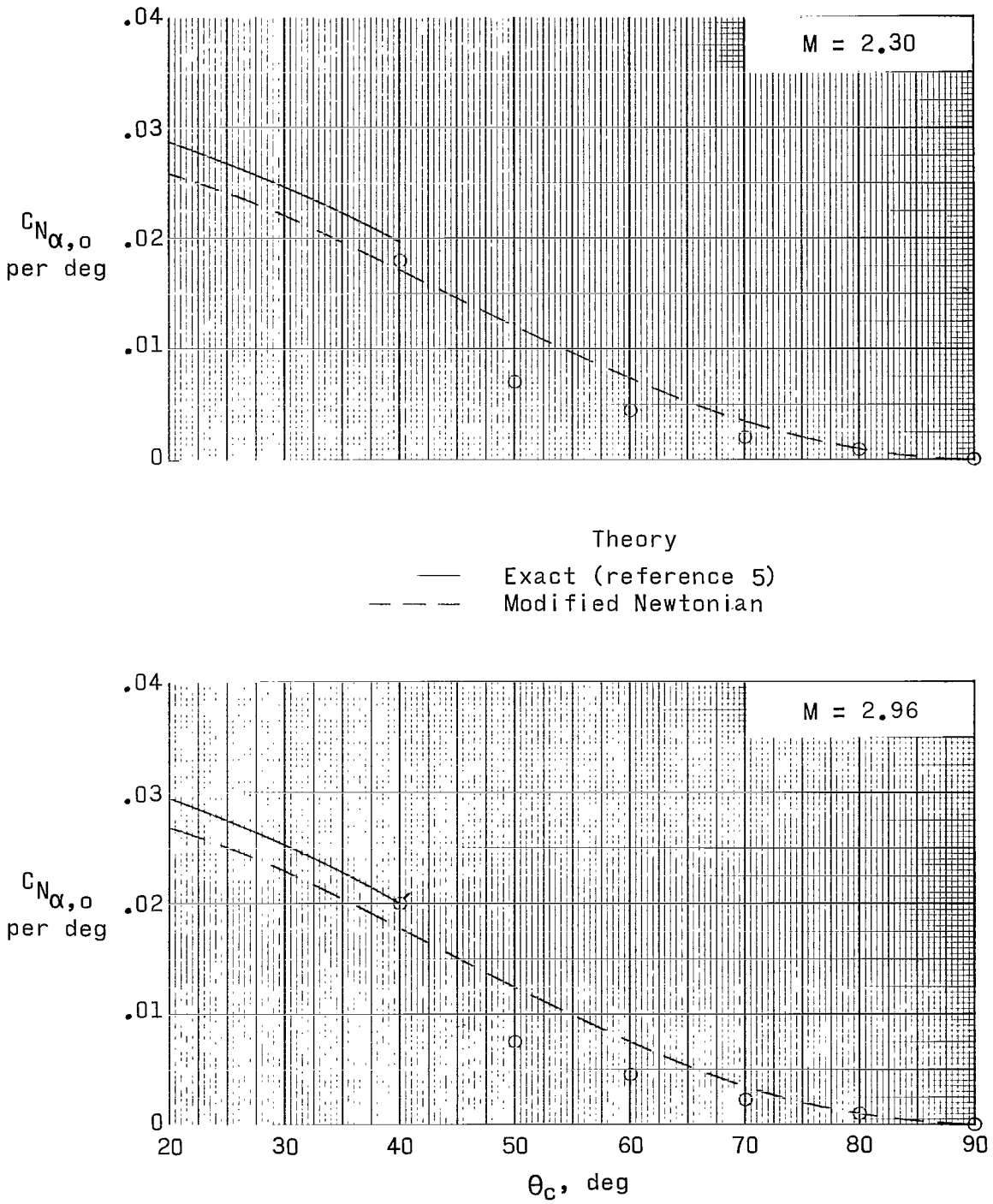

Figure 9.- Variation of normal-force slope at zero angle of attack with cone semiapex angle. (Flagged symbols indicate data from ref. 2.)

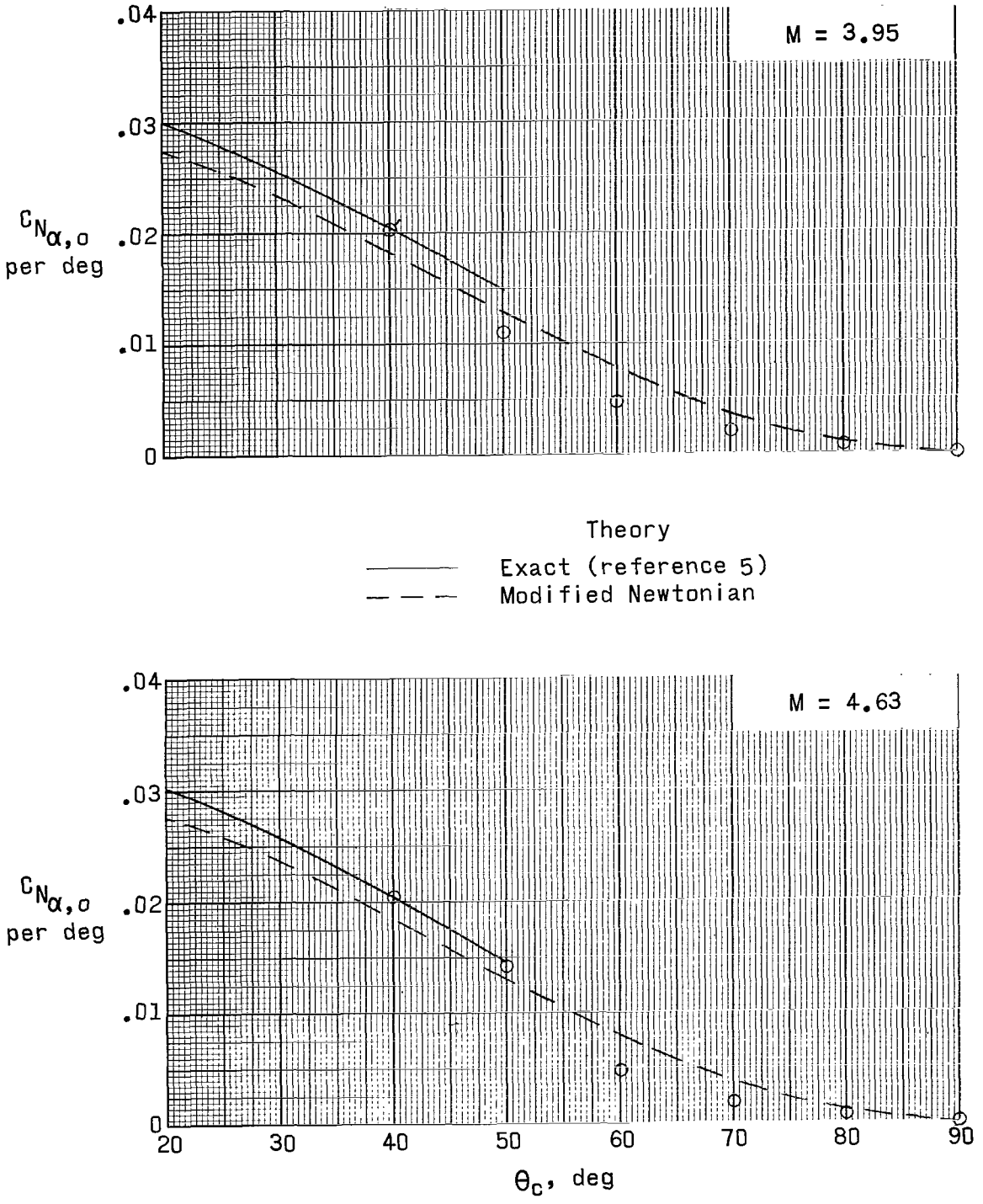

Figure 9.- Concluded.

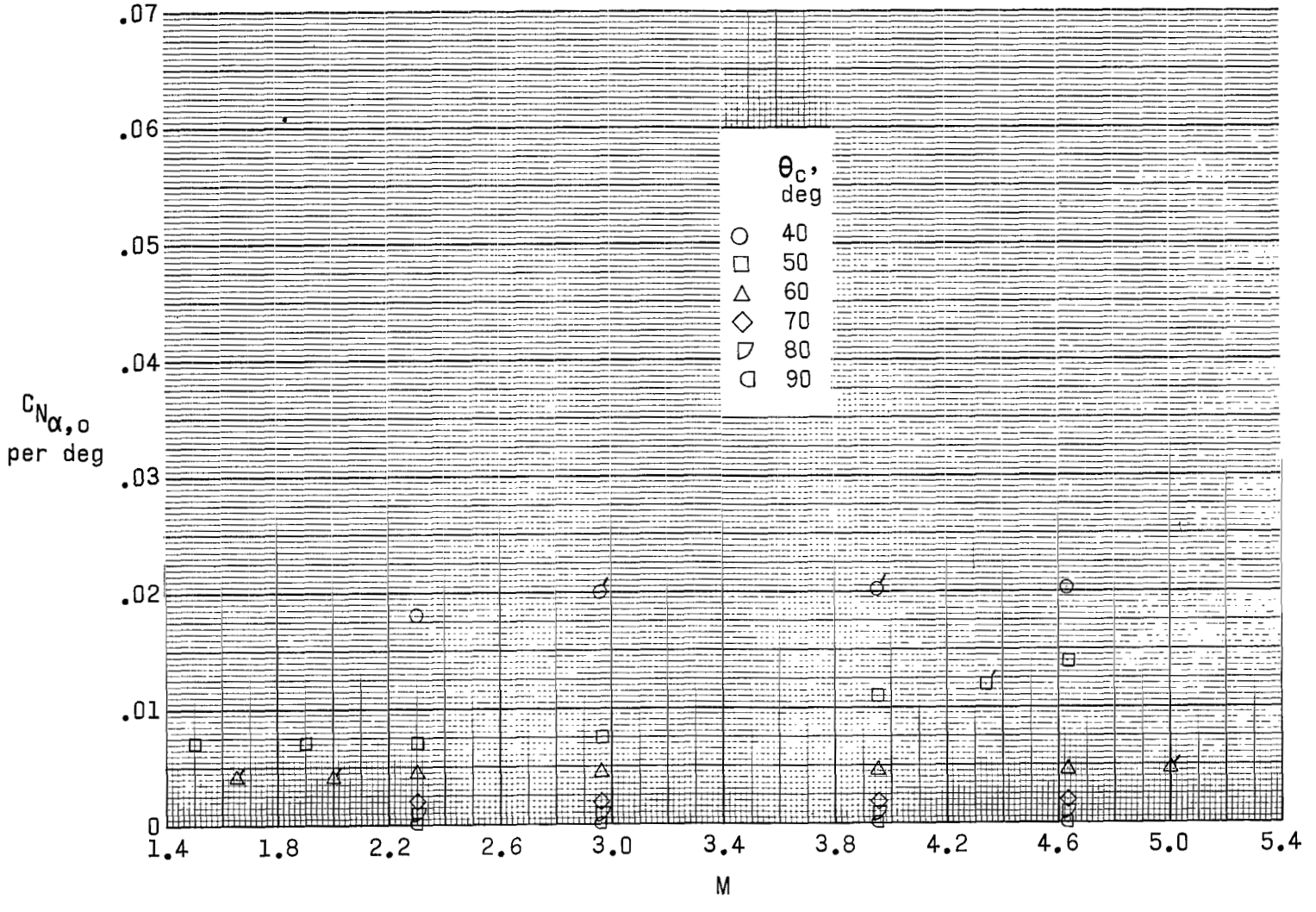

Figure 10.- Variation of normal-force slope at zero angle of attack with Mach number. (Flagged symbols indicate data from ref. 2.)

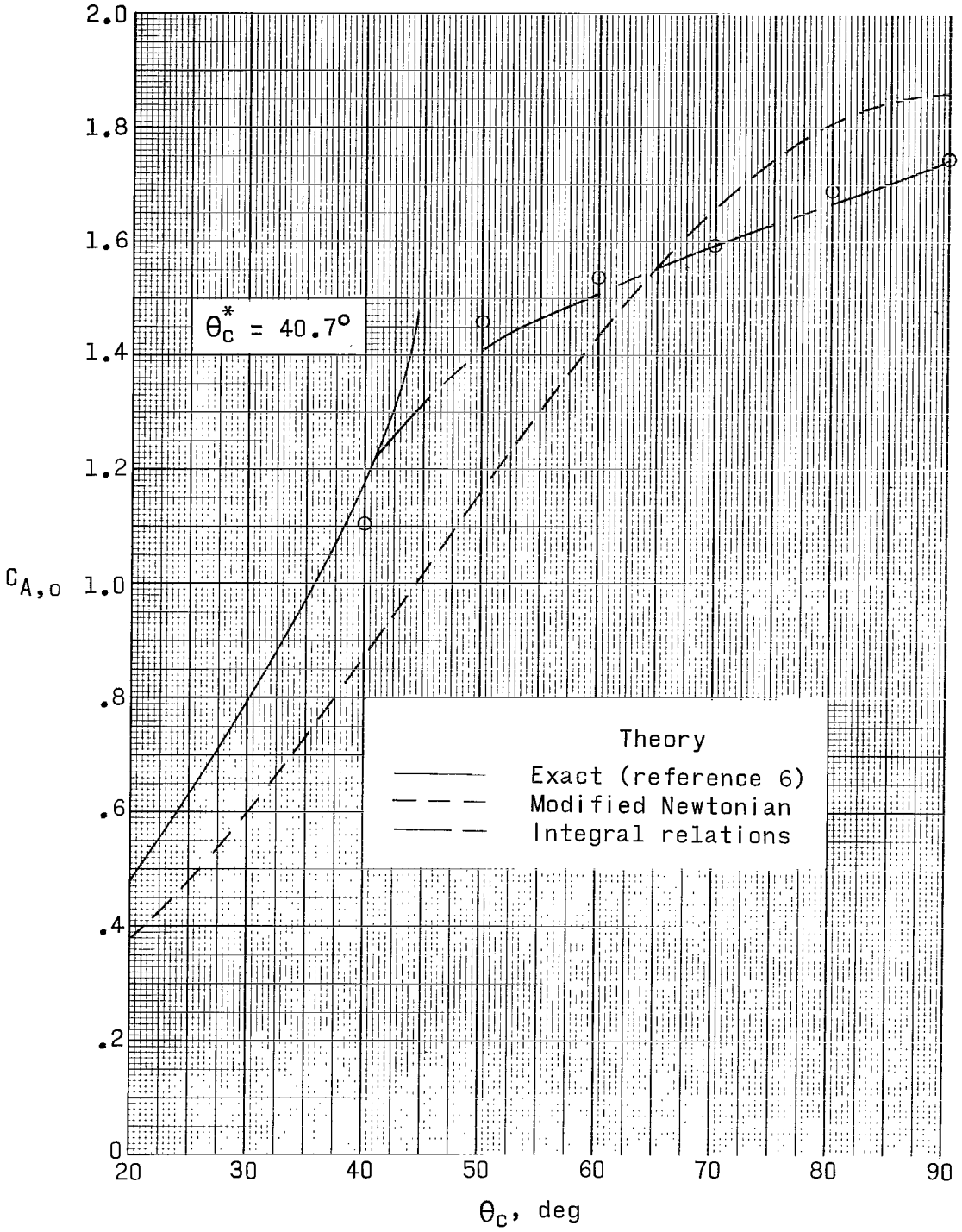

(a) M = 2.30.

Figure 11.- Variation of axial-force coefficient at zero angle of attack with cone semiapex angle. (Circular symbols represent experimental data: flagged symbols indicate data from ref. 2.)

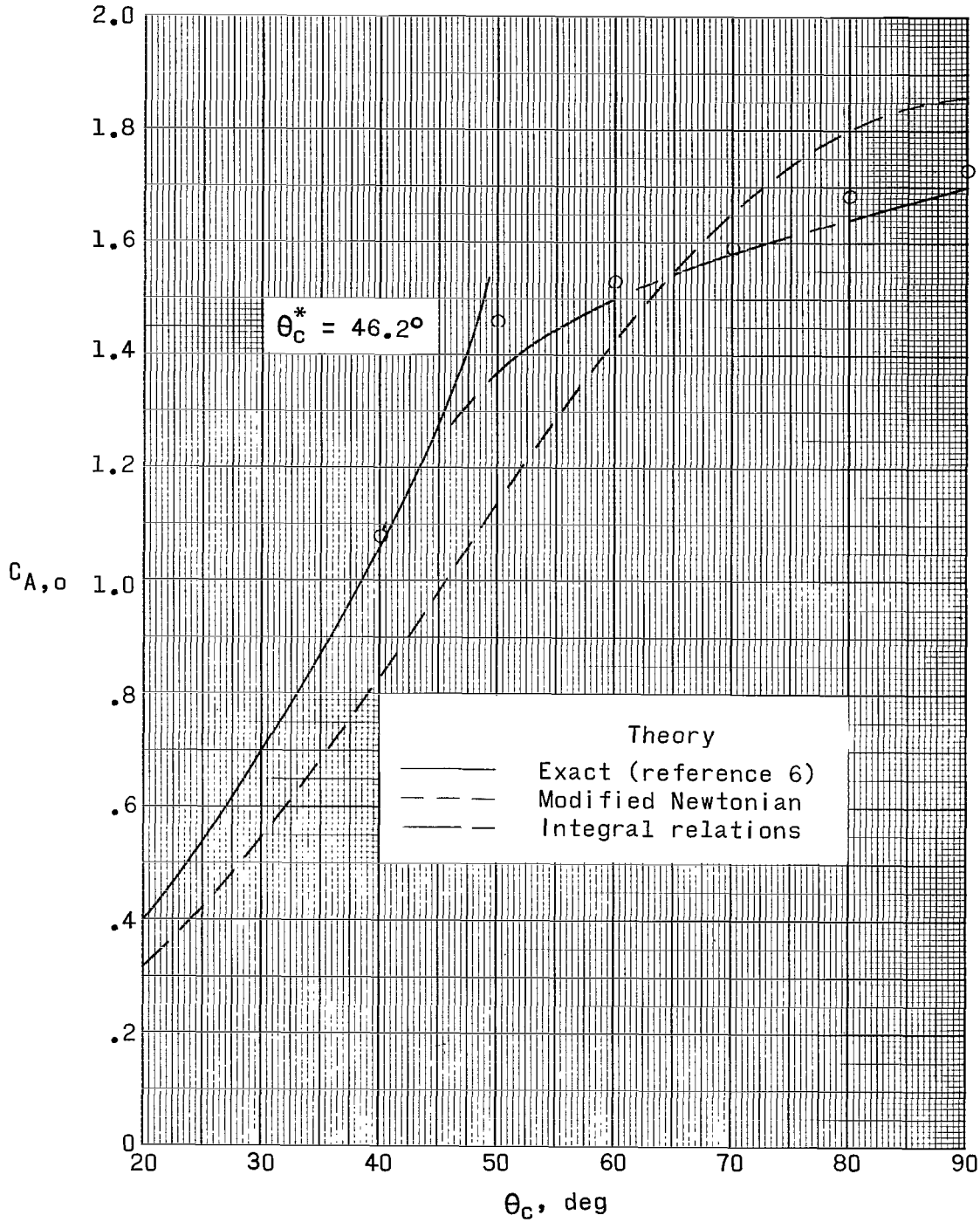

(b) M = 2.96.

Figure 11.- Continued.

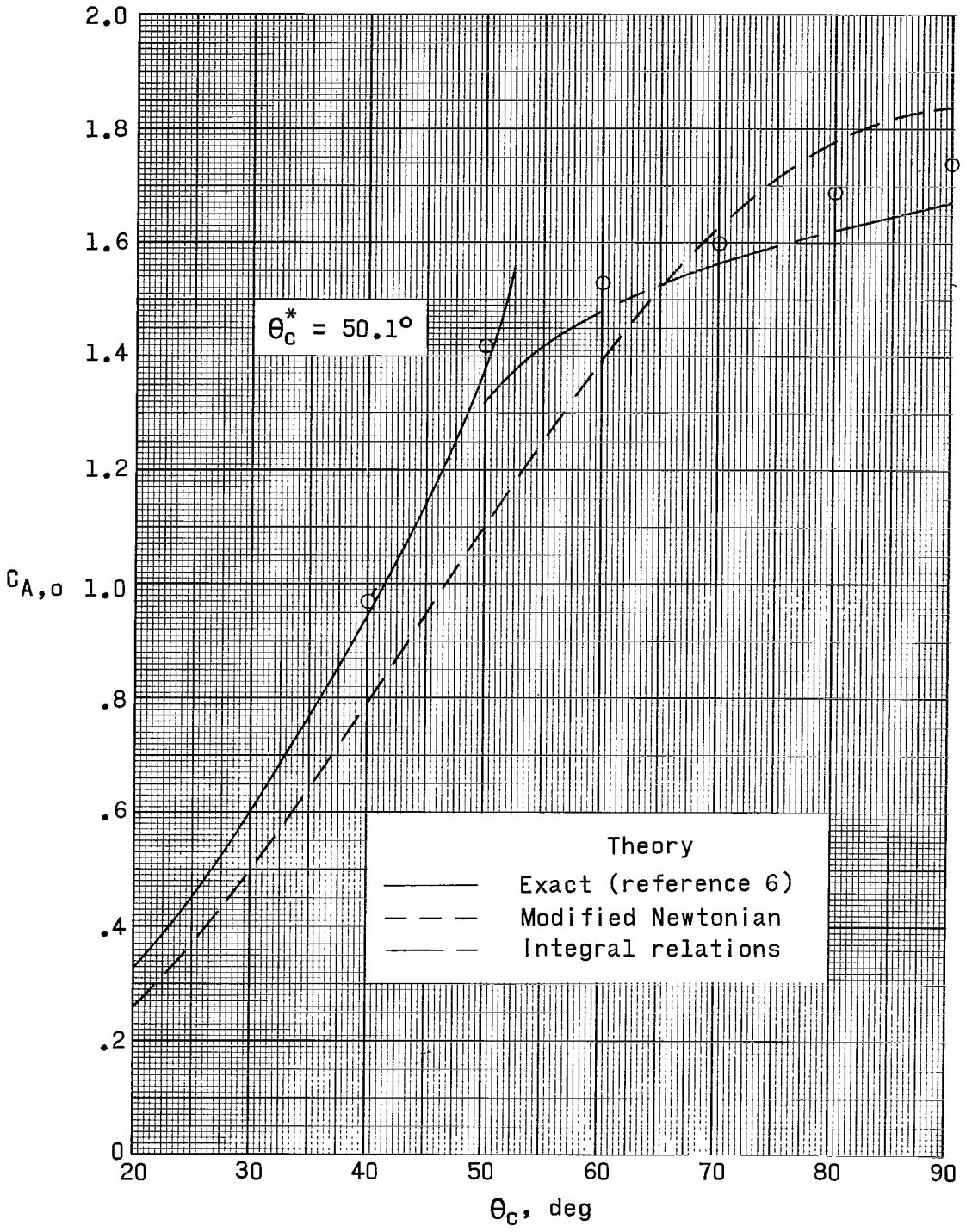

(c) M = 3.95.

Figure 11.- Continued.

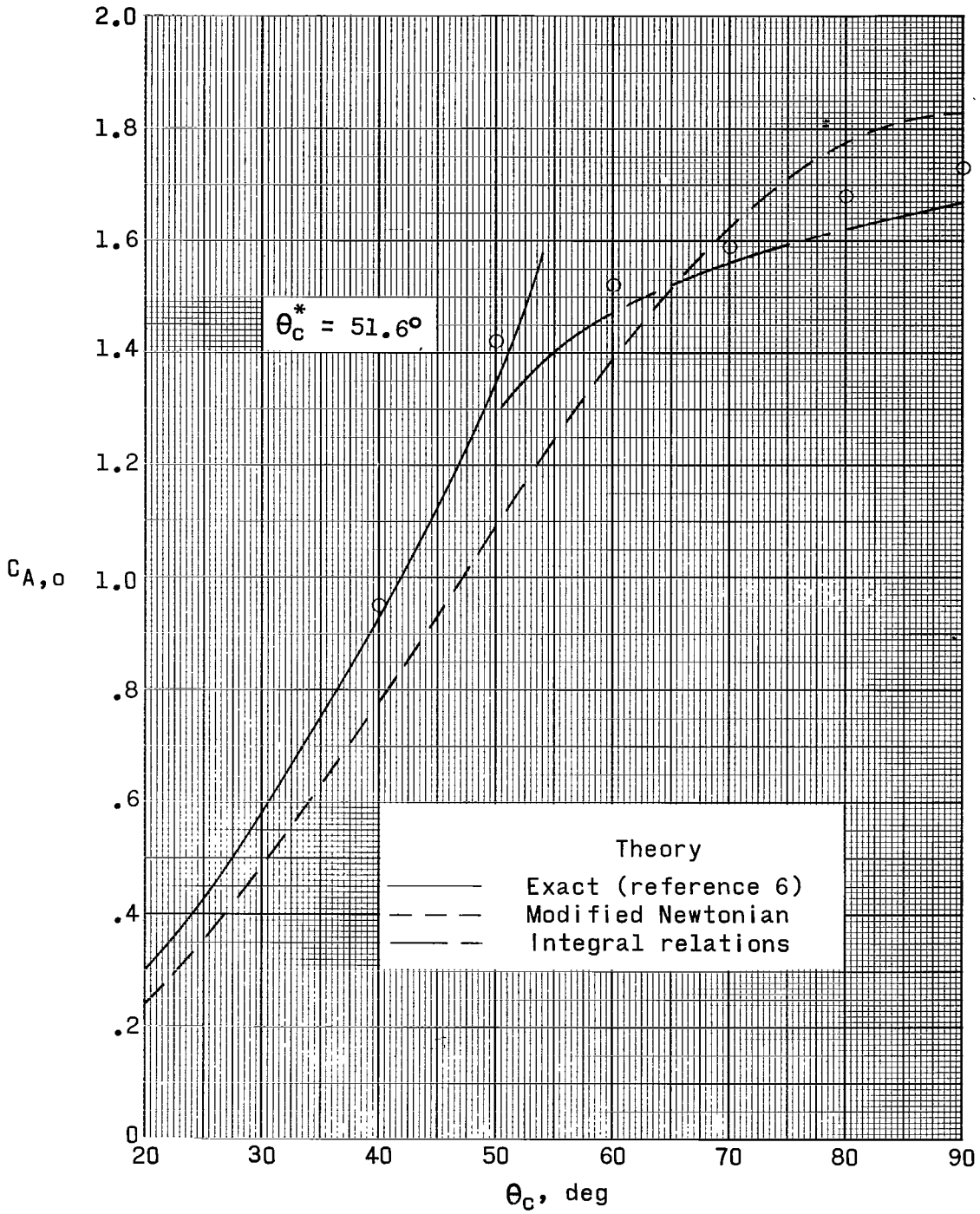

(d) M = 4.63.

Figure 11.- Concluded.

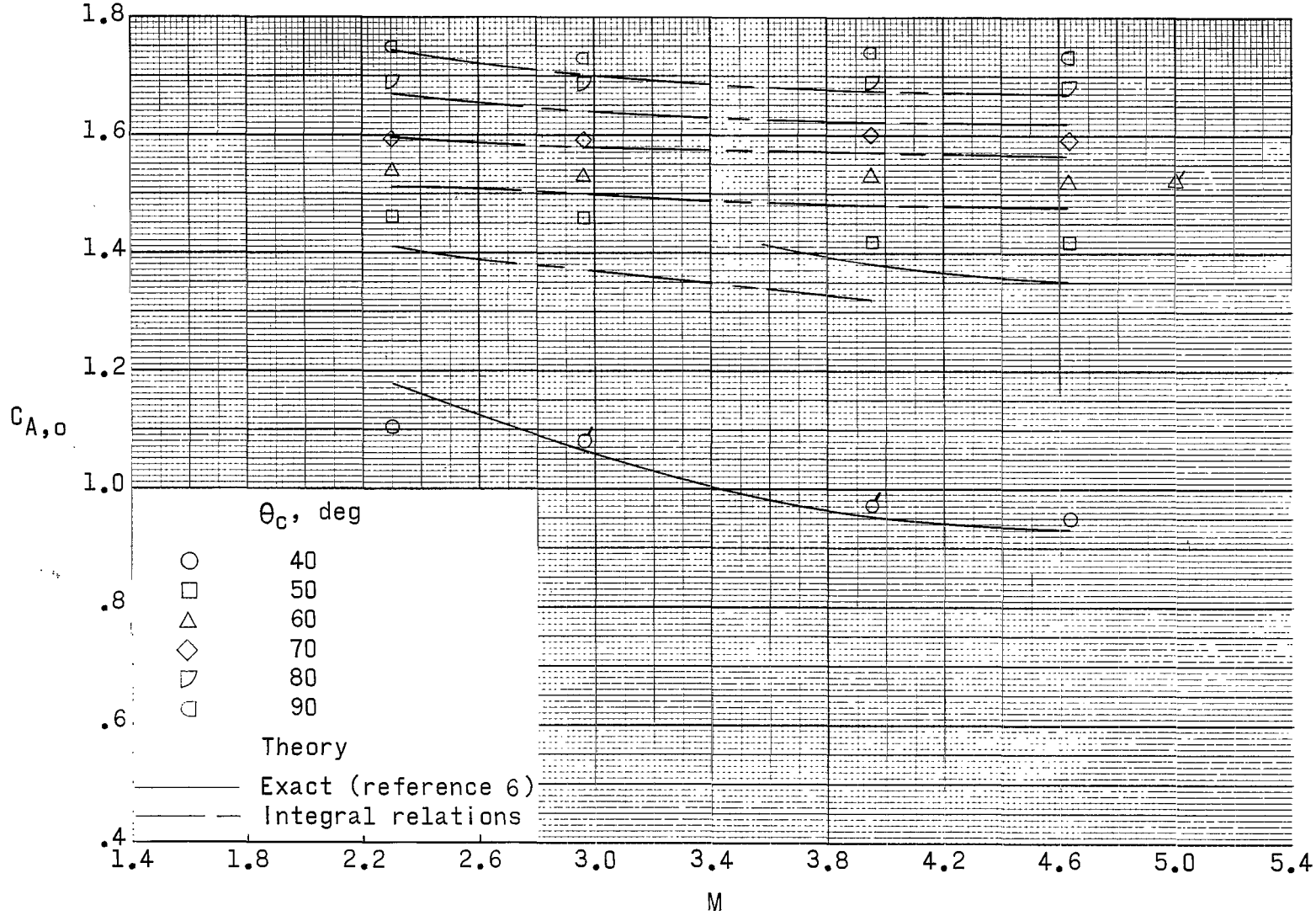

Figure 12.- Variation of axial-force coefficient at zero angle of attack with Mach number. (Flagged symbols indicate data from ref. 2.)

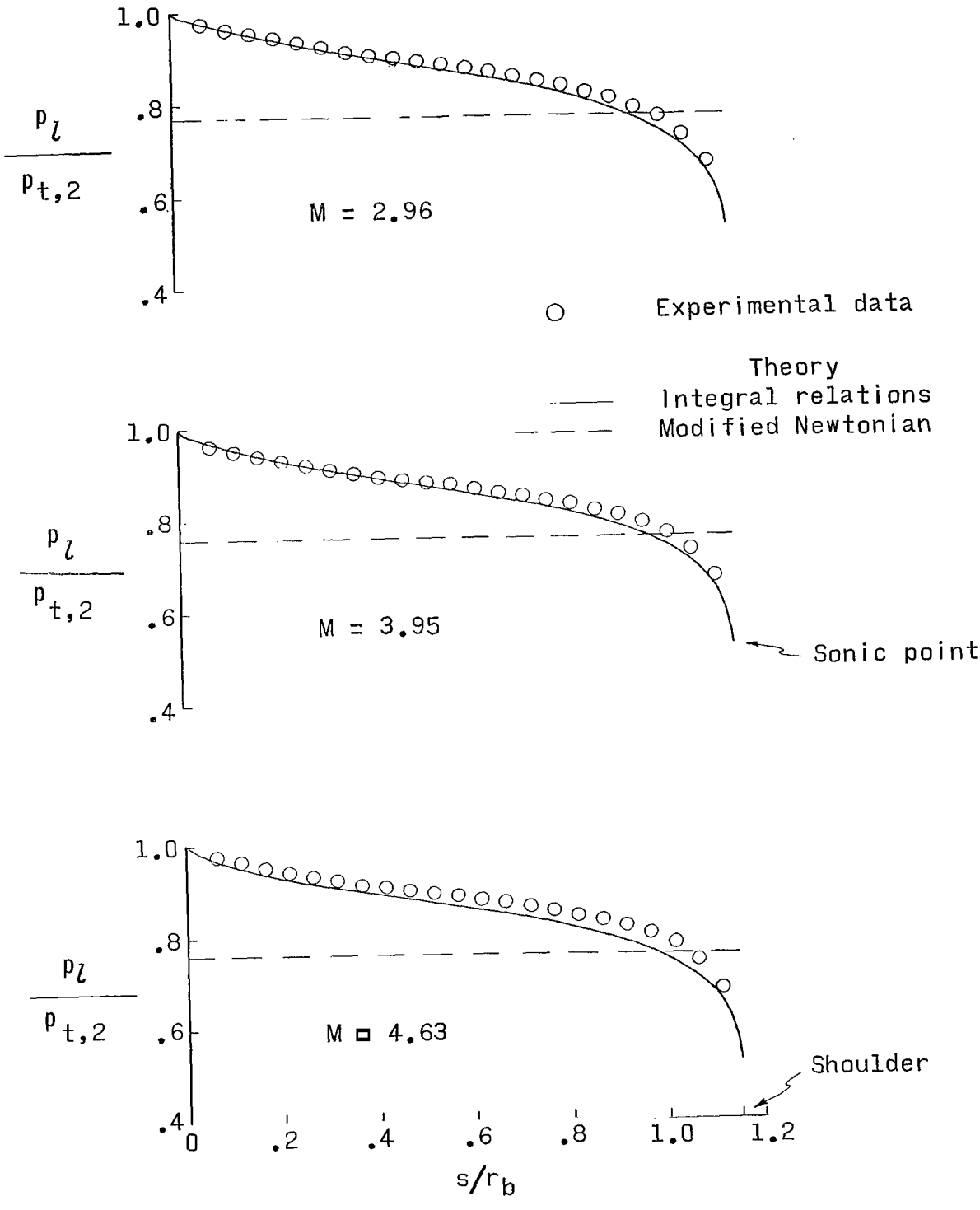

Figure 13.- Frontal surface pressure distribution on 60° semiapex angle cone. $\alpha \approx 0^{\circ}$.

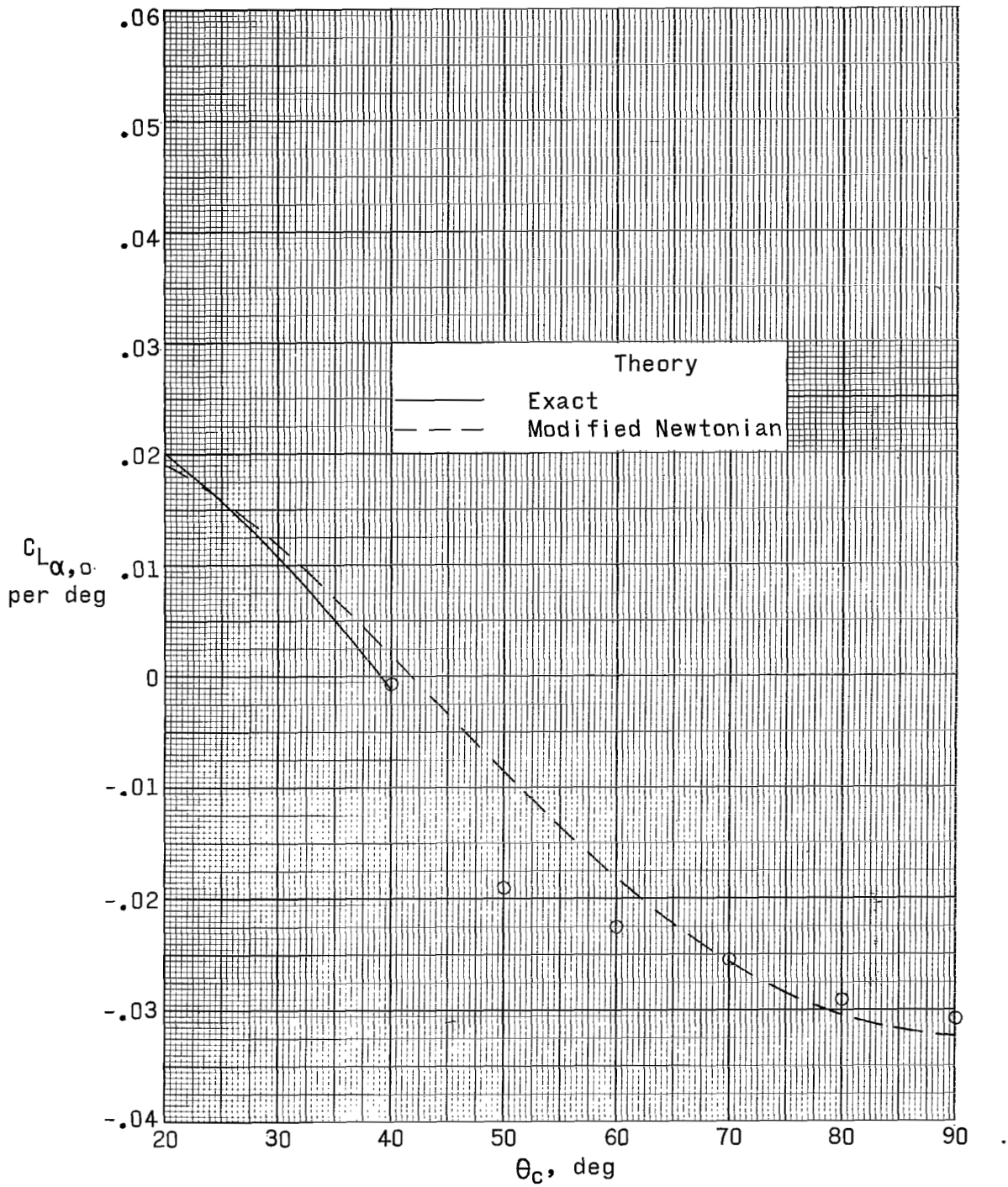

(a) M = 2.30.

Figure 14.- Variation of lift-curve slope at zero angle of attack with cone semiapex angle. (Flagged symbols indicate data from ref. 2.)

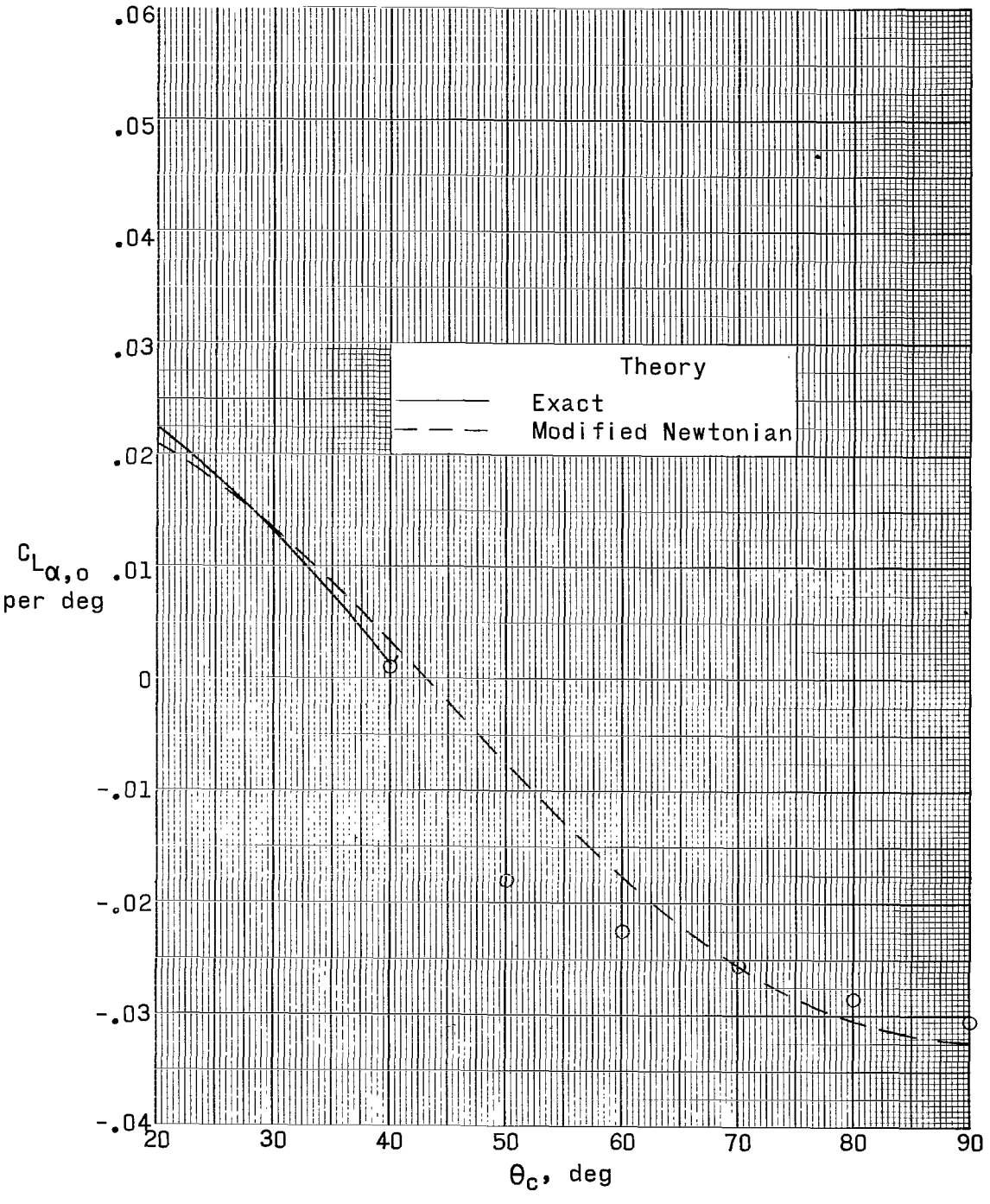

(b) M = 2.96.

Figure 14.- Continued.

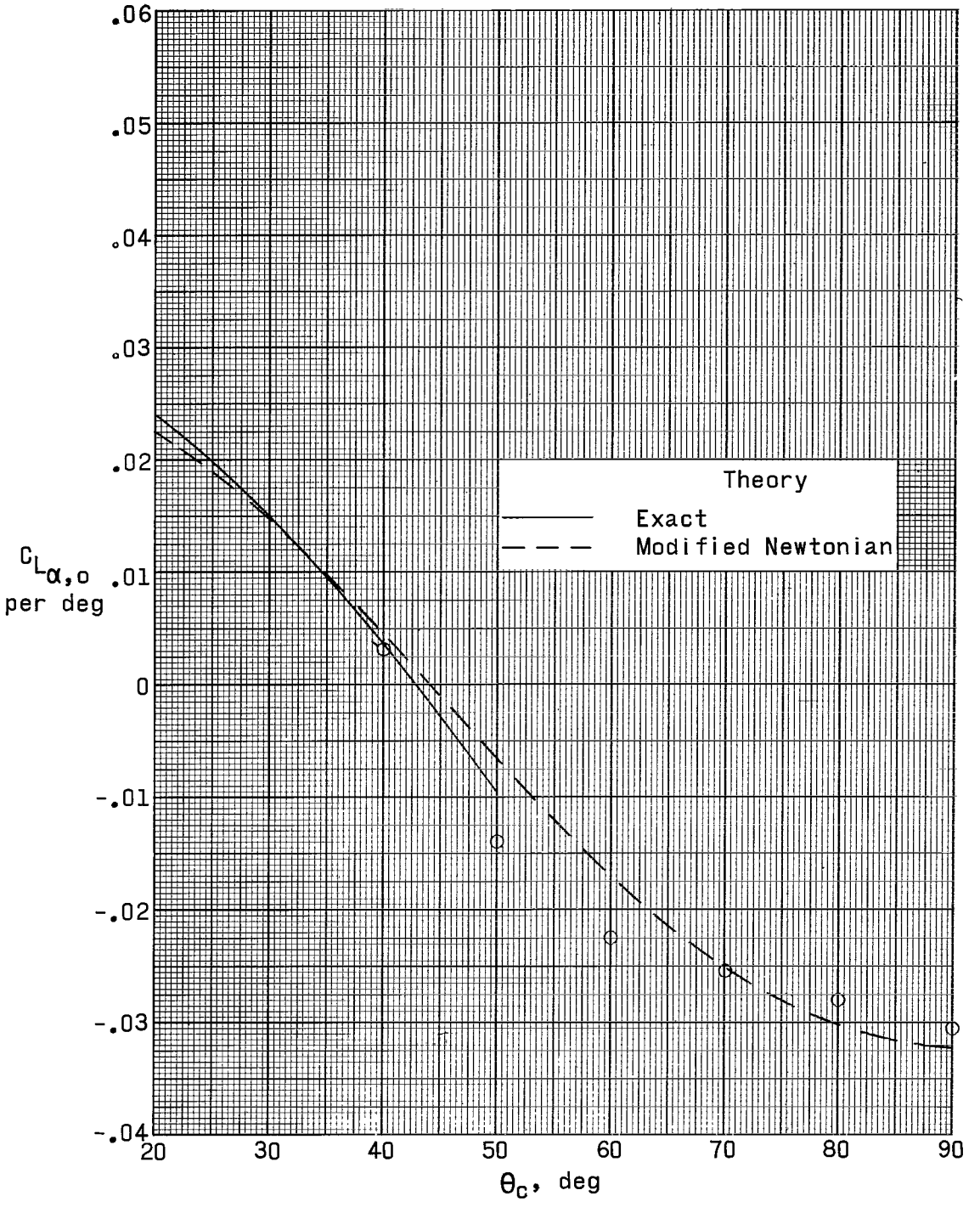

(c) M = 3.95.

Figure 14.- Continued.

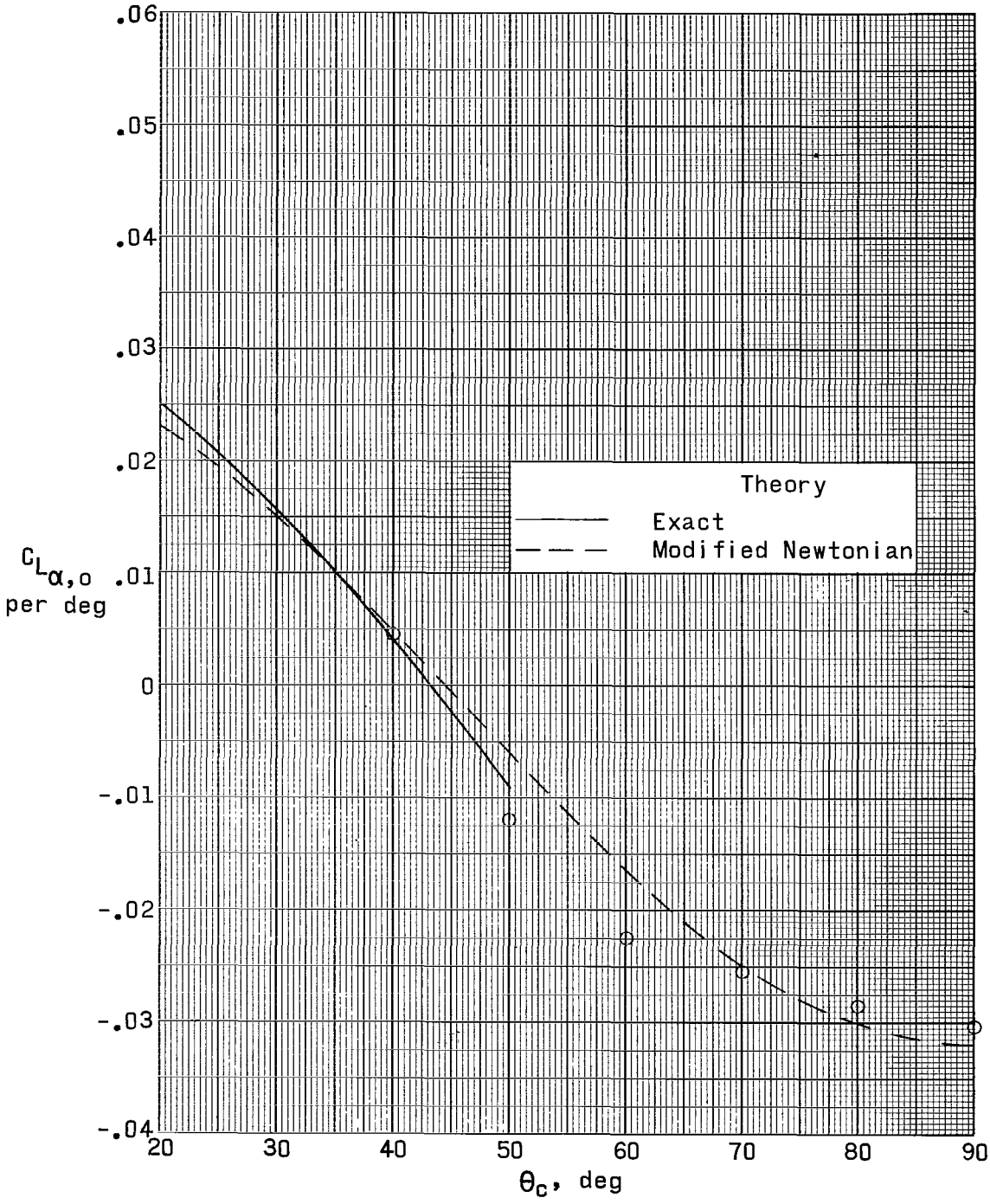

(d) M = 4.63.

Figure 14.- Concluded.

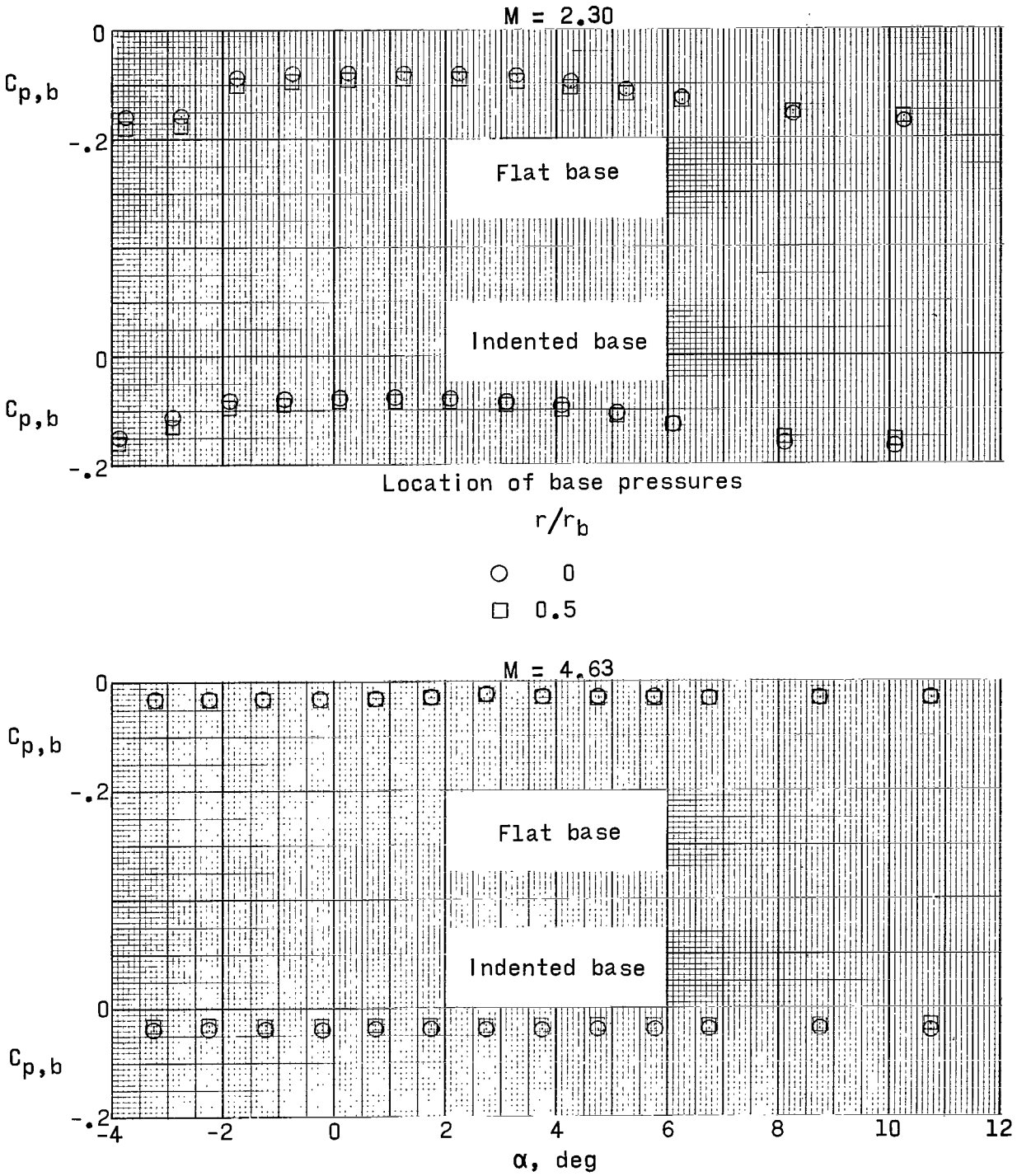

(a) $\theta_c = 40^0$.

Figure 15.- Variation of base pressure coefficient with angle of attack for test configurations.

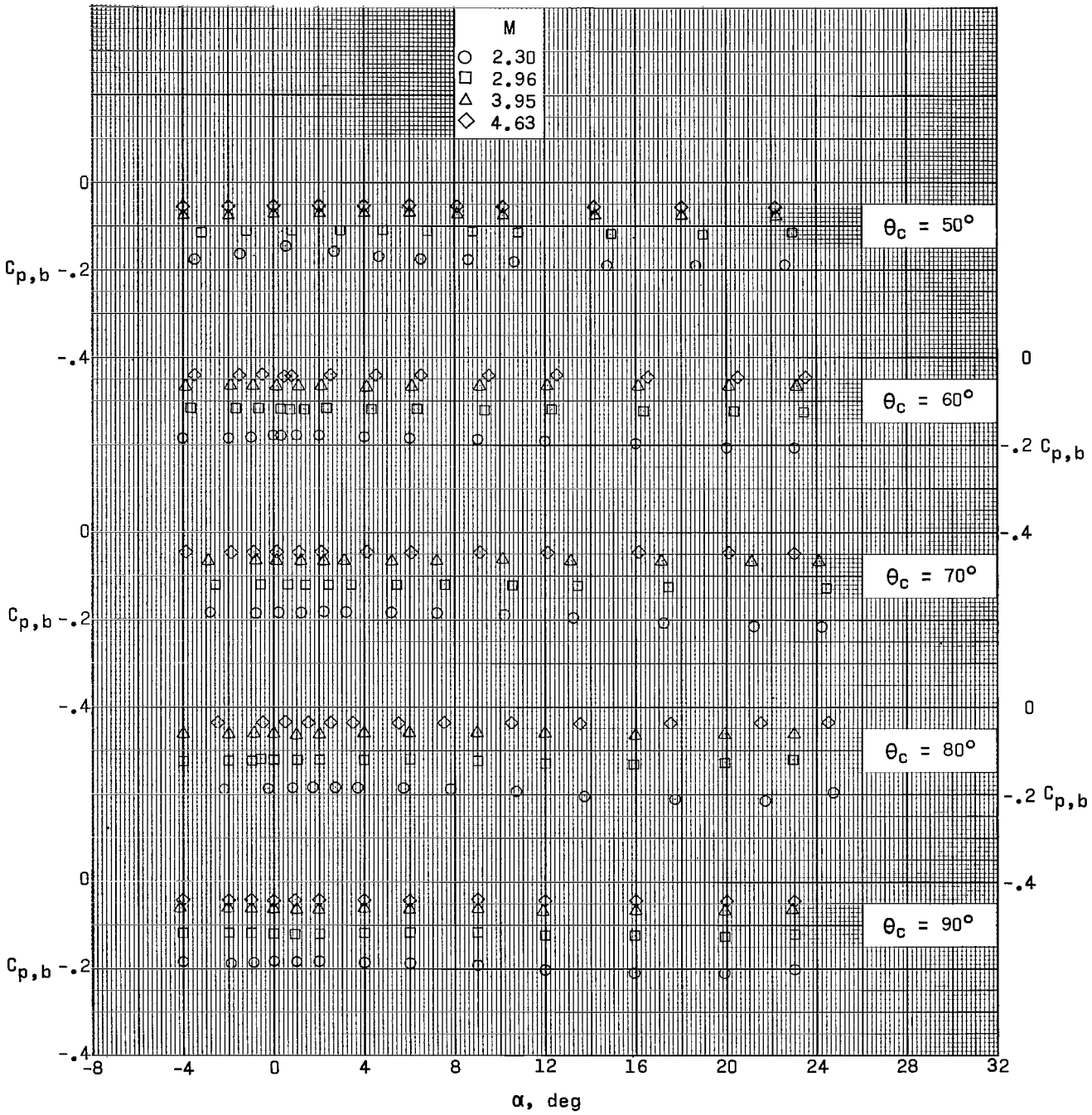

(b) $\theta_c = 50^0$, 60^0, 70^0, 80^0, and 90^0.

Figure 15.- Concluded.

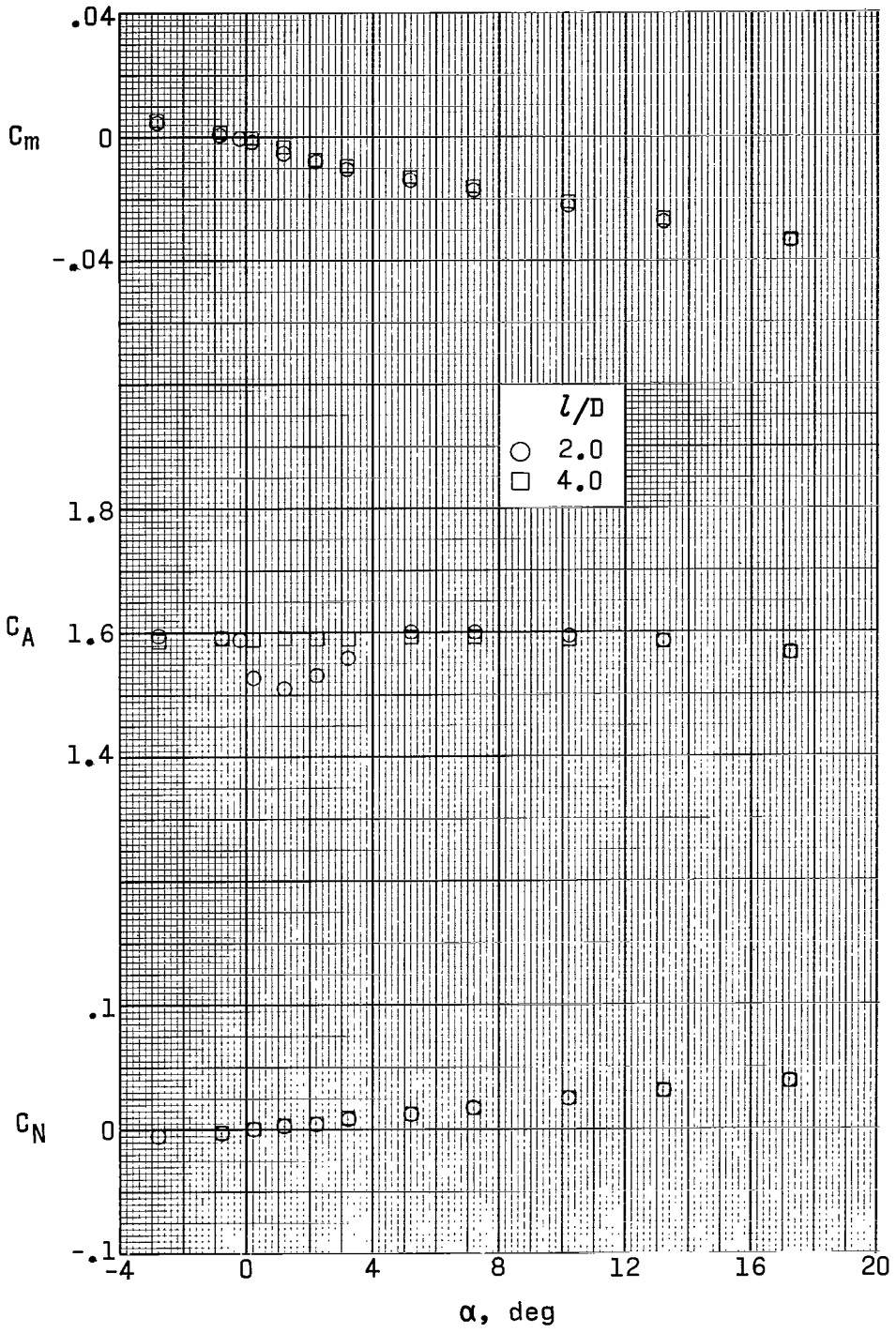

(a) M = 2.30.

Figure 16.- Effect of sting length on longitudinal aerodynamic characteristics. $\theta_c = 70^o$.

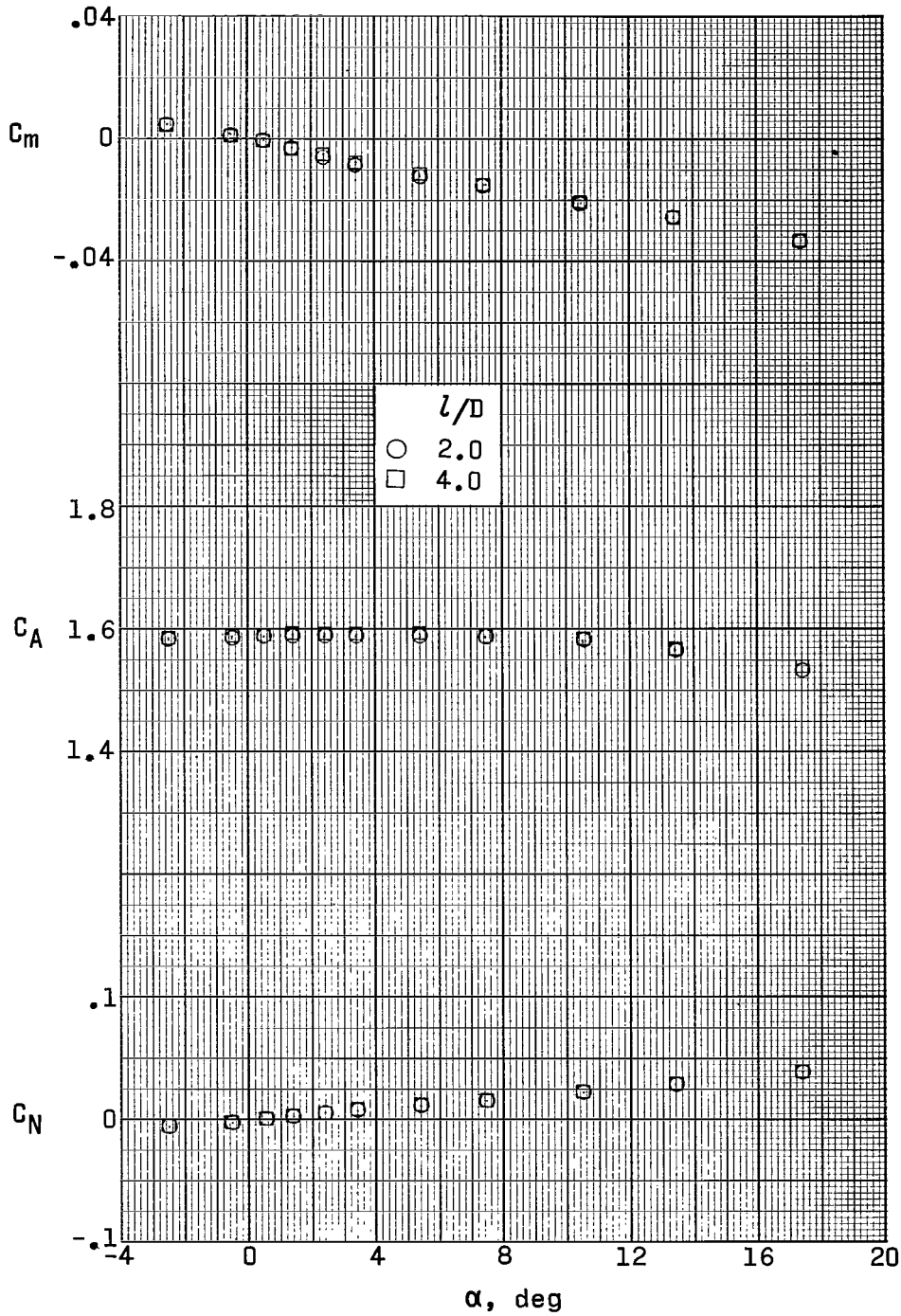

(b) M = 2.96.

Figure 16.- Concluded.

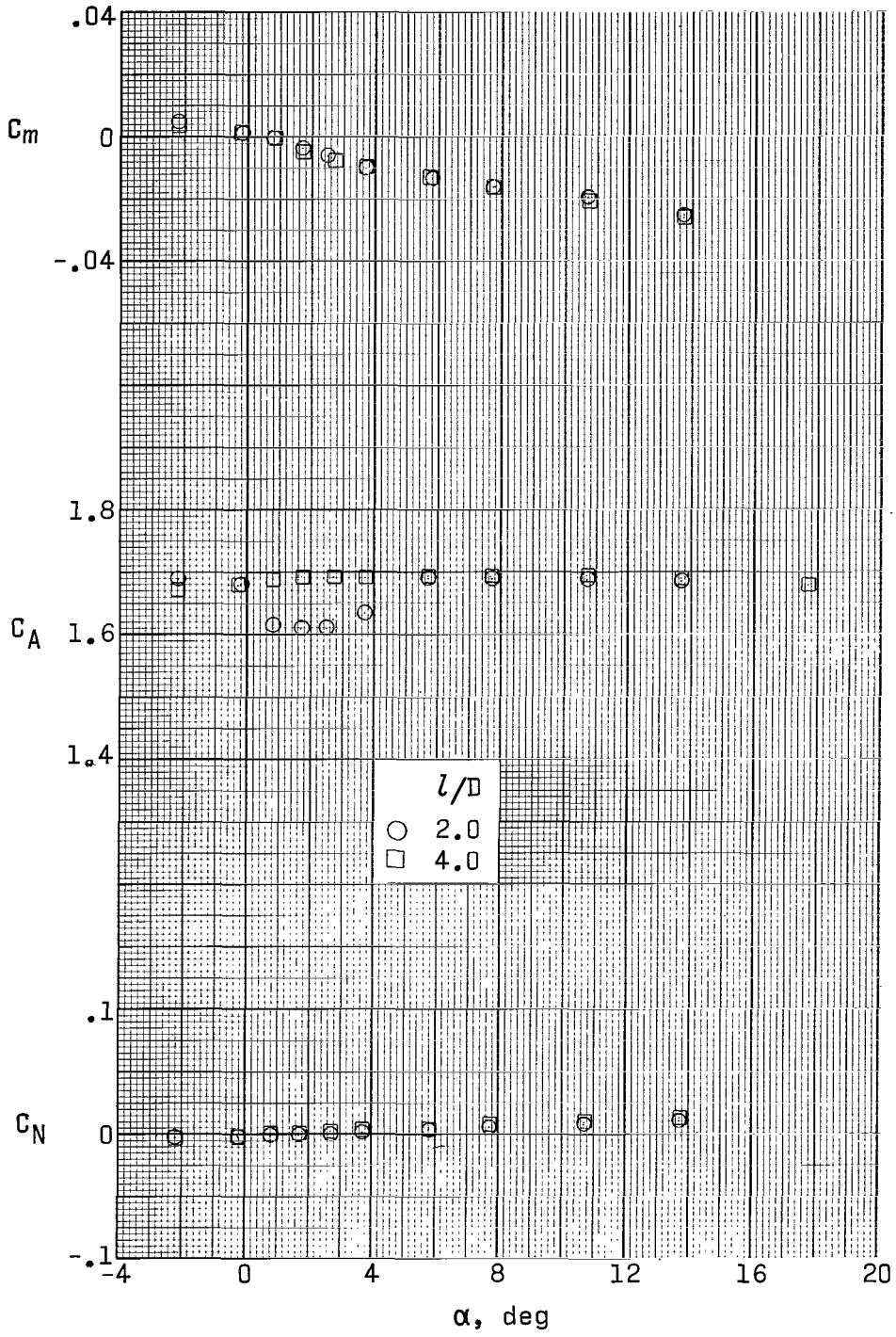

(a) M = 2.30.

Figure 17.- Effect of sting length on longitudinal aerodynamic characteristics. $\theta_c = 80^0$.

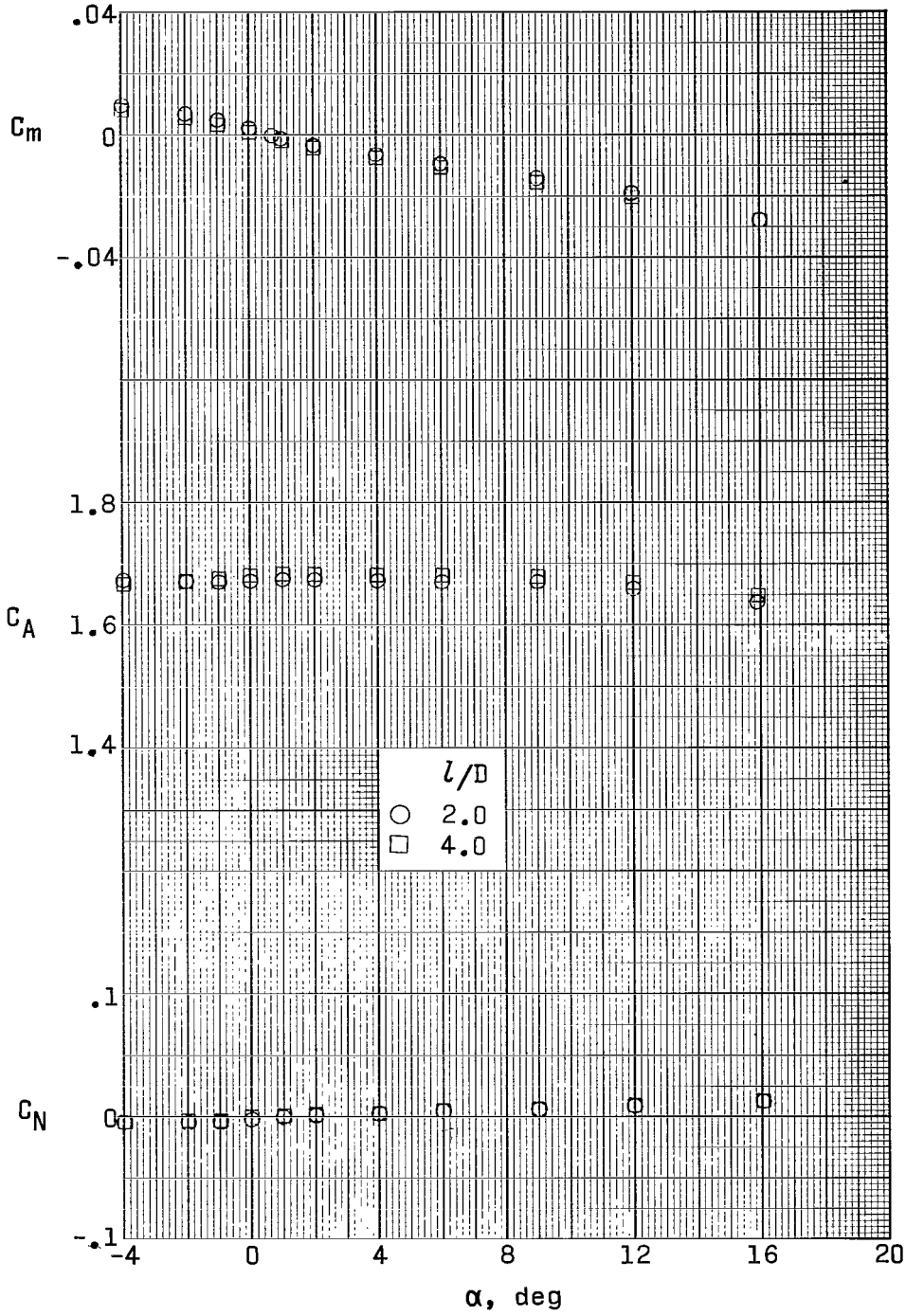

(b) M = 2.96.

Figure 17.- Concluded.

M = 2.30

M = 2.96

l/D = 2.0

$\overline{M}$ = 2.30

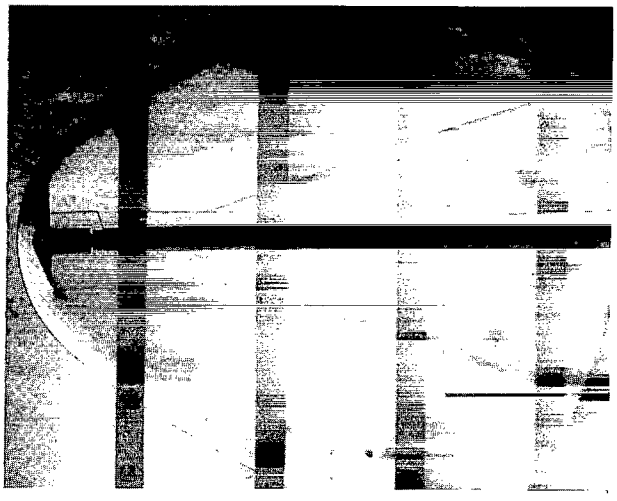

M = 2.96

l/D = 4.0

(a) $\theta_c = 70^0$.

L-68 5601

Figure 18.- Schlieren photographs for several cone models with two sting lengths. $\alpha \approx 0^0$.

M = 2.30 M = 2.96

l/D = 2.0

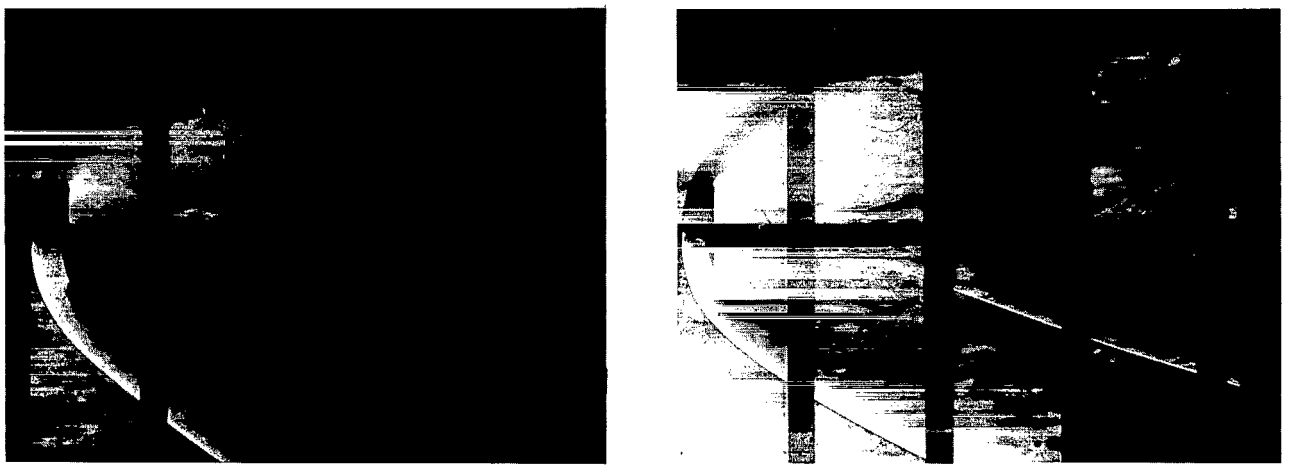

M = 2.30 M = 2.96

l/D = 4.0

(b) $\theta_c = 80^o$. L-68 5602

Figure 18.- Concluded.

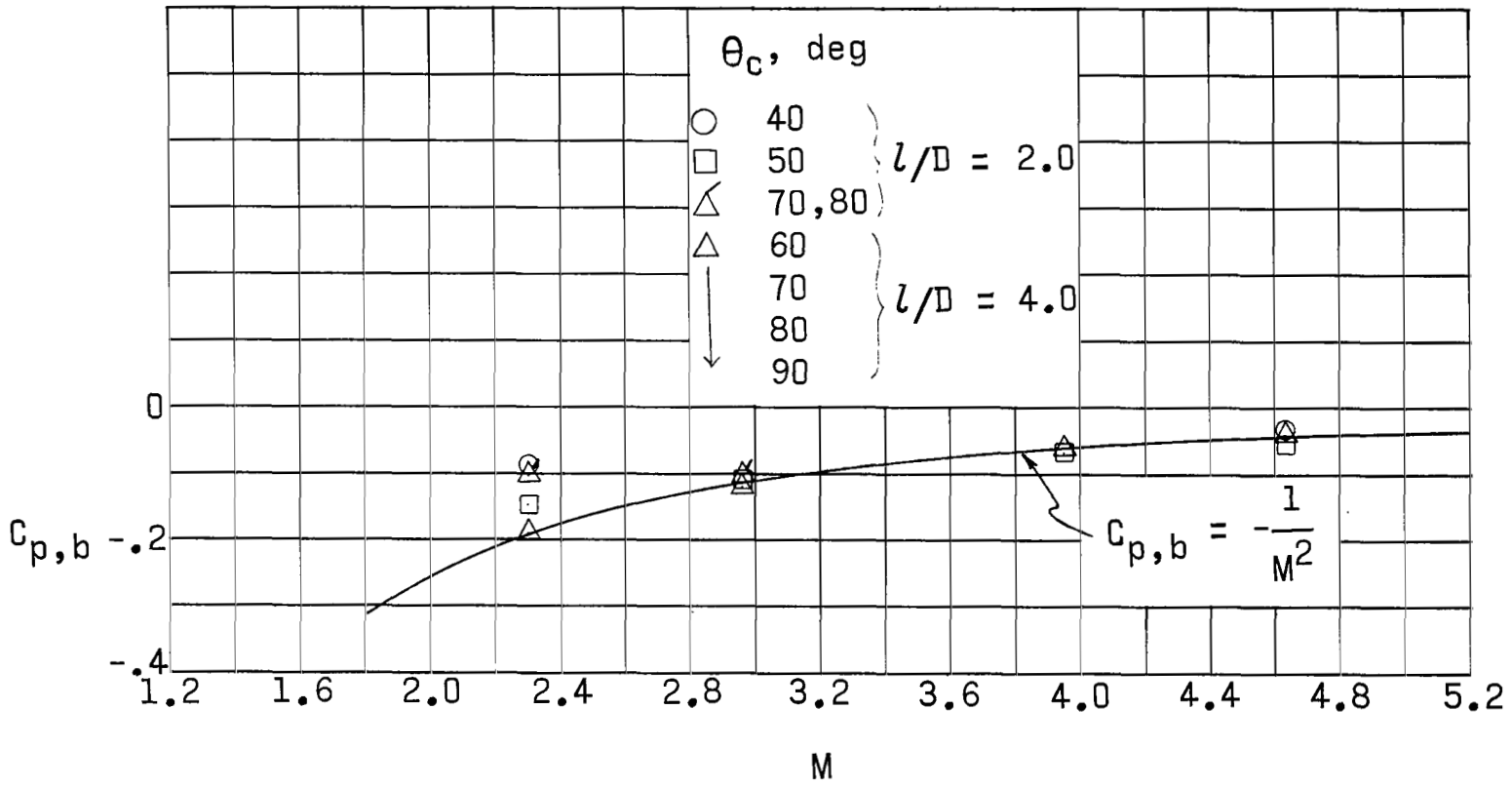

Figure 19.- Effect of sting length and Mach number on base pressure coefficient. Flagged symbols represent shorter sting; $\alpha \approx 0°$

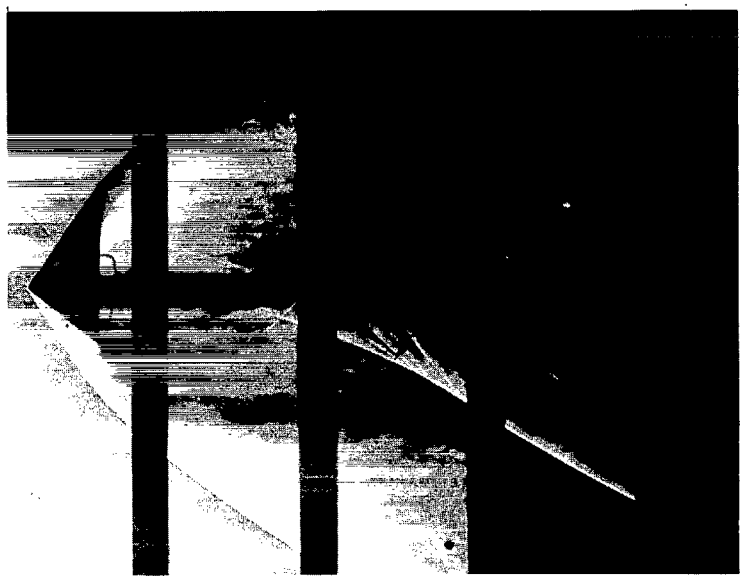

M = 2.30

M = 4.63

(a) $\theta_c = 40^o$.

L-68 5603

Figure 20.- Schlieren photographs for test models at $\alpha \approx 0^o$.

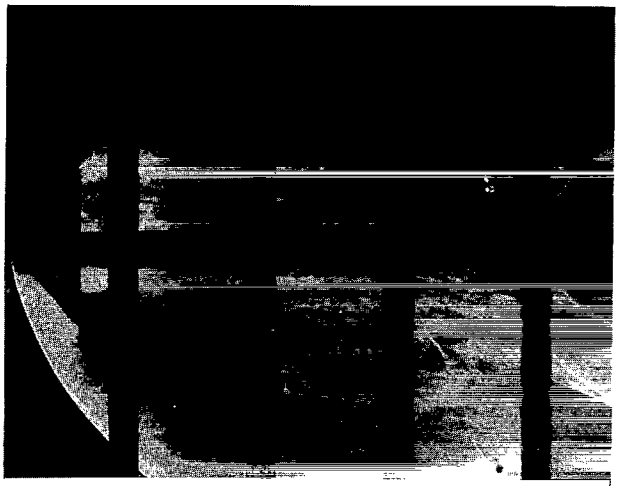

M = 2.30

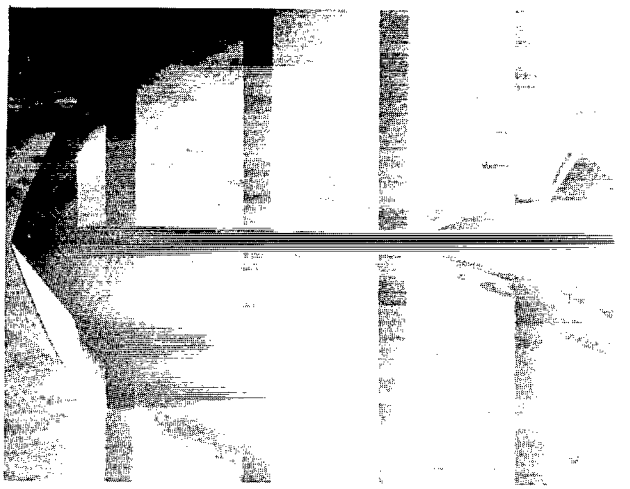

M = 2.96

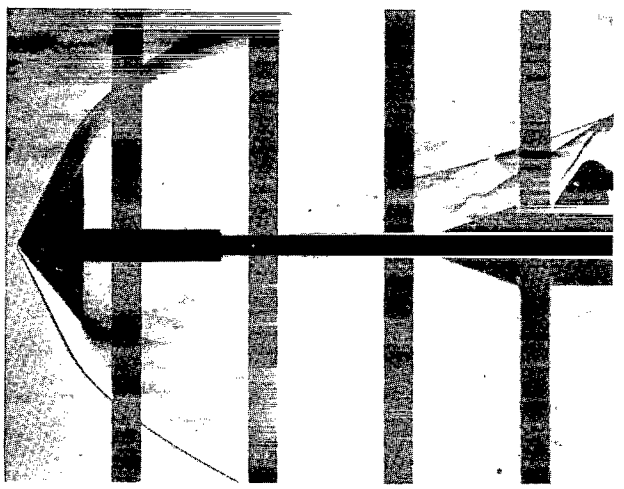

M = 3.95

M = 4.63

(b) $\theta_c = 50^o$. L-68 5604

Figure 20.- Continued.

M = 2.30

M = 2.96

M = 3.95

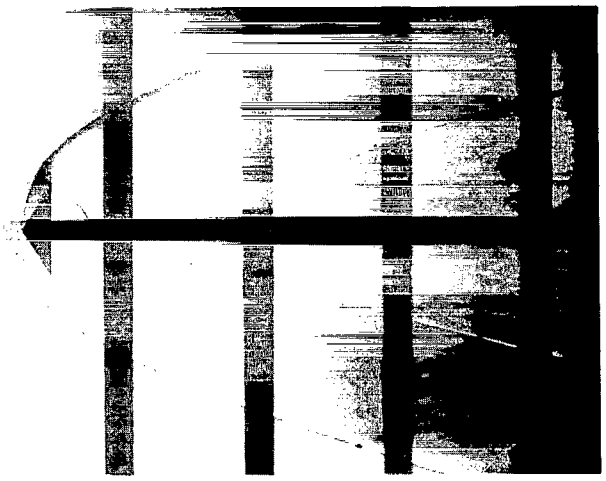

M = 4.63

(c) $\theta_c = 60^0$. L-68-5605

Figure 20.- Continued.

M = 2.30

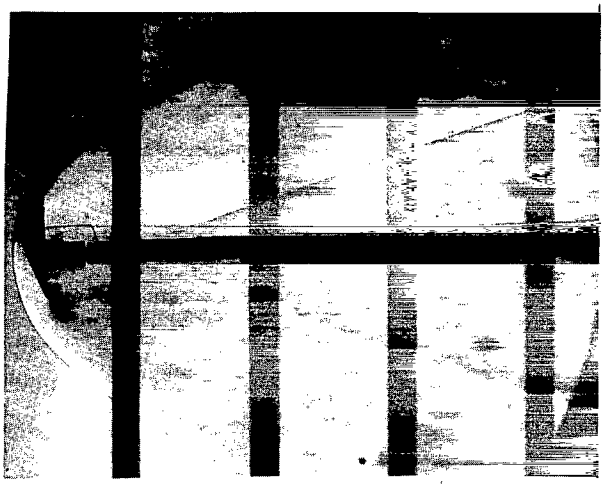

M = 2.96

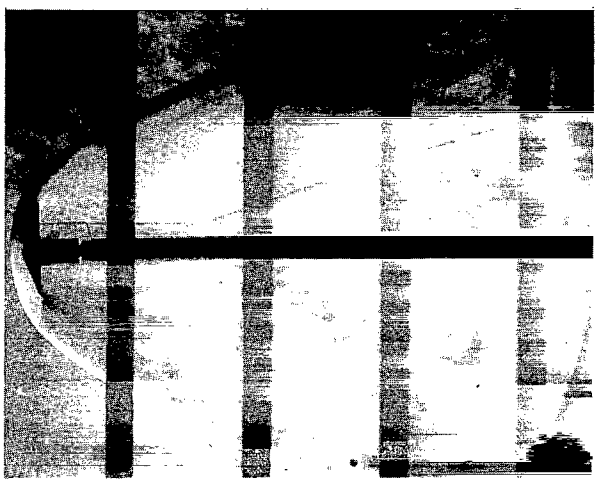

M = 3.95

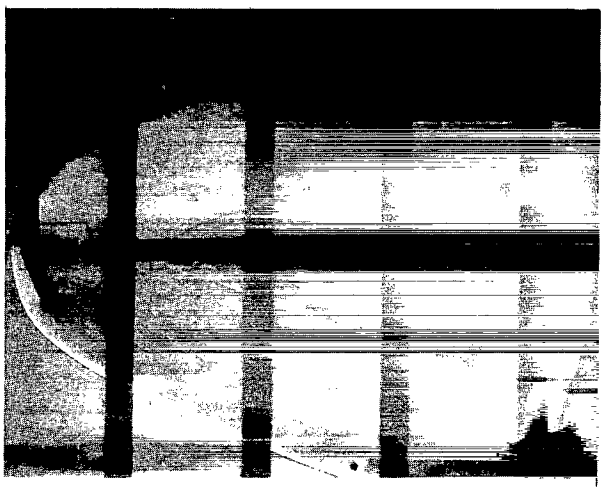

M = 4.63

(d) $\theta_c = 70^o$. L-68-5606

Figure 20.- Continued.

M = 2.30

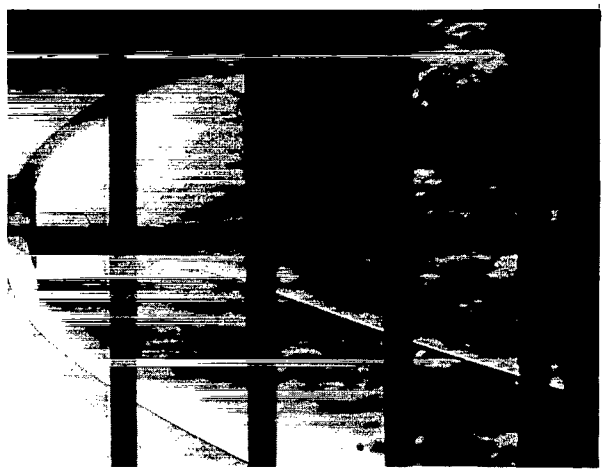

M = 2.96

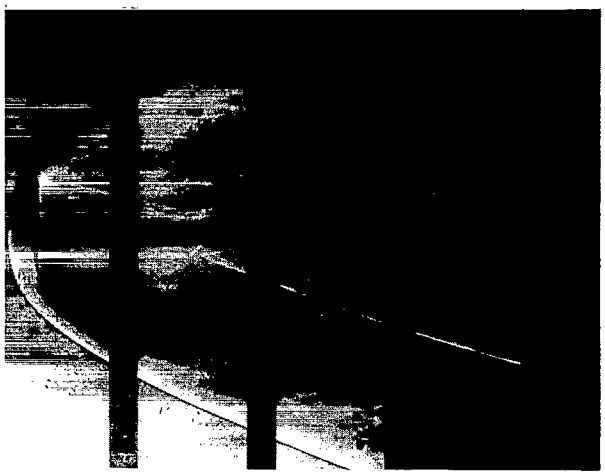

M = 3.95

M = 4.63

(e) $\theta_c = 80^o$. L 68-5607

Figure 20.- Continued.

M = 2.30

M = 2.96

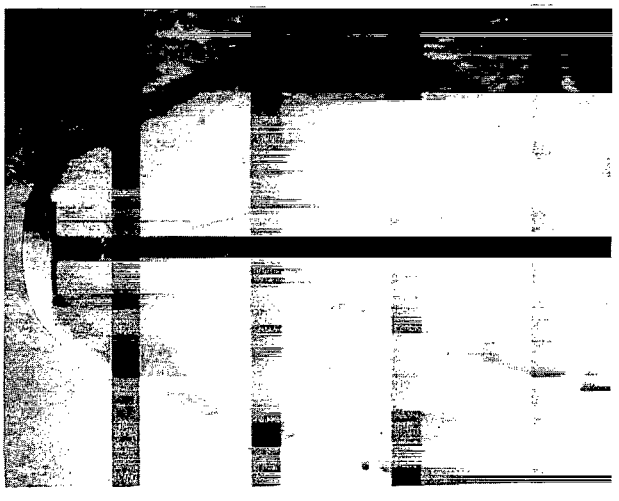

M = 3.95

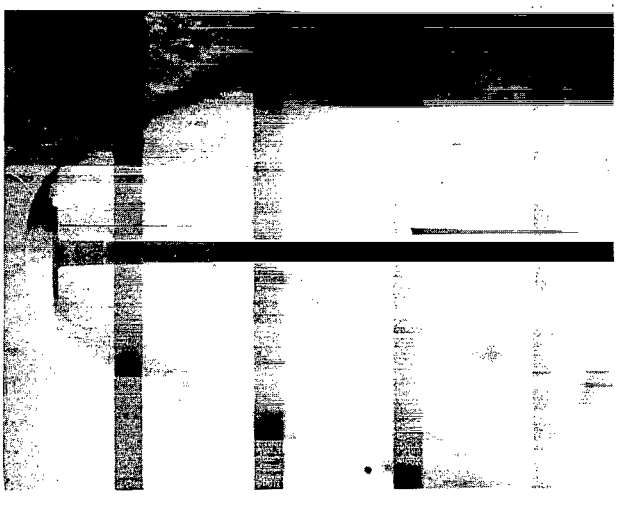

M = 4.63

(f) $\theta_c = 90^o$.

L-68-5608

Figure 20.- Concluded.

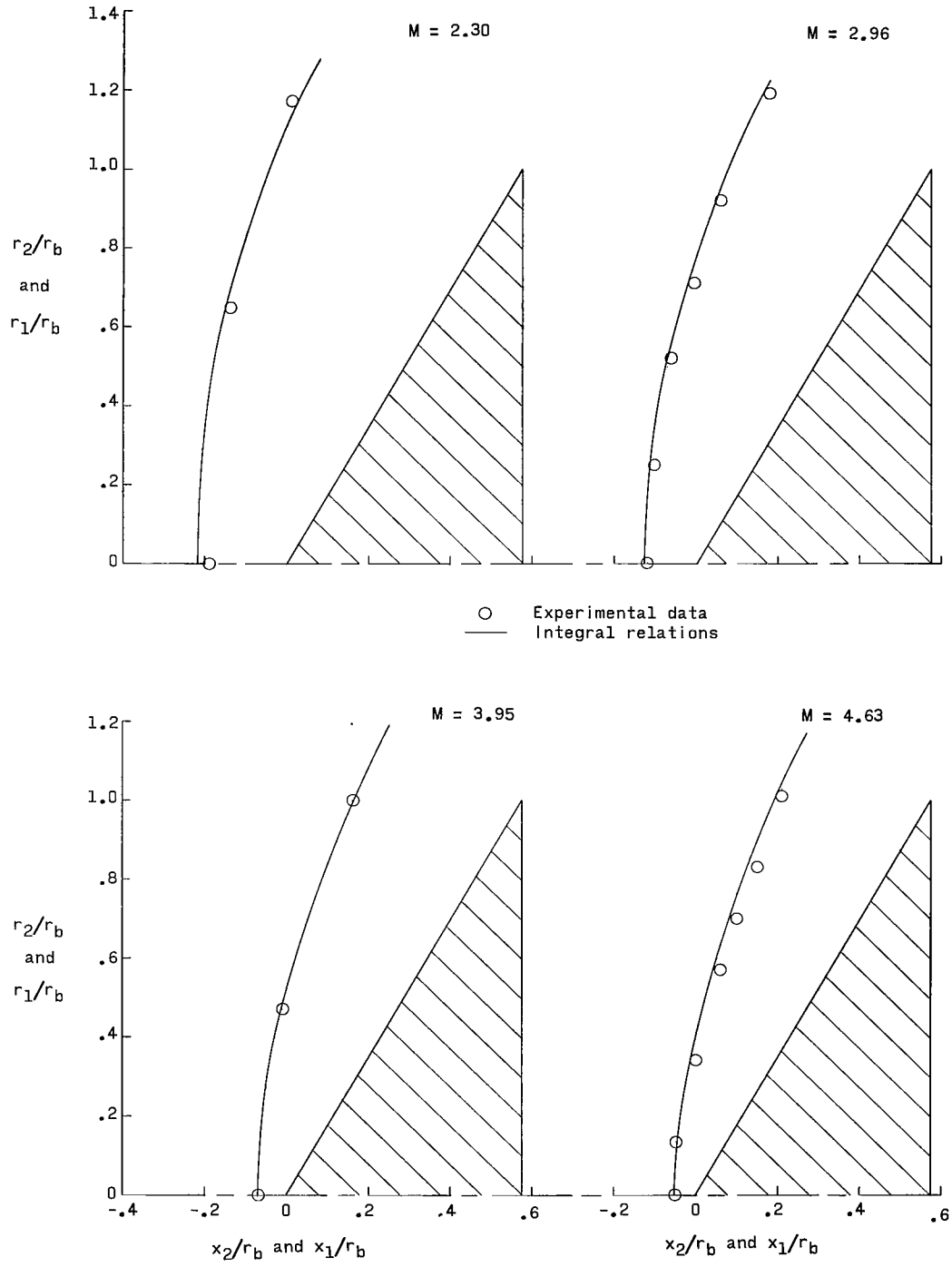

(a) $\theta_c = 60^0$.

Figure 21.- Shape of the detached shock wave for the test configurations.

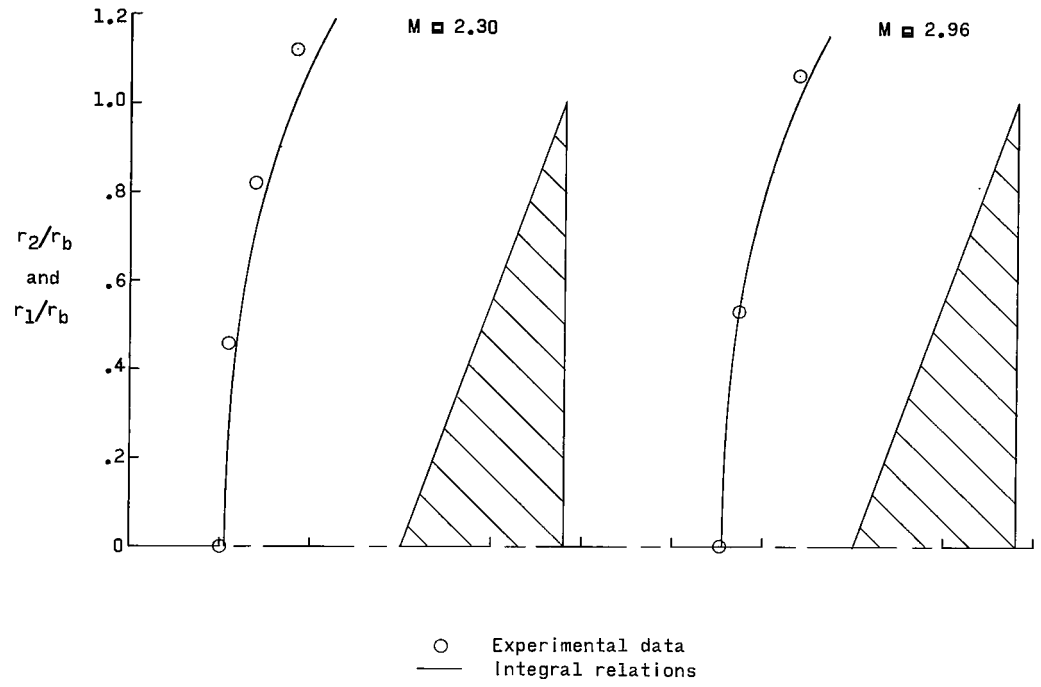

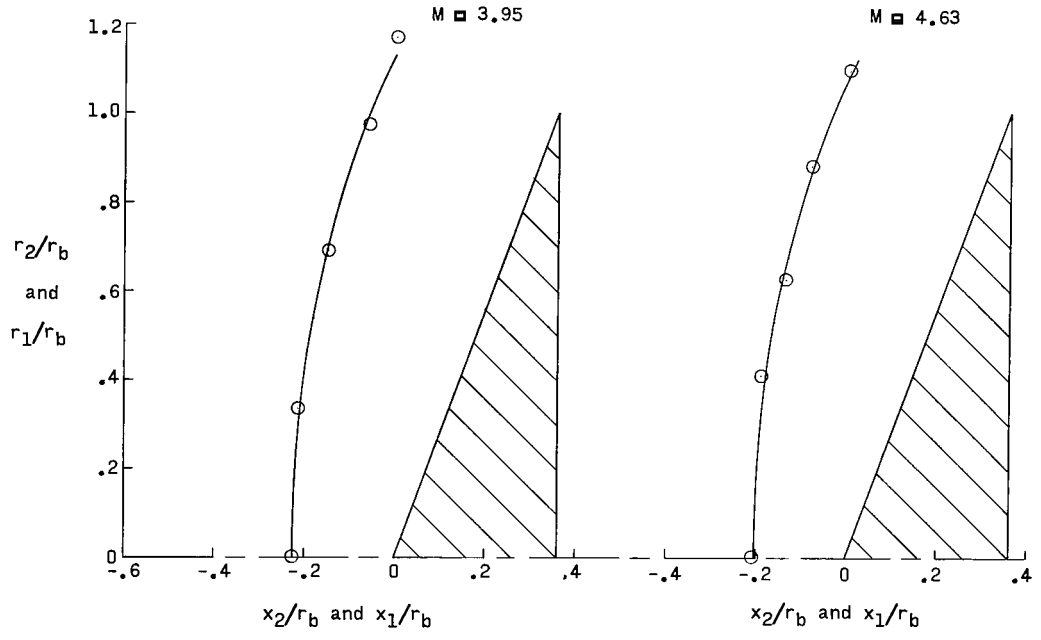

(b) $\theta_c = 70^0$.

Figure 21.- Continued.

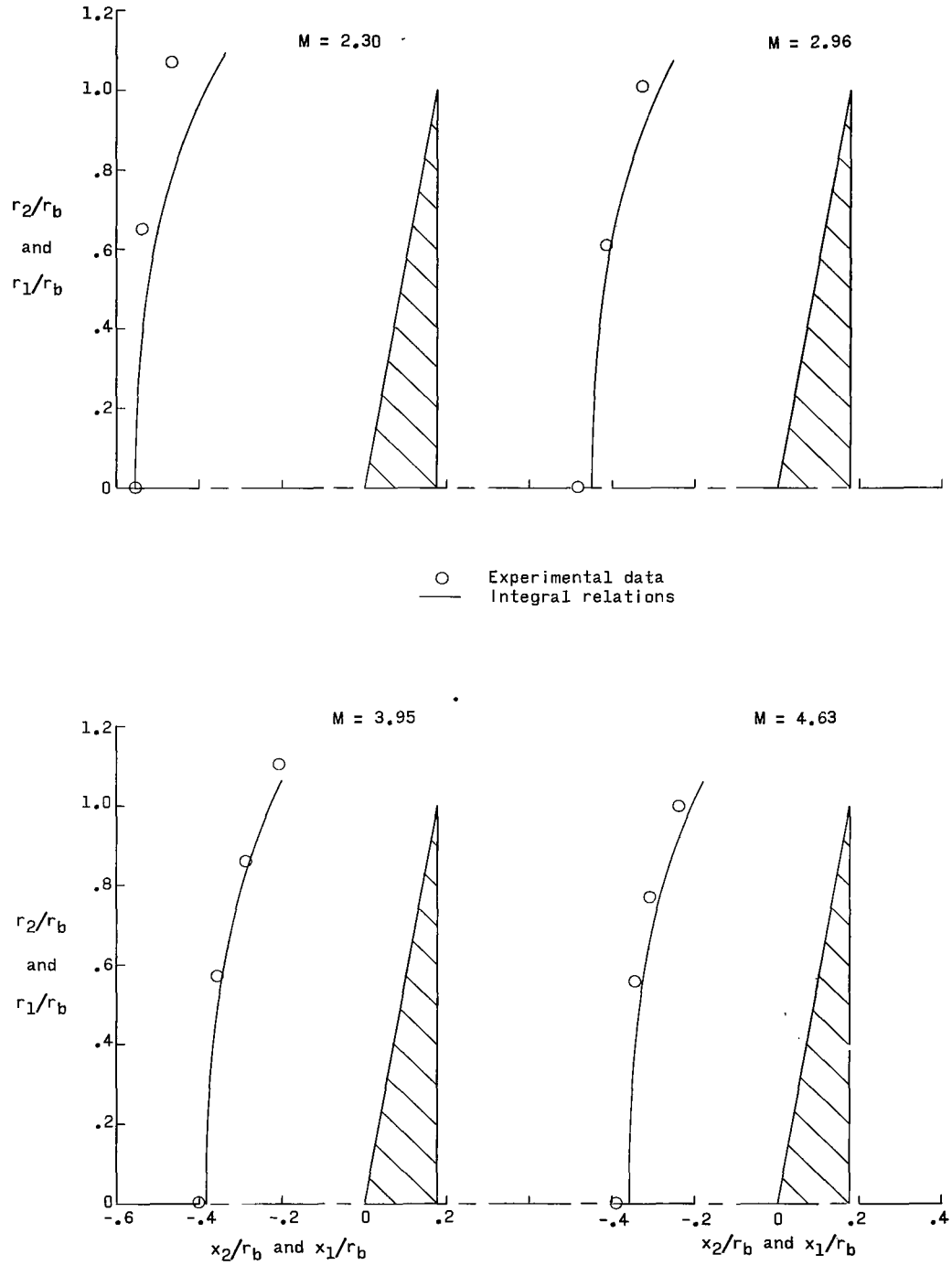

(c) $\theta_c = 80^0$.

Figure 21.- Continued.

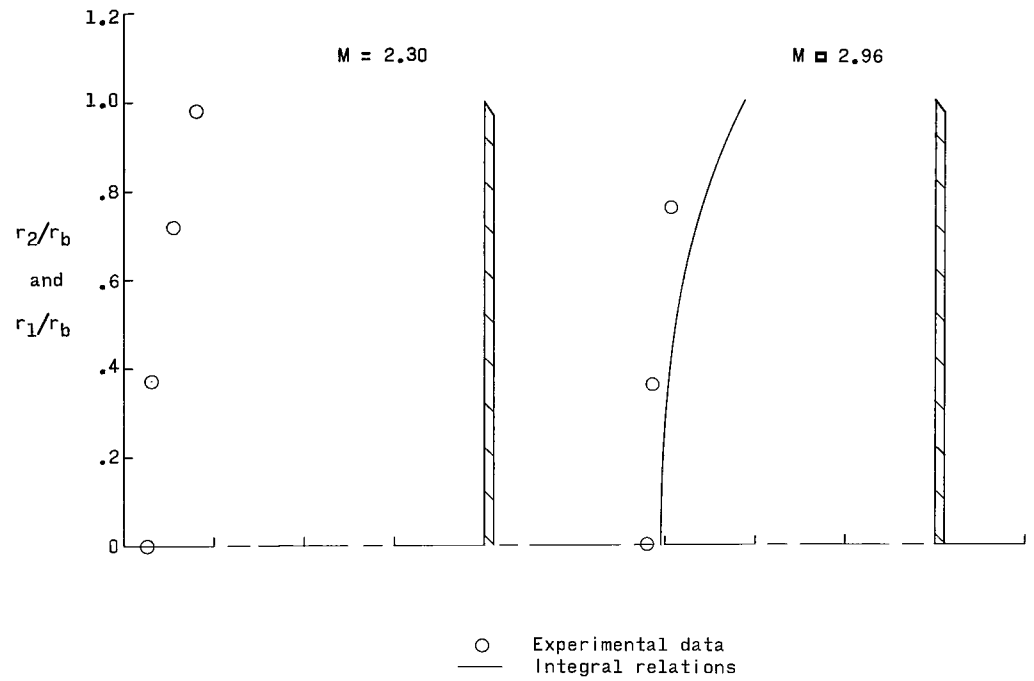

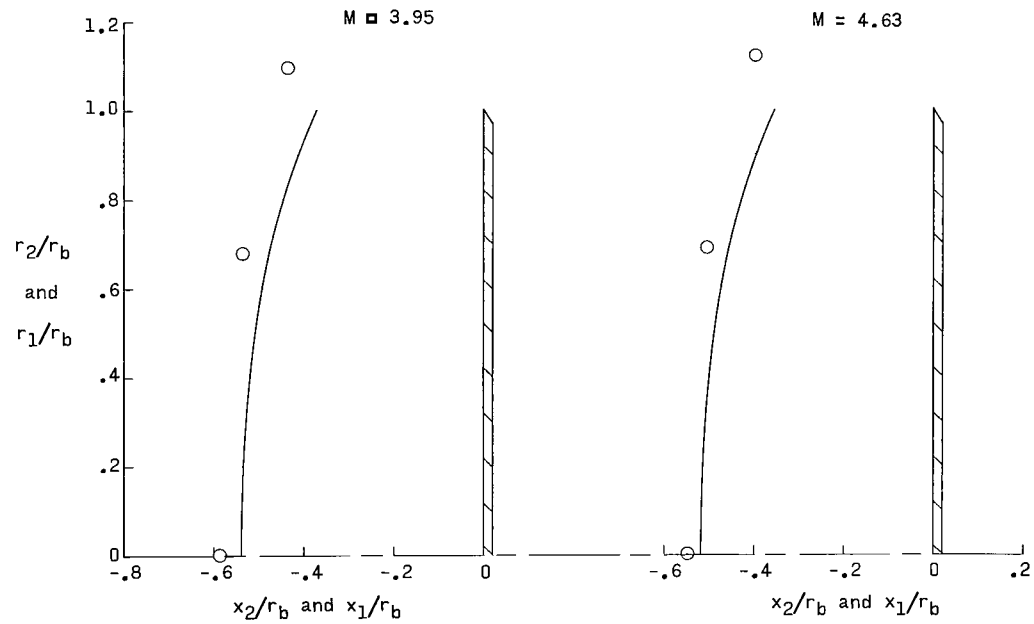

(d) $\theta_c = 90^0$.

Figure 21.- Concluded.

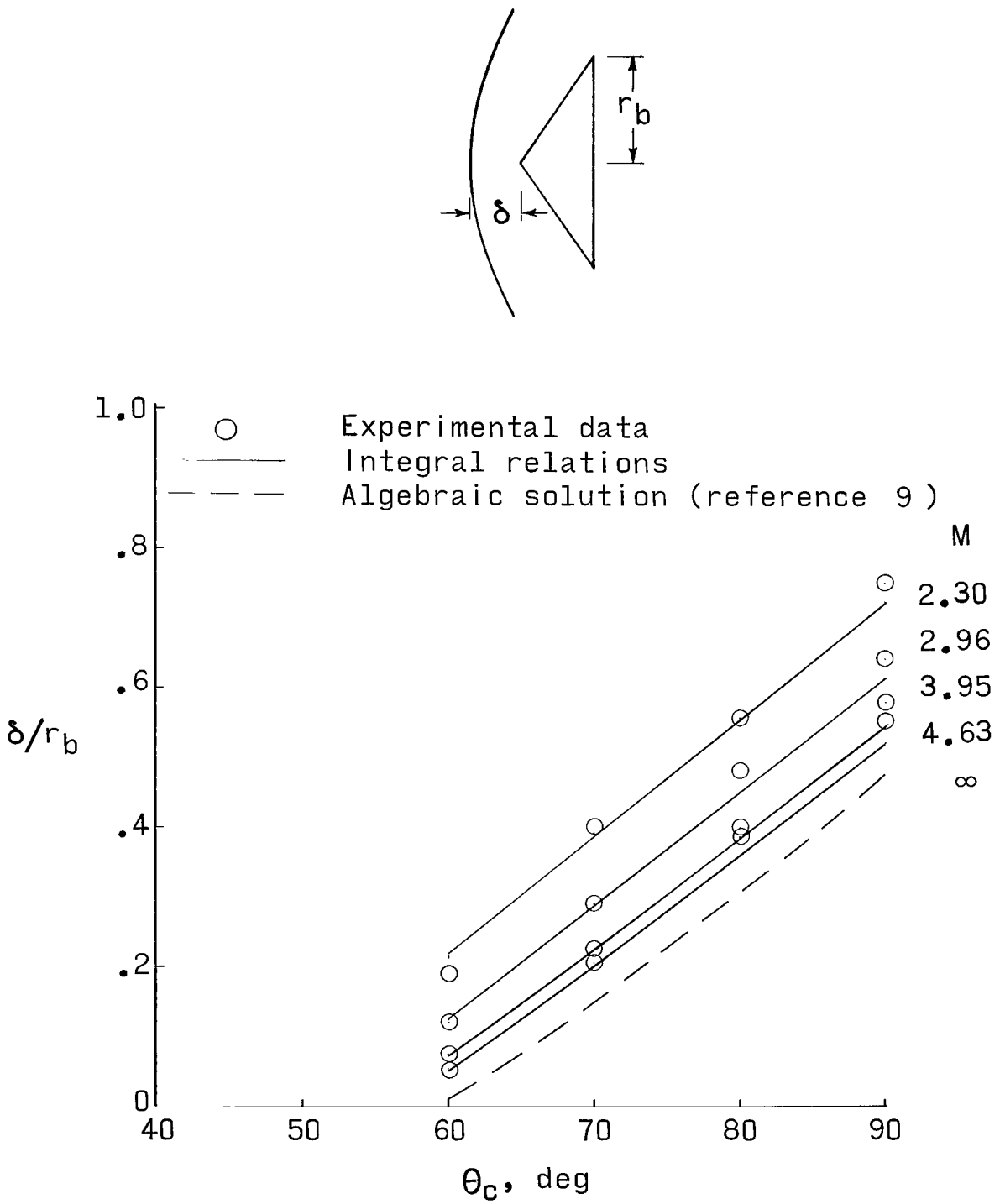

Figure 22.- Variation of nondimensionalized shock standoff distance with cone semiapex angle.

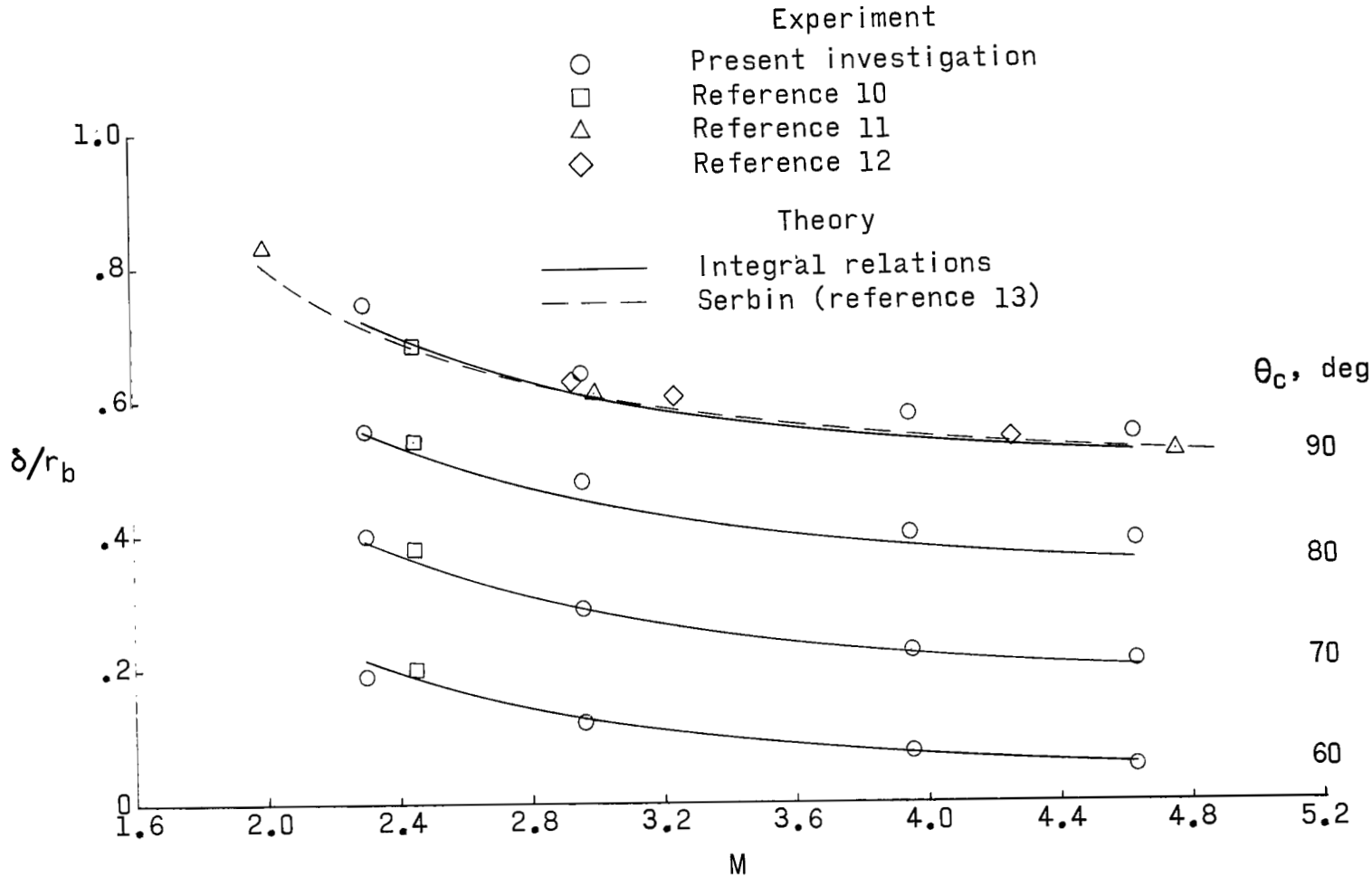

Figure 23.- Variation of nondimensionalized shock standoff distance with Mach number.

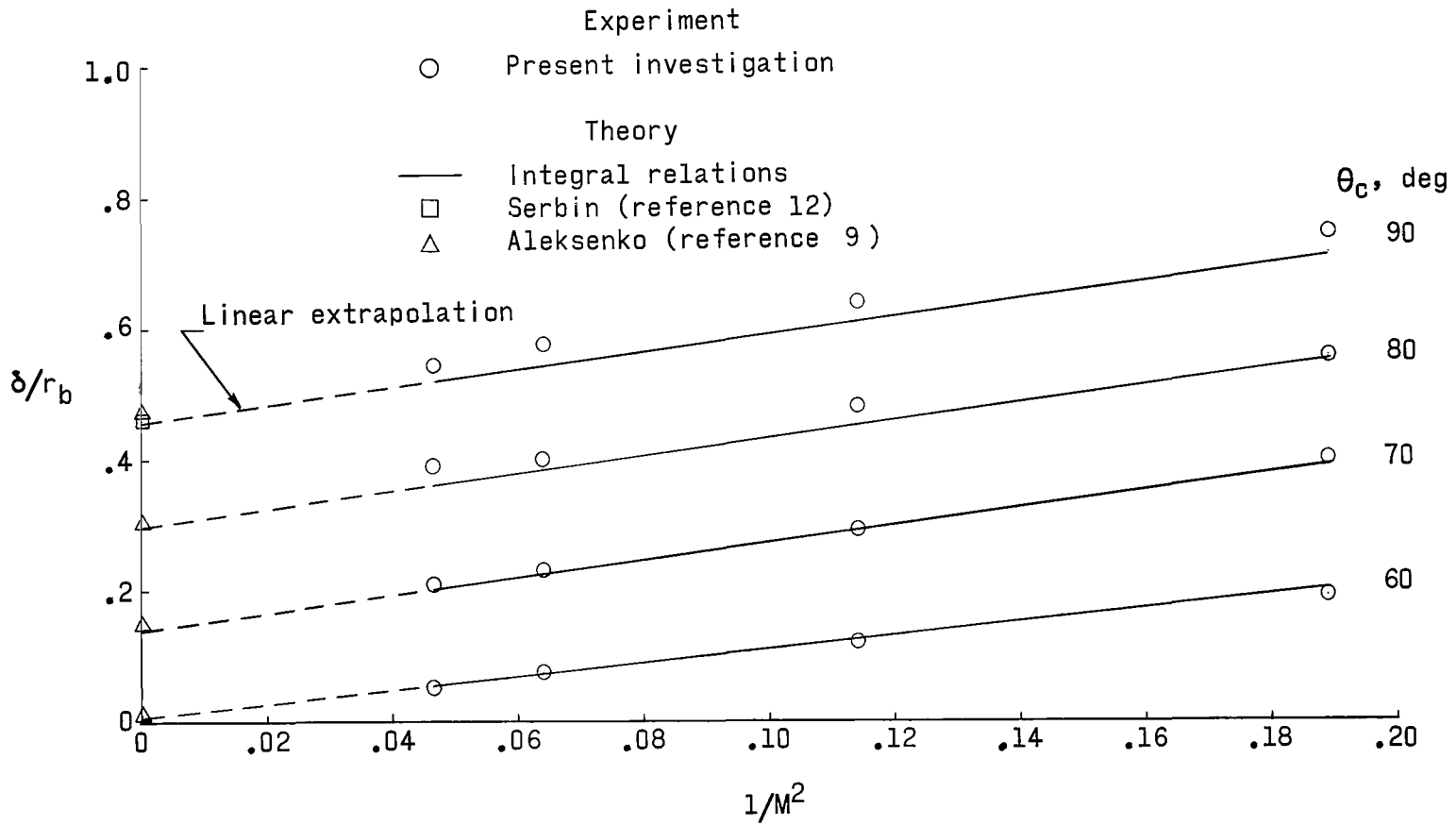

Figure 24.- Variation of nondimensionalized shock standoff distance with $1/M^2$.

"The aeronautical and space activities of the United States shall be conducted so as to contribute . . . to the expansion of human knowledge of phenomena in the atmosphere and space. The Administration shall provide for the widest practicable and appropriate dissemination of information concerning its activities and the results thereof."

—NATIONAL AERONAUTICS AND SPACE ACT OF 1958

NASA SCIENTIFIC AND TECHNICAL PUBLICATIONS

TECHNICAL REPORTS: Scientific and technical information considered important, complete, and a lasting contribution to existing knowledge.

TECHNICAL NOTES: Information less broad in scope but nevertheless of importance as a contribution to existing knowledge.

TECHNICAL MEMORANDUMS: Information receiving limited distribution because of preliminary data, security classification, or other reasons.

CONTRACTOR REPORTS: Scientific and technical information generated under a NASA contract or grant and considered an important contribution to existing knowledge.

TECHNICAL TRANSLATIONS: Information published in a foreign language considered to merit NASA distribution in English.

SPECIAL PUBLICATIONS: Information derived from or of value to NASA activities. Publications include conference proceedings, monographs, data compilations, handbooks, sourcebooks, and special bibliographies.

TECHNOLOGY UTILIZATION PUBLICATIONS: Information on technology used by NASA that may be of particular interest in commercial and other non-aerospace applications. Publications include Tech Briefs, Technology Utilization Reports and Notes, and Technology Surveys.

Details on the availability of these publications may be obtained from:

SCIENTIFIC AND TECHNICAL INFORMATION DIVISION

NATIONAL AERONAUTICS AND SPACE ADMINISTRATION

Washington, D.C. 20546